Studies of Miniature Tear Glucose Sensors and Electromodulated Nitric Oxide Delivery Devices

by

Bo Peng

A dissertation submitted in partial fulfillment
of the requirements for the degree of
Doctor of Philosophy
(Chemistry)
in The University of Michigan
2013

Doctoral Committee:

Professor Mark E. Meyerhoff, Chair
Associate Professor Nicolai Lehnert
Assistant Professor Stephen Maldonado
Professor Levi T. Thompson

DEDICATIONS

This Work is Dedicated To:

My parents and grandparents
for their support and unconditional love.

ACKNOWLEDGEMENTS

I was truly fortunate to have spent the past five years completing my doctoral work with numerous wonderful people in Ann Arbor. First and foremost, I sincerely thank my advisor, Dr. Mark E. Meyerhoff, for being the best mentor I can ever find. His optimism, passion for science, and patience for students have and will always be an inspiration to me. He encouraged me through research bottle-necks, rejoiced with me at breakthroughs, and finally guided me to the end of the tunnel.

Thank you to Dr. Stephen Maldonado, Dr. Nicolai Lehnert and Dr. Levi T. Thompson for serving on my committee. I appreciate the comments and suggestions each of you have had and your valuable time. I have to especially thank Dr. Maldonado for taking me as a rotation student and teaching me the fundamentals of electrochemistry in my first semester at Michigan.

Part of my research is highly collaborative work that involves researchers across the university. My gratitude goes to Terry C. Major at the Extracorporeal Life Support Research Laboratory for conducting the rabbit procedures with me, and for teaching me lessons on the blood sampling and animal handling. I also thank Dr. Bruce Cohan and Zvi Flanders from EyeLab Group for stimulating monthly discussions. A special thank you also extends to Jing Lu for providing insightful suggestions on the statistics relevant to my tear glucose data.

I was privileged to be in the Meyerhoff lab with a group of extraordinary scientists, including many former and present graduate students: Wansik Cha, Zhengrong Zhou, Mike Shen, Biyun Wu, Lin Wang, Jun Yang, Laura Zimmerman, Qinyi Yan, Natalie Crist, Wenyi Cai, Teng Xue, Si Yang, Andrea Bell, Liz Brisbois, Alex Wolf, Alex Ketchum, Hang Ren, and Zheng Zheng; and post docs: Fenghua Zhang, Kun Liu, Kebede Gemene, Lajos Höfler, Gary Jensen, and Dipankar Koley. Thank you all for providing continuous support and assistance for my research, especially for spending time on all my often-too-long practice talks, and our incredibly fun group nights. Special thanks go to Natalie Crist, Lahdan Refahiyat, and Drew Robison for their careful proof-reading efforts and for teaching me some real American English over these years.

During my doctoral research, I was honored to mentor several undergraduates and rotation students. In particular, Dakota Suchyta, Anant Balijepalli, and Peipei Hu have been of great assistance on two of my major projects. They impressed me with the real "Michigan Difference". Thank you for helping to save my time and I learnt a lot by working with each of you.

I would like to thank Roy Wentz, our departmental glassblower for efficiently turning my various sketchy designs into decent experimental gadgets. I also thank James Windak for training me on LC-MS, GC-MS, ICP-OES, FT-IR, for lending me the IR gas cell, and for answering my many questions. Patti Fitzpatrick's patient help in ordering chemicals and reimbursement is very much appreciated as well.

I am grateful to all my friends around the globe. I thank Juan Wen, Min Gong, Xiaoling Luo, and Jingting Shen in China for their continuous support and encouragement. I thank Si Yang, Yueyang Zhong, J.Y. Lee, Jing Nie, Yipei Wang,

Wenjing Chen, Jing Chen, Chenxi Shen, Tracy Liu, and Yu-Jui Huang for all the good times together in Ann Arbor.

Finally, I wish to express my love and gratitude to my family, without them this doctoral journey would not have been successful. I thank my parents (Shuijin Peng and Lixing Li), grandparents (Xiaolian Zhang, Xianzao Li, and Suyun Zeng), aunts, uncles, cousins, for their unending love and support on every decision I ever made.

TABLE OF CONTENTS

LIST OF FIGURES

LIST OF SCHEMES

ABSTRACT

Studies of Miniature Tear Glucose Sensors and Electromodulated Nitric Oxide Delivery Devices

by

Bo Peng

Chair: Mark E. Meyerhoff

In this dissertation, classic enzyme-based electrochemical sensors were fabricated for tear glucose measurements. Moreover, electrochemically modulated nitric oxide (NO) delivery systems were investigated to potentially improve the biocompatibility of indwelling medical devices.

First, miniature amperometric and coulometric biosensors were coupled with a glass micro-capillary to detect low levels (0.62 μM and 0.32 μM, S/N=3, respectively) of glucose in 3 microliters of tear fluid. The sensors were employed to selectively measure tear glucose in anesthetized rabbits with insulin administration over a wide range of blood glucose values. A positive correlation (r^2=0.86 and 0.83 for

amperometric and coulometric sensors) between the glucose levels in tear fluid and blood was found. This method may provide a supplementary tool to aid routine point-of-care blood glucose monitoring.

Nitric oxide (NO) plays critical roles in platelet inhibition, vasodilation, and antimicrobial activity. Two novel electromodulated approaches were studied to deliver NO on demand from a reservoir of donor species. Nitric oxide was previously reported to be the common product produced from electrochemical reduction of various *S*-nitrosothiols (RSNO) at physiological pH. However, studies here show that RSNO species are reduced to nitrous oxide (N_2O), not NO, at pH 7.4. Interestingly, at pH 4.0, a proton coupled one-electron reduction of RSNOs takes place and generates quantitative NO release on a gold working electrode. Therefore, it is further demonstrated that it is possible to use a reservoir of RSNOs at low pH to create catheters that can electrochemically generate NO at fluxes of $0.5\sim4\times10^{-10}$ mol cm^{-2} min^{-1} to possibly prevent clotting and infection.

In addition, pH sensitive NO donors, inorganic nitrite salts and diazeniumdiolated species, were employed to design a controlled NO release catheter via electrochemical modulation. Protons produced by water oxidation can lower the local pH and release NO in a thin layer in proximity to an anode surface. Catheters filled with NO donor solutions and a simple two-electrode circuit are shown to be able to electrochemically turn "on" and "off" at fluxes above 1×10^{-10} mol cm^{-2} min^{-1} of NO release for 8 h.

CHAPTER 1

INTRODUCTION

1.1 Role of Electrochemistry in Modern Medicine

Since Clark and Lyons proposed the first concept of an enzyme based electrode for glucose measurement in 1962,[1] electrochemical sensing has developed into a relatively mature field that continuously remains an active area of research with combined efforts of biologists, physicists, chemists, and engineers. The use of electrochemical techniques, in which the potential, current, or charge in an electrochemical cell serves as the signal for analytical methods has been widely explored. Electrochemical sensors are advantageous in measurement science, including environmental analysis and clinical diagnosis, due to various inherent properties. For example, they are relatively inexpensive, capable of real-time monitoring, and are easy to miniaturize and ultimately be implanted to facilitate *in vivo* tests without complex sample preparations. They also possess the ability to enhance selectivity and sensitivity by electrode modification and/or applied electrochemical methods optimization.

In general, electrochemical sensors can involve any of the five different measurement principles:

1. Potentiometry is a method that measures the potential difference between two electrodes. It is based on a reversible recognition between the target analyte (usually an ionic species) and a receptor under zero-current conditions. In theory, the potential (E) observed is proportional to the activity (a) of the target ion in the sample (Nernst equation, $E = K + \frac{0.0592}{z} log a$, K: constant, z: charge of ion, T=25℃). As examples, the classic pH electrode and K^+ sensors are routinely employed in modern clinical lab analyzers.[2] Further, simple Ag/AgCl electrodes are generally applied to measure electrical signals associated with heart function (e.g., EKG or ECG).

2. Amperometry includes measuring the electrochemical reduction or oxidation current with a constant voltage applied to the system. The steady-state current is directly related to the concentration of analyte. Many commercial handhold glucose meters are amperometric devices. In addition, the Clark style oxygen sensor[3] can be made as an implantable biomedical amperometric device.

3. Voltammetry monitors the current from electrochemical reactions (similar to amperometry) but with application of varying applied voltage. Usually, three electrodes are required, including the working, reference, and auxiliary electrodes. Two main types of voltammetric methods are cyclic voltammetry and linear sweep voltammetry, and other methods include stripping analysis and pulsed voltammetry as well. In principle, pulsed and square wave voltammetry techniques are suitable for lower concentration applications due to their excellent signal to noise ratios when compared to cyclic voltammetry or linear sweep voltammetry. Further, the anodic stripping voltammetry method is commonly employed in clinical microarray

analyzers to detect lead and other toxic heavy metal ions with high sensitivity in complex biological samples (blood, urine, and saliva).[4]

4. Coulometry is a technique that integrates the electrical currents passed through two electrodes in contact with the test solution, and the total electrical charge is correlated to the concentration of target species. This method counts the absolute amount of charge generated in the system, and therefore, in theory, does not need calibration. It is an attractive tool for environmental applications when fast response, low detection limit, and easy operation are required.[5]

5. Impedance is a method that reveals the capacitive properties and charge-transfer kinetics of an electrode under electrochemical perturbations/reactions. It generally employs a series of sinusoidal voltages that is close to the formal potential (with amplitude of 5-20 mV) to the working electrode with variable frequencies. This technique provides a powerful tool to reach extremely low detection limit in biological target measurements such as for specific DNA, antibodies, and other proteins.[6]

In this dissertation, a special interest of research is focused on employing classic amperometric and coulometric sensors for unconventional glucose measurements in microliter volumes of accessible tear fluid. Further, the feasibility of creating an electrochemically modulated nitric oxide delivery method to prevent clotting and bacterial growth on catheter devices is also examined.

1.2 Non/Minimally Invasive Glucose Measurements

According to current statistics from the World Health Organization (WHO), an estimated 346 million people have diabetes mellitus worldwide. Diabetes has been well recognized as one of the major causes of death and disabilities in developed countries, and the mortality rate of individuals diagnosed with diabetes is expected to double by 2030.[7] Early diagnosis and tight glycemic management are crucial in helping to prevent and control diabetes and its complications, such as cardiovascular disease, kidney failure, and blindness.[8, 9]

Conventional point-of-care glucose monitoring systems generally involve finger pricks to obtain drops of blood to be analyzed with an electrochemical strip-based glucometer. The sample volume of blood is drawn into a test strip loaded with glucose oxidase or glucose dehydrogenase, which reacts with sample glucose and reports a reading of plasma glucose concentrations in a few seconds. For Type 1 diabetics, it is recommended that their blood glucose concentration be monitored up to eight times a day. These repeated finger pricks may result in patient discomfort and, therefore, less frequent blood glucose checks that can lead to further complications.[10, 11]

1.2.1 Current Research on Non-Invasive Glucose Measurements

A number of new techniques have been examined that might provide a minimally invasive and/or non-invasive approach to blood glucose monitoring to improve patient compliance and glycemic control. These include near-infrared spectroscopy,[12, 13] Raman spectroscopy,[14] fluorescence affinity sensors,[15] photoacoustic probes,[16] and a photonic crystal method.[17] Unfortunately, none of these techniques have yet achieved the required

analytical performance necessary to fully substitute for conventional blood glucometer devices. Other investigations have suggested testing glucose levels in accessible surrogate body fluids, such as interstitial fluids,[18, 19] saliva,[20] urine,[21, 22] and tears[23] as viable alternatives to finger pricks.

Most notably, a commercial automatic glucose monitor called the GlucoWatch® 2 Biographer (Cygnus Inc., Redwood City, CA) received United States Food and Drug Administration (FDA) approval in 2001. It measured glucose continuously from subcutaneous fluid that was brought to the skin surface by reverse iontophoresis via application of a small electric voltage. An AutoSensor composed of a replaceable adhesive polymer pad was placed at the back of the device to collect interstitial fluids that further undergo an enzymatic reaction with glucose oxidase at an electrochemical sensor surface, similar to the traditional glucometer (Figure 1.1). It automatically measured glucose levels through the skin and reported results on a screen every 10 min.

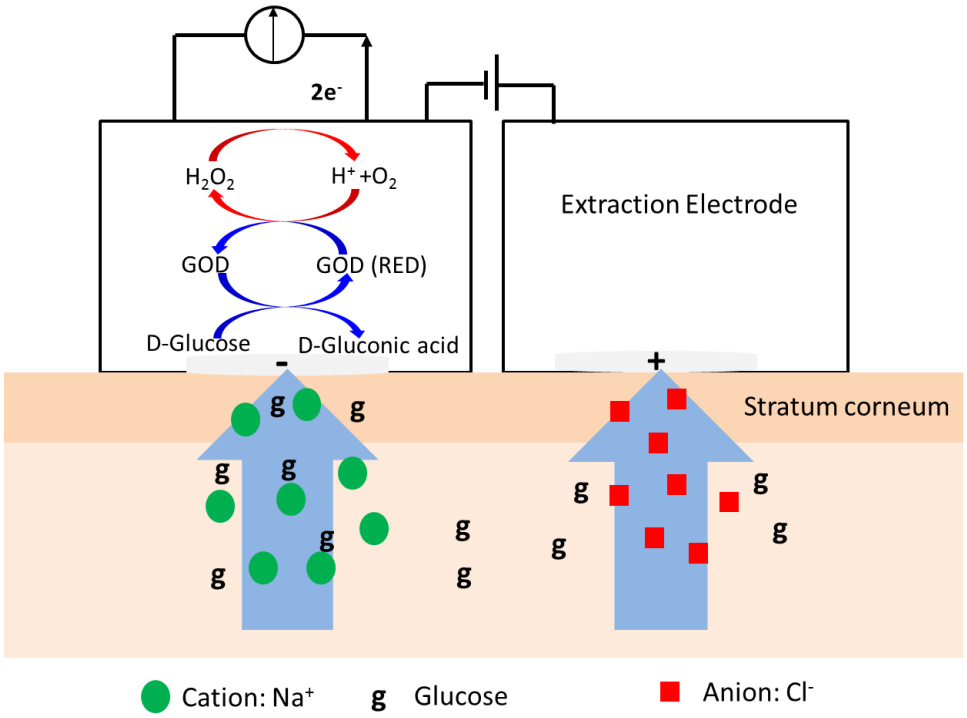

Figure 1.1. Schematic diagram of the ionotophoresis process during an interstitial glucose measurements using GlucoWatch.

However, clinical researchers reported only a 78.4% correlation coefficient ($p<0.05$) between these automated measured glucose values and a finger-prick glucometer.[24] Due to poor accuracy, the device required repeated calibration every 5 measurements. Further, according to the FDA, at least half of the users experienced skin irritation or itching from the electric discharge, and thus the patients had to rotate the device site so as to avoid repeated skin irritation. Sweating was recognized as another factor that led to additional inaccuracy. Due to the lack of reliability and accuracy, the GlucoWatch® G2 Biographer system is no longer produced, effective July 31, 2007.

There are also other approved and readily commercially available continuous glucose monitoring (CGM) systems. They are usually operated to measure interstitial

glucose levels for up to a few days at a time until the glucose sensor needs to be replaced, while the patients continues daily activities at home. These include: (1) the Navigator CGM device (Abbott Diabetes Care, Alameda, CA); (2) the Seven Plus (DexCom, San Diego, CA); and (3) the Guardian (Medtronic Diabetes, Northridge, CA). These continuous glucose monitoring system provide a very helpful tool for tight glycemic control and predicting necessary therapeutic treatment. However, these available systems must be coupled with the conventional finger-prick glucometer to be calibrated each day, or multiple times per day. In addition, the glucose levels measured in interstitial fluids are reported to have a significant lag time from blood glucose concentrations ranging from 5-15 min.[25]

The use of urine samples for the estimation of blood glucose concentrations has received considerable attention. This method is non-invasive and particularly useful for people who are unable to use a blood glucometer or that reside in rural areas in developing countries. It usually involves the use of a special reagent strip or dipstick that contains color-sensitive reagents to react with glycosuria (glucose in urine). The color developed on the strip provides quantitative information of detected glycosuria levels by referring to a standard color scale. A more recent study, using gold nanoparticles with immobilized glucose oxidase, measured urine glucose at a lower threshold of 0.56 mM (10 mg/dL), and a color change from red to blue that can be differentiated by the naked eye. However, the preparation is complicated, requiring gold nanoparticle fabrication and enzyme immobilization.[22] Also, glucose will only show up in the urine once it has reached high levels in the blood, i.e. 10 mM (180 mg/dL), which is already a pathological value. Additionally, urine is a complex sample matrix and the correlation between

glycosuria and blood sugar is possible only if renal plasma flow and filtration is normal; in case of reduced plasma flow, the renal glucose threshold will be higher. As a result, a glycosuria test is not an ideal alternate to routine blood glucose monitoring and diabetic treatments.

1.2.2 Tear Fluid as Surrogate for Glucose Measurements

Tear fluid has unique properties among other accessible body fluids and is known to contain glucose.[26] Compared to saliva and urine that have a variable dilution effects, tear fluid that bathes the eye is maintained at a miniscule and relatively stable volume (~4 μL). Tear fluid is continuously replenished by the lacrimal gland and other accessory glands at a rate of production in the range of 0.5-2.2 μL/min.[27] A thin film of tear fluid (~8 μm thick) keeps the cornea and conjunctiva continuously moist, without any stimulation (Figure 1.2).[28]

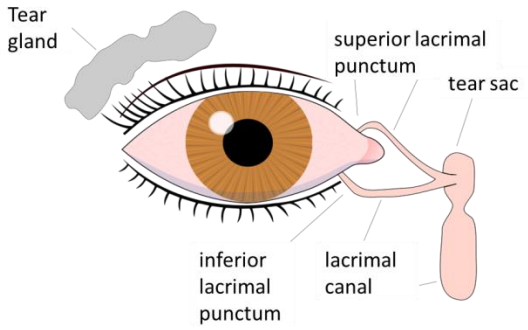

Figure 1.2. Schematic diagram of the eye and tear production.

The interest in monitoring glucose levels in tear fluid dates back to 1937 when Michail et al. demonstrated an increase of tear glucose concentration in diabetics.[29] Tear

glucose measurements provide the possibility of developing a relatively simple and minimally invasive method of monitoring glucose levels, provided that the tear glucose concentrations can be shown to correlate closely to the blood glucose concentrations in individuals. If a good correlation between the two types of samples can be established over a wide glycemic range, tear glucose monitoring could be an attractive alternate for conventional blood glucose measurements within the normal (4-6 mM) as well as hyperglycemic and hypoglycemic ranges. During the measurement, it is important for tear fluid to be collected using a method that will not impact/perturb the eye or cause any damage to the blood capillaries within the eye. Indeed, it is necessary to prevent any capillary glucose leakage into the tear film that would result in false high glucose levels compared to the actual glucose present in the tear fluid. Furthermore, tear fluid must be collected in a manner that will not increase tear production, which would further dilute the glucose concentrations in such samples.

1.2.3 Current Research on Tear Glucose Measurements

There has been much research focused on the determination of glucose in tears with different methods. For any technique to be effective, it requires a low detection limit, since glucose is present at levels of 50-100 times lower than in blood,[28] high selectivity over active interferences such as uric acid and ascorbic acid,[30] and the ability to quantitatively measure small sample volumes in a short time period (1-5 min). While most of the studies reported to date have found a positive correlation between tear and blood glucose levels, discrepancies still exist in terms of the actual lacrimal glucose concentrations (7-600 μM) and the degree of correlation between blood and tear levels,

mainly due to different tear glucose measurement and sampling methods (e.g., filter paper and micro-capillaries). [31-33]

LeBlanc et al.[32] reported a tear glucose concentration analysis system using high-performance liquid chromatography with a pulse amperometric detector (HPLC-PAD). They concluded from 44 paired samples from 5 patients that poor correlation existed between tear and blood glucose in critically ill patients, and that glucose measurement in tear fluid failed to provide an alternative method to blood glucose monitoring. Later, Lane[28] applied a similar chromatographic (LC-PAD) system in 121 diabetic and non-diabetic patients and found a correlation between tear glucose and capillary blood glucose concentrations. In a recent paper, La Belle and co-workers[34] introduced a disposable microfluidics system that measured glucose at levels as low as 43.4 μM using an integrated electrochemical sensor. The authors proposed this device to be a future prototype for a non-invasive glucose testing, but did not provide real sample data. An enzyme immobilized Pt electrode on the surface of a poly-dimethyl silicone (PDMS) was reported to be able to measure tear glucose levels in a rabbit to be 0.12 mmol/L.[35] However, no blood samples were collected to validate any relationship between tear and blood glucose levels.

In perhaps the most significant studies to date, Baca and Asher[36] employed liquid chromatography coupled with electrospray ionization mass spectrometry (LC-ESI-MS) to detect glucose concentrations in 1 μL samples of tear fluid. They were able to obtain significant correlations between this method and a contact lens-based sensor device. In fact, attempts to continuously monitor tear glucose concentrations using disposable contact lenses have received much research focus as most diabetic patients have

complications that need visual correction as well.[37] In 2004, March and co-workers published the first clinical trial test of five fasting Type 2 diabetic patients using a fluorescent contact lens tear glucose sensor, where the fluorescent signal increases with higher concentrations of glucose in tear fluid. The tear glucose levels measured in a 3 h experiment by the lens sensor tracked the trend of blood glucose well.[38] Later, the Asher and other research groups developed a series of photonic crystal glucose sensing materials for the non-invasive tear glucose monitoring system.[39-41] An intelligent platform of polymerized crystalline colloidal array (PCCA) was employed. The PCCA consists of highly ordered crystalline colloidal material that responds to the volume changes of the hydrogel on the principle that the observed diffraction wavelength is directly related to the spacing between lattice planes.[40] Therefore, by tethering the boronic acid molecule which can reversibly recognize glucose to the hydrogel materials, a contact lens optical sensor was created. By proper design, a change of color as a function of glucose concentration occurs based on a change in the diffraction properties of the lens material as glucose binds to the anchored boronic acid sites. One major challenge in the boronic acid doped contact lens system is the complex receptor design and the need for irradiation to initiate the diffraction based color change.

Despite these and other research efforts, discrepancies exist on whether there is a clinically useful correlation between tear glucose and blood glucose, as well as a stable true concentration of tear glucose in normal and diabetic subjects. Consequently, more research is needed to develop more sensitive detection techniques and less invasive sampling methods that can be used very close to the patient, so that evaporation or other issues associated with very small tear sample volumes can be prevented.

1.3 Nitric Oxide (NO) and NO Precursors

1.3.1 Biological Functions of NO

Since nitric oxide (NO) was first discovered as the elusive endothelial-derived relaxing factor (EDRF) in 1987,[42] there has been a significant research effort to explore and understand the many other important physiological activities of NO.[43]

Nitric oxide is the smallest biological messenger in the human body.[43] It functions as a vasodilator, an inhibitor of platelet adhesion and activation, an antimicrobial mediator and a neurotransmitter.[44] Endothelial cells (EC) that line the inner surfaces of all blood vessels possess an enzyme that produces NO called NO synthase (eNOS). The mechanism for NO production starts with a two-electron oxidation of L-arginine in the presence of oxygen and one molecule of NADPH, forming a N-hydroxy-L-arginine intermediate. Thereafter, a three-electron oxidation occurs, which is supported by oxygen and 0.5 molecule of NADPH, resulting in the formation of L-citrulline and NO in a 1:1 stoichiometry (Figure 1.3, left).[45] Once the diatomic radical is synthesized in the endothelium, it can diffuse into underlying smooth muscle cells and further activates soluble guanylyl cyclase, ultimately resulting in the relaxation of smooth muscle cells and promoting vessel dilation (Figure 1.3, right). Further, emission of NO at the blood/surface interface is critically important since the local levels of NO produced by the endothelium prevents platelet activation and adhesion to this highly thromboresistant surface. However, NO does not exist to any significant degree in blood due to its rapid reaction with oxyhemoglobin (to form methemoglobin and nitrate) and its oxidation by oxygen.

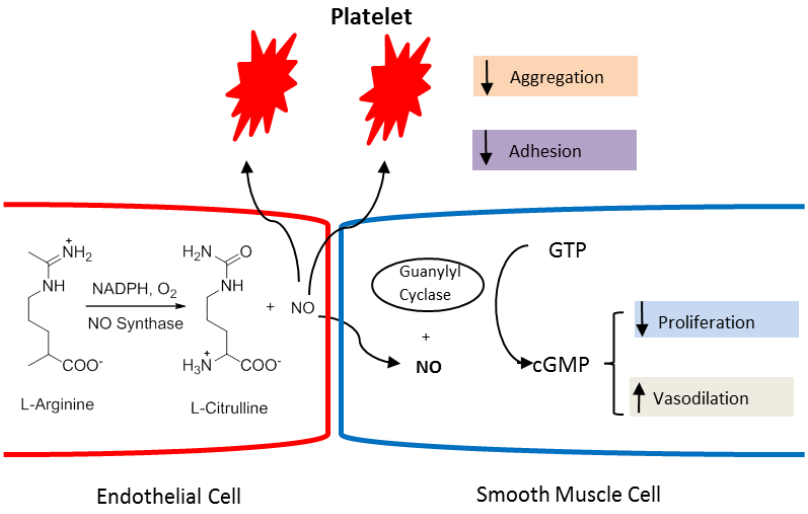

Figure 1.3. Scheme of production and biological functions of NO in human blood.

1.3.2 NO Donors: S-Nitrosothiols, Diazeniumdiolates, and Nitrite Salts

S-Nitrosothiols (RSNOs) have proven to be a potent donor of transient NO with much better stability and longer half-life (most RSNOs are stable for hours in the presence of metal ion chelator).[46] The functions of RSNOs mirror that of NO in biological processes including vasodilation, contraction of heart and skeletal muscle, and neurotransmission.[47] For instance, RSNOs have been shown to increase in response to inflammatory stimuli[48] and also are elevated in septic shock.[49] Up to now, normal plasma RSNOs have been detected over a wide range of concentrations, from trace nanomolar to tens of micromolar levels,[47] due to differences in the individual species as well as the sampling and analytical methodologies used.

Endogenous RSNOs are formed *in vivo* from the reaction between thiols and NO, or its reactive intermediates. A fraction of NO produced by NOS in the vasculature (approximately 20%) escapes inactivation by hemoglobin and is oxidized to HNO_2 (Eq.

1.1) and subsequently N_2O_3 (Eq. 1.2), which spontaneously decomposes to produce nitrite (NO_2^-) and nitrosonium ions (NO^+) (Eq. 1.3). The NO^+ serves as a nitrosating agent, and can react with free thiols (including cysteine residues within proteins) to form low concentrations of *S*-nitrosothiols (Eq. 1.4).[50]

$$NO + metHb\big(Fe(III)\big) \rightarrow deoxyHb\big(Fe(II)\big) + 2H^+ + 2NO_2^- \qquad (1.1)$$

$$2HNO_2 \leftrightarrow H_2O + N_2O_3 \qquad (1.2)$$

$$N_2O_3 \leftrightarrow NO^+ + NO_2^- \qquad (1.3)$$

$$RSH + NO^+ \rightarrow RSNO + H^+ \qquad (1.4)$$

Scheme 1.1. Reactions leading to the formations of endogenous RSNOs.

Chemically, RSNOs are thioesters of nitrite with the nitroso moieties covalently bound to a sulfhydryl group (Figure 1.4). *S*-Nitrosothiols are assumed to act as stable stores of NO and can release local transient NO under physiological conditions via different decomposition pathways (thermal, light, thiol, catalytic metal ion reduction, etc.). Hence, there are increasing research interests to utilize such NO generating processes in order to modify different surfaces with RSNOs and then release NO in a controlled manner.

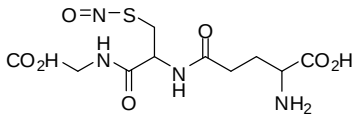

S-nitrosoglutathione (GSNO)

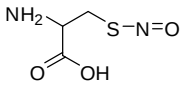

S-nitrosocysteine (CysNO)

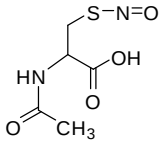

S-nitroso-N-acetylcysteine(SNAC)

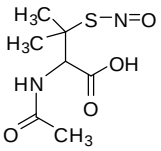

S-nitroso-N-acetyl-DL-penicillamine (SNAP)

Figure 1.4. Chemical structures of some *S*-nitrosothiols (RSNOs)

N-Diazeniumdiolates, compounds containing two molecules of NO combined with an amine (*N*) or other nucleophilic site, which are called NONOates, were first investigated by Drago in the 1960s.[51, 52] Later in the 1990s, with the discovery of NO's important biological functions, diazeniumdiolates became an ideal NO precursor candidate for proton-mediated NO release to tackle pharmacological and biomedical research problems.[53, 54] Diazeniumdiolates are usually prepared via exposing primary or secondary amine compounds to NO gas at an elevated pressure (i.e., 5 atm).[55] Diazeniumdiolates have a generic structure of $R_1R_2NN(O)=NOR_3$ (Figure 1.5), with rich structural diversity allowing for the design of different derivative groups with various half-lives and NO release rates.

For example, depending on the identity of the R_3 groups, diazeniumdiolates can be divided into two categories: zwitterionic (or intramolecular) and anionic (i.e., R_3 is Na^+).[56] Some zwitterionic salts have to undergo metabolism and/or hydrolysis to remove the covalent R_3 group to free the anion before spontaneously releasing NO. Therefore, by

choosing the proper R_3 groups that can be specifically cleaved by certain enzymes, a cell or organ selective NO releasing agent can be prepared.[57, 58] On the other hand, some anionic diazeniumdiolate salts have been widely employed as potent NO precursors to achieve the release of NO when exposed to aqueous media.[59] Figure 1.5 illustrates some examples of diazeniumdiolates and their half-lives (in pH 7.4 phosphate buffer at 37 ℃), as used in this dissertation work.

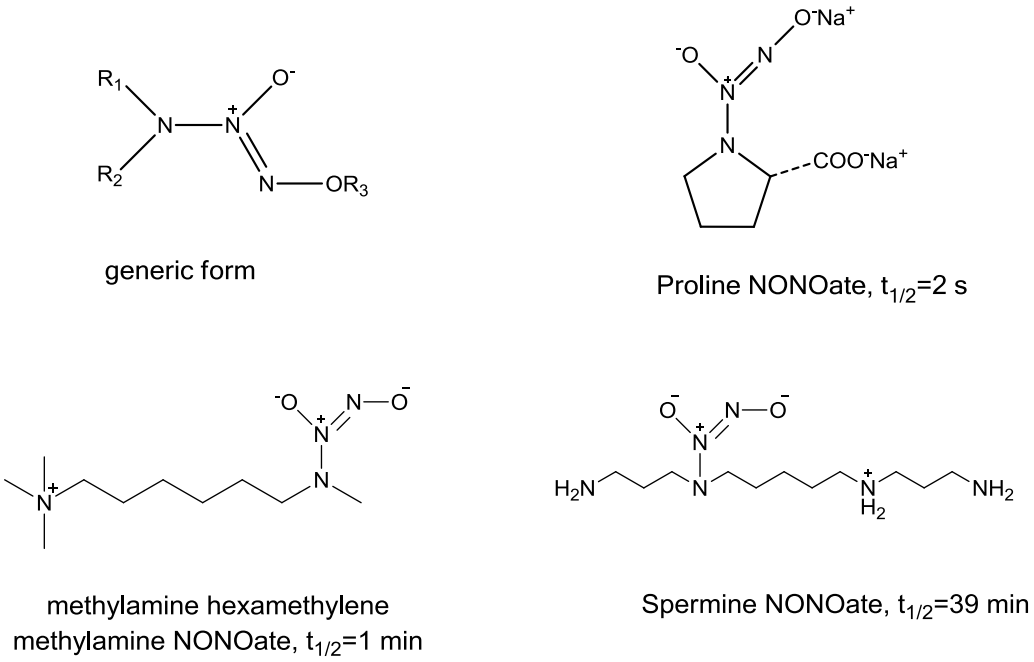

Figure 1.5. Structures and half-lives ($t_{1/2}$) in pH 7.4 phosphate buffer at 37˚C of some diazeniumdiolates.

The release of NO from diazeniumdiolates is proton and/or thermally driven. Therefore, exposure of these NO precursors to physiological conditions will stimulate NO release. Figure 1.6 depicts the NO releasing mechanism from anionic diazeniumdiolates.

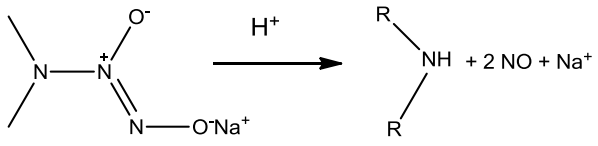

Figure 1.6. The proton driven NO releasing mechanism from anionic diazeniumdiolates.

In biology, the inorganic anion, nitrite, is generally viewed as the oxidative end-product of endogenous NO metabolism. However, recent studies from two independent groups have shown that nitrite can recycle *in vivo* to form NO through the protonation of nitrite in the stomach.[60, 61] These were the first two reports on NOS-independent NO formation. More importantly, they represent an alternative source of endogenous NO, especially under hypoxia conditions, when the classic oxygen-dependent NO generation from L-arginine/NO synthase may be dysfunctional. Nitric oxide levels in the stomach are in the range of 10-100 ppm, several orders of magnitude higher than required for vasodilation. At such high concentrations, the gastric NO is toxic to a wide range of microorganisms, and may function as a possible antibacterial agent. The researchers tested this hypothesis by exposing pathogenic Enterobacteriaceae *E. Coli* and *C. Albicans* to the combination of acids and nitrite, and found them to be destroyed.[61] A more recent study by Bjorne and co-workers investigated the antibacterial effect of human gastric juice mixed with saliva, with a high concentration of nitrite in saliva.[62] These studies have provided good indications that nitrite and NO play an important role in gastric host defense against swallowed pathogens.

When nitrite (p*K*a 3.4) is acidified, it produces nitrous acid (HNO_2, Eq. 1.5) first, which spontaneously decomposes to NO and nitrogen dioxide (NO_2). (Eq. 1.6 and 1.7)

$$H^+ + NO_2^- \leftrightarrow HNO_2 \quad (1.5)$$

$$2HNO_2 \rightarrow N_2O_3 + H_2O \quad (1.6)$$

$$N_2O_3 \rightarrow NO + NO_2 \quad (1.7)$$

Scheme 1.2. NO release mechanism from nitrite acidification.

1.4 Anti-Thrombotic and Anti-Bacterial Medical Devices with NO Release

As mentioned above, nitric oxide is a potent anti-thrombotic and anti-bacterial agent that functions widely in the cardiovascular and immune systems at various concentrations (ppb to ppm levels). Therefore, synthetic polymer materials that can mimic the nature of endothelial cells (EC) to release localized NO at equal or greater fluxes to that of the EC will enable the preparation of potentially thrombus resistant and bactericidal surfaces. By immobilizing NO delivery coatings onto clinically relevant blood-contacting and implantable medical devices (i.e., vascular grafts, intravascular catheters and sensors, extracorporeal blood-loop, oxygenators etc.), the risk of thrombus formation and inflammation/infection can be reduced, and ultimately the *in vivo* performance and life-time of such devices can be improved.

1.4.1 Current Methods of Continuous Nitric Oxide Release

Indeed, over the past two decades, there have been considerable research efforts on the design of polymeric materials with NO releasing/generating properties, mainly based on incorporating NO precursors into a variety of polymers including poly(vinyl chloride) (PVC), polyurethane (PU), silicone rubber (SR), and polymethacrylate (PM).

The amount of local NO flux and the release rates can be modulated by changing the chemical structure of NO precursors and/or polymer backbones. To effectively modify these polymer matrices with NO releasing/generation function, two different approaches have been pursued: (1) incorporation of discrete NO precursor (i.e., diazeniumdiolate and RSNO) species into films of the hydrophobic polymers; or (2) covalently tethering of NO release agents onto the backbone of the given polymer.

In 1996, the Smith and Keefer group reported the first diazeniumdiolate based NO releasing polymers using both of the two above mentioned methods.[63] Diethylamine NONOate and spermine NONOate were blended into poly(ethylene glycol) (PEG) and poly(caprolactone) (PCL) matrices and the resulting polymers retained the active NO releasing surface over 5 to 7 weeks of storage as a solid under ambient conditions. By incorporating diazeniumdiolates into hydrophobic polymer solids of low hydrogen ion activity, the rate of NO release was slowed down. Later, Mowery[64] and Schoenfisch[65] blended zwitterionic diazeniumdiolated dimethylhexane diamine (DMHD/NONOate) into different polymer matrices to achieve continuous NO release for 10-72 h when incubated at 37℃ in PBS. By dip coating the surface of an implantable oxygen catheter with a diazeniumdiolated doped silicone rubber, superior analytical accuracy and significantly reduced thrombus formation was observed on the coated catheter surface as compared to the control catheter without the NO release coating. Zhou et al.[66] synthesized water-soluble diazeniumdiolated poly(ethylenimine) (PEI) for its potential use as an NO release agent within the dialysate fluid in hemodialysis systems. By tuning the specific structure of the polymer and the use of exogenous additives (i.e., sodium salt of poly(acrylic acid) to accelerate NO releasing rate of high molecular weight PEI

NONOate), the polymers were able to provide steady and well controlled physiological levels of NO flux (0.5×10^{-10} mol cm^{-2} min^{-1}) through the fiber of dialysis devices.

In addition to diazeniumdiolated NO releasing materials, RSNOs have also been employed as an active precursor to generate localized NO from hydrophobic polymer materials. The labile nitroso bond of RSNO molecules can be decomposed and release NO via various pathways, including pH, light, heat, and catalytic metal ions.[67] Copper ion (Cu (II)/Cu (I)) is one of the most widely utilized catalytic reagents,[68, 69] in the presence of a reducing agent such as thiols. A slow reduction of Cu (II) by the thiols to form Cu (I) (Eq. 1.8) can further reduce RSNO into RS^- and NO free radicals, with the regeneration of thiolate and Cu (II) (Eq. 1.9) at the same time, yielding a catalytic cycle. Therefore, only a trace amount of copper ion is needed to release NO from RSNOs.[69]

$$RS^- + Cu^{2+} \rightarrow \frac{1}{2}RSSR + Cu^+ \qquad (1.8)$$

$$R'SNO + Cu^+ \rightarrow R'S^- + NO + Cu^{2+} \qquad (1.9)$$

Scheme 1.3. Copper (I/II) ion mediated catalytic NO generation from RSNO species.

Our laboratory has previously investigated the feasibility of both doping hydrophobic PVC polymers with lipophilic copper complexes[70] as well as covalently linking a Cu (I/II)-cyclen complex into a polymethacrylate matrix for the *in situ* generation of nitric oxide from endogenous RSNOs in blood.[71] The potential advantage of employing catalytic polymeric materials *in vivo* is that the NO generated from local

endogenous RSNO species are likely to be sustained, provided the subject maintains a constant RSNO supply (assumed to be μM levels) by blood circulation.

Besides metal ions, certain enzymes have also been reported to be able to decompose RSNOs to NO. One example is glutathione peroxidase (GPx), a peroxidase found in erythrocytes of mammals that reduce lipid hydroperoxides to their corresponding alcohols, and therefore help prevent lipid peroxidation of the cell membrane. The crystal structure of GPx shows the enzyme contains 4 subunits, each with a selenocysteine residue in a depression on the surface. Studies have shown that GPx can activate GSNO to liberate NO in the presence of H_2O_2.[72] Further studies suggested that diselenides along with free thiols can also catalyze the decomposition of RSNO into NO in a stepwise manner.[73] The initial activation is assumed to involve the interchange reaction of the diselenide and the thiol (Eq. 1.10). The selenolate generated from first step further reacts with RSNO to release NO (Eq. 1.11 and Eq. 1.12). The first three reactions represent the stepwise catalytic cycle with the presence of thiol, R'SH, as the reducing agent and diselenide being a catalyst. Equation 1.13 occurs even without the presence of reducing agent, but in a very slow process.[74]

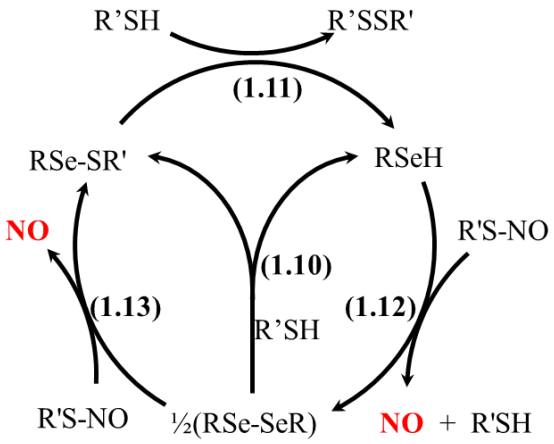

$$RSe - SeR + R'SH \leftrightarrow RSe - SR' + RSe^{-} + H^{+} \qquad (1.10)$$

$$RSe - SR + R'SH \leftrightarrow R'S - SR' + RSe^{-} + H^{+} \qquad (1.11)$$

$$R'S - NO + RSe^{-} + H^{+} \leftrightarrow \frac{1}{2}RS - SR + R'SH + NO \qquad (1.12)$$

$$2R'S - NO + RSe - SeR \leftrightarrow 2RSe - SR' + 2NO \qquad (1.13)$$

Scheme 1.4. Organoselenium species mediated catalytic NO generation from RSNO.

Cha and Meyerhoff reported the first NO generating polymer matrix (i.e., cellulose filter paper and polyethylenimine) with immobilized organoselenium species to mimic GPx and observed the catalytic decomposition of endogenous RSNO into NO with the corresponding free thiol.[74] Later, Yang and co-workers[75] assembled a universal NO generating surface via the Layer-by-Layer coating of sodium alginate and organoselenium modified polyethyleneimine on polymeric substrates. A stable and constant NO flux (1×10^{-10} mol cm^{-2} min $^{-1}$) was generated from a quartz slide coated with $(SePEI/Alg)_{10}$ even after prolonged contact with sheep whole blood (24 h at 4℃). More recently, Cai et al.[76] synthesized an aromatic carboxyl-ebselen based polyethylenimine

film that was assembled via the Layer-by-Layer technique onto quartz slide and polyurethane catheters. The catalytic film was able to continuously generate physiological levels of NO from RSNO after blood soaking, suggesting the potential application as an anti-thrombotic and anti-bacterial coating for medical devices. However, one potential obstacle of employing the catalytic NO generating system in clinical applications is the various concentrations of RSNO species available in the blood stream for each individual subject, as the actual endogenous blood RSNO levels (including *S*-nitrosoglutathione, *S*-nitrosocysteine, and *S*-nitrosoalbumin) are still debatable.[77, 78]

1.4.2 Current Methods to Modulate Nitric Oxide Release

There is an increasing interest in the development of new NO releasing materials capable of liberating NO at a predictable rate. Indeed, rapid and precise spatial and temporal control of localized NO release will allow fundamental studies to define useful NO fluxes required to achieve specific therapeutic effects. However, to the best of our knowledge, most reported studies employed continuous modes to release or generate NO. For example, the release of NO is initiated once a diazeniumdiolated polymer is exposed to aqueous media, and the NO releasing flux can only be roughly tuned by switching to different polymer materials or using different structures of NO donors. This usually involves complex synthesis work to ultimately formulate the ideal polymer-precursor compositions. Further, the life time of a diazeniumdiolate based NO releasing system is also greatly limited by the initial reservoir of NO precursors. Moreover, since the endogenous concentration of RSNOs varies, this is an issue for the long term NO

generating system. Therefore, more work is needed in order to maintain truly long term active NO releasing/generating polymers.

Previous research in the Meyerhoff lab has incorporated synthetic RSNOs into a polymer matrix through covalent linkage and it was shown that controlled fluxes of NO can be emitted from the polymers by exposure to light through a homolytic cleavage of the S-N bond.[79] More specifically, the photo-switchable NO releasing material was prepared with synthetic RSNO (*S*-nitroso-N-acetyl-DL-penicillamine) modified fumed silica particles that were further doped into silicone rubber films. Notably, the specific amount of NO flux can be controlled by the intensity of light. The on/off light trigger is environmentally friendly, readily available and easily manipulated, providing an elegant tool to deliver NO into biological sites on demand.

Recently, our group has also utilized electrochemical techniques in thin films of polymeric materials to create and modulate the release of NO at physiologically relevant levels based on the reduction of nitrite ions at the surface of copper electrodes.[80] Hofler and colleagues created a novel catheter configuration filled with a concentrated and buffered sodium nitrite precursor (pH 6.8), along with a copper working electrode and a Ag/AgCl reference electrode inserted in the catheter lumen. The control of the potential applied to the Cu electrode can "turn on" and "turn off" the release of NO through the walls of the 1 mm diameter catheter tubing. A cathodic pulse at at -0.7 V (*vs.* NHE) to refresh the Cu^o surface, followed by another positive potential step at +0.2 V (*vs.* NHE) to produce Cu^+ that can react with nitrite to release NO (Eq. 1.14).

$$Cu^+ + NO_2^- + 2H^+ \rightarrow Cu^{2+} + NO + H_2O \qquad (1.14)$$

In theory, an ca. 150 μm thick layer of nitrite solution on a copper mesh or copper wire is enough to produce a physiologically relevant 1×10^{-10} mol cm^{-2} min^{-1} NO flux continuously for 100 days in a planar or cylindrical arrangement. The catheter was tested over a week in a biofilm dispersion study and showed that the electromodulated catheter that releases NO had 97% less viable *E. coli* on its surfaces. At the same time, a 98% decrease was observed in the number of *A. baumannii* cells, in the presence of low NO flux (0.6×10^{-10} mol cm^{-2} min^{-1}) from the catheter surface.

Active and modulated release of NO from polymer surfaces used to prepare indwelling catheters can be extremely valuable in extending the longevity of catheter placement with a given supply of NO precursors. The ability to switch on/off the NO release may help to yield extended lifetimes since it is not necessary to have a continuous flux of NO to kill biofilm forming microbes.

1.4.3 Nitric Oxide Detection via Chemiluminescence

The analytical evaluation of nitric oxide release from devices/materials is quite challenging due to NO being a free radical, with unique physical and chemical properties, such as rapid diffusion, high reactivity, short half-life, and a broad range of local concentrations (picomolar to micromolar) in physiological milieus.[81] Despite these difficulties, a variety of analytical approaches have been employed for the detection of NO. These methods include chemiluminescence,[82] absorbance[83] and fluorescence-based spectroscopic techniques,[84] electron paramagnetic resonance (EPR),[85] and electrochemistry.[86]

An ozone-based chemiluminescence method is by far the gold standard for the detection of NO released from materials due to its reliability, accuracy and sensitivity.[87] The released NO gas is continuously purged with nitrogen gas and is carried with a sweep nitrogen gas into an reaction chamber. Here, NO then undergoes a rapid oxidation reaction in the gas phase with ozone and yields nitrogen dioxide (NO_2*) in an excited state. As the excited electron returns to its ground state, a photon is emitted and is detected as chemiluminescence. The emitted light is detected and amplified by a photomultiplier tube (PMT) (Figure 1.7). Such a method can detect NO at concentration as low as 0.5 ppb, with a dynamic range up to ~500 ppm.[81]

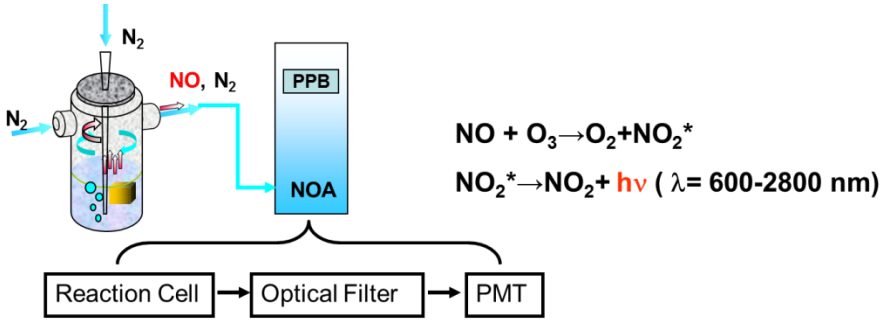

Figure 1.7. Schematic representation of the chemiluminescence NO measurement setup.

1.5 Statement of Research

In this dissertation, the design of enzyme-based non/minimally invasive electrochemical tear glucose sensors coupled with a glass micro-capillary fluid collection configuration is proposed as a potential supplementary tool for routine point-of-care glycemic management. In addition, this thesis work has focused on developing a new electrochemically modulated approach to deliver NO to a given site at physiological levels from NO precursor species residing in silicone rubber catheter tubing.

Chapter 2 introduces two simple needle-type enzyme electrode devices (amperometric and coulometric) to selectively detect tear glucose in anesthetized rabbits with insulin administration to achieve a wide range of blood glucose values (2-20 mM). A positive correlation between glucose levels in tear fluids and blood was found using this animal model. However, the slope of correlation varies from animal to animal. This suggests that the ratio between blood and tear glucose varies significantly from animal to animal. Therefore, to ultimately use tear fluid as an alternate sample to evaluate blood glucose for human subjects, the approach will likely require a pre-calibration step to obtain the exact ratio between blood and tears for each individual. Once this correlation is established for a given eye, the proper algorithm can be employed for the reported tear glucose results in order to reflect a corresponding value of blood glucose. Eventually, a disposable single use strip-type sensor that is similar to the commercial blood glucometer strip sensor will probably be the desired configuration for point-of-care tear glucose measurements.

Chapter 3 reexamines previous literature on NO being the reported common product generated from the direct electrochemical reduction of various RSNOs at physiological pH. However, headspace gas analysis using infrared absorption spectroscopy suggests that RSNO species are electrochemically reduced to nitrous oxide (N_2O) at pH 7.4, and can only be converted back to NO by switching to a more oxidizing applied voltage. Interestingly, at pH 4.0, a proton coupled one-electron reduction of RSNOs appears to take place and generates quantitative NO release at a gold working electrode at a cathodic potential of -0.8 V (v.s. Ag/AgCl). Based on preliminary results obtained, it seems possible to use a reservoir of RSNOs at this lower pH to create biomedical devices (e.g., intravascular catheters) in which electrochemically modulated release of NO can be achieved to prevent clotting and infection.

Chapter 4 describes a novel method that utilizes proton driven NO release from inorganic nitrite salts and diazeniumdiolated species to electrochemically modulate the NO flux from biomedical catheters. This was achieved by lowering the local pH by generating protons from water oxidation in a thin layer in close proximity to an anode surface. Silicone rubber catheters filled with such NO precursor solutions, as well as a simple two-electrode (working and reference electrodes) could release physiological levels ($0.5\text{-}4.0 \times 10^{-10}$ mol cm^{-2} min^{-1}) of NO by voltammetric control for up to 8 h.

Chapter 5 summarizes the findings and conclusions of this dissertation work and provides an outlook for future directions. Improvements of the tear glucose sensor configuration that would require less than 1 μL tear fluid for future human tests are discussed. Future long term experiments and biological studies on the anti-thrombotic

and anti-bacterial applications for the electrochemical modulated NO releasing catheters are also discussed.

1.6 References

1. L.C. Clark and C. Lyons, *Ann. N.Y. Acad. Sci.*, **1962**, *102*, 29-45.

2. H.F. Osswald, R. Asper, W. Dimai, and W. Simon, *Clin. Chem.*, **1979**, *25*, 39-43.

3. L.C. Clark, R. Wolf, D. Granger, and Z. Taylor, *J. App. Physiol.*, **1953**, *6*, 189-193.

4. W. Yantasee, Y. Lin, K. Hongsirikarn, G.E. Fryxell, R. Addleman, and C. Timchalk, *Environ. Health Perspect.*, **2007**, *115*, 1683-1690.

5. H.B. Yildiz and L. Toppare, *Biosens. Bioelectron.*, **2006**, *21*, 2306-2310.

6. J. Baur, C. Gondran, M. Holzinger, E. Defrancq, H. Perrot, and S. Cosnier, *Anal. Chem.*, **2009**, *82*, 1066-1072.

7. *http://www.who.int/mediacentre/factsheets/fs312/en/index.html*.

8. M. Muggeo, *Diabetic Medicine*, **1998**, *15*, S60-S62.

9. Y. Zhao, W. Ye, K.S. Boye, J.H. Holcombe, and R. Swindle, *Diabetic Medicine*, **2009**, *26*, 61-69.

10. C.L. Gay, F. Chapuis, N. Bendelac, F. Tixier, S. Treppoz, and M. Nicolino, *Diabetes & Metabolism*, **2006**, *32*, 159-165.

11. S. Greene, *Medicine*, **2002**, *30*, 60-65.

12. A. Sämann, C. Fischbacher, K.U. Jagemann, K. Danzer, J. Schüler, L. Papenkordt, and U.A. Müller, *Exp Clin Endocrinol Diabetes*, **2000**, *108*, 406-413.

13. D. Abookasis and J.J. Workman, *J. Biomed. Opt.*, **2011**, *16*, 027001-027009.

14. N. Dingari, I. Barman, G. Singh, J. Kang, R. Dasari, and M. Feld, *Analytical and Bioanalytical Chemistry*, **2011**, *400*, 2871-2880.

15. R. Ballerstadt, C. Evans, A. Gowda, and R. McNichols, *Diabetes Technol. Ther.*, **2006**, *8*, 296-311.

16. R. Weiss, Y. Yegorchikov, A. Shusterman, and I. Raz, *Diabetes Technol. Ther.*, **2007**, *9*, 68-74.

17. J.H. Holtz, J.S.W. Holtz, C.H. Munro, and S.A. Asher, *Anal. Chem.*, **1998**, *70*, 780-791.

18. S. Woderer, N. Henninger, C.-D. Garthe, H.M. Kloetzer, M. Hajnsek, U. Kamecke, N. Gretz, B. Kraenzlin, and J. Pill, *Analytica Chimica Acta*, **2007**, *581*, 7-12.

19. E. Cengiz and W.V. Tamborlane, *Diabetes Technol. Ther.*, **2009**, *11*, S-11-S-16.

20. M. Yamaguchi, M. Mitsumori, and Y. Kano, *IEEE Eng. Med. Biol. Mag.*, **1998**, *17*, 59-63.

21. J. Lu, R.F. Bu, Z.L. Sun, Q.S. Lu, H. Jin, Y. Wang, S.H. Wang, L. Li, Z.L. Xie, and B.Q. Yang, *Diabetes Research and Clinical Practice*, **2011**, *93*, 179-186.

22. C. Radhakumary and K. Sreenivasan, *Anal. Chem.*, **2011**, *83*, 2829-2833.

23. J.G. Lewis, *British Medical Journal*, **1957**, *1*, 585.

24. S.Y. Rhee, S. Chon, G. Koh, J.R. Paeng, S. Oh, J.-t. Woo, S.W. Kim, J.-W. Kim, and Y.S. Kim, *J Korean Med Sci*, **2007**, *22*, 70-73.

25. B. Wilhelm, S. Forst, M.M. Weber, M. Larbig, A. Pfützner, and T. Forst, *Diabetes Technol. Ther.*, **2006**, *8*, 146-155.

26. S. Iwata, *International Ophthalmology Clinics*, **1973**, *13*, 29-46.

27. Y. Ohashi, M. Dogru, and K. Tsubota, *Clinica Chimica Acta*, **2006**, *369*, 17-28.

28. J.D. Lane, D.M. Krumholz, R.A. Sack, and C. Morris, *Current Eye Research*, **2006**, *31*, 895-901.

29. D. Michail and N. Zolog, *C. R. Soc. Biol., Paris,* **1937**, *126*, 1042.

30. C.K.M. Choy, I.F.F. Benzie, and P. Cho, *Invest. Ophthalmol. Vis. Sci.*, **2000**, *41*, 3293-3298.

31. R. Chen, Z. Jin, and L.A. Colon, *J. Cap. Elec.*, **1996**, *3*, 243-248.

32. J. LeBlanc, C. Haas, G. Vicente, and L. Colon, *Intensive Care Medicine*, **2005**, *31*, 1442-1445.

33. D.K. Sen and G.S. Sarin, *Br. J. Ophthalomol.*, **1980**, *64*, 693-695.

34. J.T. LaBelle, D.K. Bishop, S.R. Vossler, D.R. Patel, and C.B. Cook, *J. Diabetes Sci. Technol.*, **2010**, *4*, 307-311.

35. M.X. Chu, T. Shirai, D. Takahashi, T. Arakawa, H. Kudo, K. Sano, S. Sawada, K. Yano, Y. Iwasaki, K. Akiyoshi, M. Mochizuki, and K. Mitsubayashi, *Biomed. Microdevices*, **2011**, *13*, 603-611.

36. J.T. Baca, C.R. Taormina, E. Feingold, D.N. Finegold, J.J. Grabowski, and S.A. Asher, *Clin. Chem.*, **2007**, *53*, 1370-1372.

37. J.T. Baca, D.N. Finegold, and S.A. Asher, *The Ocular Surface*, **2007**, *5*, 280-293.

38. W.F. March, A. Mueller, and P. Herbrechtsmeier, *Diabetes Technol. Ther.*, **2004**, *6*, 782-789.

39. V.L. Alexeev, S. Das, D.N. Finegold, and S.A. Asher, *Clin. Chem.*, **2004**, *50*, 2353-2360.

40. M.M.W. Muscatello, L.E. Stunja, and S.A. Asher, *Anal. Chem.*, **2009**, *81*, 4978-4986.

41. H. Yao, A.J. Shum, M. Cowan, I. Lähdesmäki, and B.A. Parviz, *Biosens. Bioelectron.*, **2011**, *26*, 3290-3296.

42. L.J. Ignarro, G.M. Bugga, K.S. Wood, R.E. Byrns, and G. Chaudhuri, *Proc. Natl. Acad. Sci. U.S.A.*, **1987**, *84*, 9265-9269.

43. E. Culotta and D.E.K. Jr., *Science*, **1992**, *258*, 1862-1865.

44. M. Feelisch and J. Stamler, *Methods in Nitric Oxide Research*. 1996: John Wiley & Sons.

45. H. Al-Sa'Doni and A. Ferro, *Clinical Science*, **2000**, *98*, 507-520.

46. N. Hogg, *Free Radi. Biol. Med.*, **2000**, *28*, 1478-1486.

47. D. Giustarini, A. Milzani, R. Colombo, I. Dalle-Donne, and R. Rossi, *Clin. Chim. Acta*, **2003**, *330*, 85-98.

48. J.H. Crawford, b.K. Chacko, H.M. Pruitt, B. Piknova, N. Hogg, and R.P. Patel, *Blood*, **2004**, *104*, 1375-1382.

49. S.J. Kuhl and H. Rosen, *West J. Med.*, **1998**, *168*, 176-181.

50. S. Shiva, X. Wang, L.A. Ringwood, X. Xu, S. Yuditskaya, V. Annavajjhala, H. Miyajima, N. Hogg, A.L. Harris, and M.T. Gladwin, *Nat. Chem. Biol.*, **2006**, *2*, 486-493.

51. R.S. Drago, R.O. Ragsdale, and D.P. Eyman, *J. Am. Chem. Soc.*, **1961**, *83*, 4337-4339.

52. R.S. Drago and F.E. Paulik, *J. Am. Chem. Soc.*, **1960**, *82*, 96-98.

53. J.E. Saavedra, G.J. Southan, K.M. Davies, A. Lundell, C. Markou, S.R. Hanson, C. Adrie, W.E. Hurford, W.M. Zapol, and L.K. Keefer, *J. Med. Chem.*, **1996**, *39*, 4361-4365.

54. D.J. Waterhouse, J.E. Saavedra, K.M. Davies, M.L. Citro, X. Xu, D.A. Powell, G.J. Grimes, G.K. Potti, and L.K. Keefer, *J. Pharm. Sci.*, **2006**, *95*, 108-115.

55. J.A. Hrabie, J.R. Klose, D.A. Wink, and L.K. Keefer, *J. Org. Chem.*, **1993**, *58*, 1472-1476.

56. M.M. Reynolds, M.C. Frost, and M.E. Meyerhoff, *Free Radi. Biol. Med.*, **2004**, *37*, 926-936.

57. J.E. Saavedra, P.J. Shami, L.Y. Wang, K.M. Davies, M.N. Booth, M.L. Citro, and L.K. Keefer, *J. Med. Chem.*, **1999**, *43*, 261-269.

58. A.E. Maciag, H. Chakrapani, J.E. Saavedra, N.L. Morris, R.J. Holland, K.M. Kosak, P.J. Shami, L.M. Anderson, and L.K. Keefer, *J. Pharmacol. Exp. Ther.*, **2011**, *336*, 313-320.

59. K.M. Davies, D.A. Wink, J.E. Saavedra, and L.K. Keefer, *J. Am. Chem. Soc.*, **2001**, *123*, 5473-5481.

60. J.O. Lundberg, E. Weitzberg, J.M. Lundberg, and K. Alving, *Gut*, **1994**, *35*, 1543-1546.

61. N. Benjamin, F. O'Driscoll, H. Dougall, C. Duncan, L. Smith, and M. Golden, *Nature* **1994**, *368*, 502.

62. H. Björne, E. Weitzberg, and J.O. Lundberg, *Free Radi. Biol. Med.*, **2006**, *41*, 1404-1412.

63. D.J. Smith, D. Chakravarthy, S. Pulfer, M.L. Simmons, J.A. Hrabie, M.L. Citro, J.E. Saavedra, K.M. Davies, T.C. Hutsell, D.L. Mooradian, S.R. Hanson, and L.K. Keefer, *J. Med. Chem.*, **1996**, *39*, 1148-1156.

64. K.A. Mowery, M. H. Schoenfisch, J.E. Saavedra, L.K. Keefer, and M.E. Meyerhoff, *Biomaterials*, **2000**, *21*, 9-21.

65. M.H. Schoenfisch, K.A. Mowery, M.V. Rader, N. Baliga, J.A. Wahr, and M.E. Meyerhoff, *Anal. Chem.*, **2000**, *72*, 1119-1126.

66. Z. Zhou, G.M. Annich, Y. Wu, and M.E. Meyerhoff, *Biomacromolecules*, **2006**, *7*, 2565-2574.

67. D.L.H. Williams, *Acc. Chem. Res.*, **1999**, *32*, 869-876.

68. S.C. Askew, D.J. Barnett, J. McAninly, and D.L.H. Williams, *J. Chem. Soc., PERKIN TRANS 2*, **1995**, *1995*, 741-745.

69. A.P. Dicks, H.R. Swift, D.L.H. Williams, A.R. Butler, H.H. Al-Sa'doni, and B.G. Cox, *J. Chem. Soc., PERKIN TRANS 2*, **1996**, *1996*, 481-488.

70. B.K. Oh and M.E. Meyerhoff, *J. Am. Chem. Soc.*, **2003**, *125*, 9552-9553.

71. S. Hwang, W. Cha, and M.E. Meyerhoff, *Angew. Chem. Int. Ed.*, **2006**, *45*, 2745-2748.

72. J.E. Freedman, B. Frei, G.N. Welch, and J. Loscalzo, *J. Clin. Invest.*, **1995**, *96*, 394-400.

73. Y. Hou, Z. Guo, J. Li, and P.G. Wang, *Biochem. Biophys. Res. Comm.*, **1996**, *228*, 88-93.

74. C. Wansik and M.E. Meyerhoff, *Biomaterials*, **2007**, *28*, 19-27.

75. J. Yang, J.L. Welby, and M.E. Meyerhoff, *Langmuir*, **2008**, *24*, 10265-10272.

76. W. Cai, J. Wu, C. Xi, A.J. Ashe Iii, and M.E. Meyerhoff, *Biomaterials*, **2011**, *32*, 7774-7784.

77. Y. Wu, F. Zhang, Y. Wang, M. Krishnamoorthy, P. Roy-Chaudhury, B.E. Bleske, and M.E. Meyerhoff, *Clin. Chem.*, **2008**, *54*, 916-918.

78. Y. Wu, W. Cha, F. Zhang, and M.E. Meyerhoff, *Clin. Chem.*, **2009**, *55*, 1038-1040.

79. M. Frost and M.E. Meyerhoff, *J. Am. Chem. Soc.*, **2004**, *126*, 1348-1349.

80. L. Hofler, D. Koley, J. Wu, C. Xi, and M.E. Meyerhoff, *RSC Advances*, **2012**, *2*, 6765-6767.

81. E.M. Hetrick and M.H. Schoenfisch, *Annu. Rev. Anal. Chem.*, **2009**, *2*, 409-433.

82. J.N. Bates, *Neuroprotocols*, **1992**, *1*, 141-149.

83. E.M. Boon and M.A. Marletta, *J. Am. Chem. Soc.*, **2006**, *128*, 10022-10023.

84. A. Gomes, E. Fernandes, and J.F.C. Lima, *J. Fluoresc.*, **2006**, *16*, 119-139.

85. P. Kuppusamy, R.A. Shankar, V.M. Roubaud, and J.L. Zweier, *Magn. Reson. Med.*, **2001**, *45*, 700-707.

86. Y. Lee, B.K. Oh, and M.E. Meyerhoff, *Anal. Chem.*, **2004**, *76*, 536-544.

87. A. Gow, A. Doctor, J. Mannick, and B. Gaston, *J. Chromat. B*, **2007**, *851*, 140-151.

CHAPTER 2

EVALUATION OF ENZYME-BASED TEAR GLUCOSE ELECTROCHEMICAL SENSORS OVER A WIDE RANGE OF BLOOD GLUCOSE CONCENTRATIONS

2.1 Introduction

As discussed in Chapter 1, non-invasive glucose monitoring systems have an unmet need in modern medicine for tight glycemic management of diabetes. Among the accessible fluids for minimal invasive and/or non-invasive glucose measurement, miniature tear glucose sensor devices may provide an attractive supplement to conventional blood glucometer measurements, provided that the tear glucose concentrations can be shown to correlate with blood glucose concentrations over a wide range of glucose concentrations.

Tear fluid that bathes the eye is maintained at a miniscule and relatively stable volume (~4 μL). It is continuously replenished by the lacrimal gland and other accessory glands at a rate of production in the range of 0.5-2.2 μL/min.[1] A thin film of tear fluid (~8 μm thick) keeps the cornea and conjunctiva continuously moist, without any stimulation.

Previous research efforts on measuring tear glucose concentrations have reported varying lacrimal glucose levels (7-600 μM),[2, 3] and whether a close correlation between blood glucose and tear glucose concentrations exists is still debatable. This is mainly due to the different measurement methodologies and tear fluid sampling methods employed.

Indeed, the exact tear collection method is of importance for lacrimal glucose measurement.[4] An increased tear production from physical or chemical stimulation will secrete more aqueous tear volume and, therefore, falsely lower the glucose levels (via dilution). In addition, decreased tear elimination caused by dysfunction of the tear drainage system (lacrimal puncta) will also lead to accumulation of aqueous tear volume and consequently, lower tear glucose concentrations. On the other hand, loss of the lipid layer from physical or chemical perturbation will result in increased tear osmolarity and decrease the basal tear volumes.[5] Therefore, careful design of the device used for collecting tear fluid from the meniscus of the lower eye lid without irritating the eye is essential for accurate tear glucose measurements. To date, the major sampling tools applied include filter paper strips,[6] glass capillary tubes,[7] plastic capillary tubes,[8] and a contact lens.[9, 10]

Surprisingly, even though the conventional hand-held glucometers are primarily based on the electrochemical/enzymatic detection of glucose in tiny volumes of whole blood, to date there are very few reports on applying electrochemical devices for tear glucose measurements. Our group has previously proposed a small amperometric sensor for tear glucose measurement in 5 μL tear fluids and found a very positive correlation between tear and blood glucose levels using 12 anesthetized rabbits over a period of 8 h.[11] However, it is known that anesthesia will elevate blood glucose levels.[12] Therefore,

the correlation could only be validated in the high blood glucose concentrations range in all tested animals.

Herein, we employ a similar needle-type enzyme-based amperometric sensor as well as a newer coulometric enzyme electrode configuration for the detection of tear glucose within a micro glass capillary tube requiring only 3 μL of tear fluid. The sensors were applied to detect tear glucose concentrations in anesthetized rabbits, but now with insulin administration to achieve a much broader range of blood glucose values (2-20 mM). Using the miniature electrochemical devices, good correlations in glucose levels between the two types of samples is observed, suggesting that tear glucose measurement may provide an attractive supplementary method to current blood glucose self-monitoring devices.

2.2. **Materials and Methods**

2.2.1 Materials

Glucose oxidase (Type VII, from *Aspergillus niger*), D-(+)-glucose, glutaraldehyde, bovine serum albumin, sodium chloride, sodium phosphate dibasic, potassium hydroxide, potassium chloride, potassium phosphate monobascic, L-ascorbic acid, uric acid (sodium salt), acetaminophen, 1,3-diaminobenzene, resorcinol, and Nafion (5 wt% solution in a lower aliphatic alcohols/H_2O mix) were purchased from Sigma-Aldrich (St. Louis, MO) and used without further purification. Platinum/iridium and silver wires with Teflon® coatings were obtained from A-M Systems (Sequim, WA).

Heat shrinkable tubing was product of Advanced Polymers (Salem, NH). Micro glass capillary tubes were obtained from Drummond (Broomall, PA).

2.2.2 Fabrication of Tear Glucose Sensors

The sensing devices are based on immobilizing glucose oxidase on a Pt/Ir wire and anodically detecting the liberated hydrogen peroxide from the enzymatic reaction (Figure 2.1). Inner selective layers of Nafion® and an electropolymerized film of 1,3-diaminobenzene/resorcinol greatly enhance the selectivity for glucose over known electroactive interferents, including ascorbate, urate and acetaminophen.[13] The amperometric sensor was fabricated from the Teflon® coated Pt/Ir (wt%, 95:5) with 1 mm active cavity of the exposed Pt wire providing a total working area of 0.40 mm^2. At the same time, a coulometric sensor configuration was designed similarly except that a larger surface area on the Pt/Ir working electrode was exposed and covered with active layers (including enzyme) so that substantial consumption of glucose can take place during measurements within the capillary tubes. Indeed, for the coulometric device, 10 mm of the Pt/Ir (of 80 mm total) wire with an area of 4.0 mm^2 was exposed to the sample as the working electrode. The Ag/AgCl reference/auxiliary electrode was prepared by dipping an 8 cm bare Ag (from a 16 cm Teflon coated Ag wire) into a 0.2 M $FeCl_3$ in 1 M HCl solution. Ten layers of glucose oxidase (5% in Bovine Serum Albumin) crossed-linked with another 5 layers of glutaraldehyde (2.5% in PBS) was alternately dip coated onto the coulometric Pt electrode surface. With these sensor configurations, 3 μL of calibrating solution or tear fluid is required and collected into marked micro capillary tubes (0.58 mm i.d.), and the sensor is then inserted.

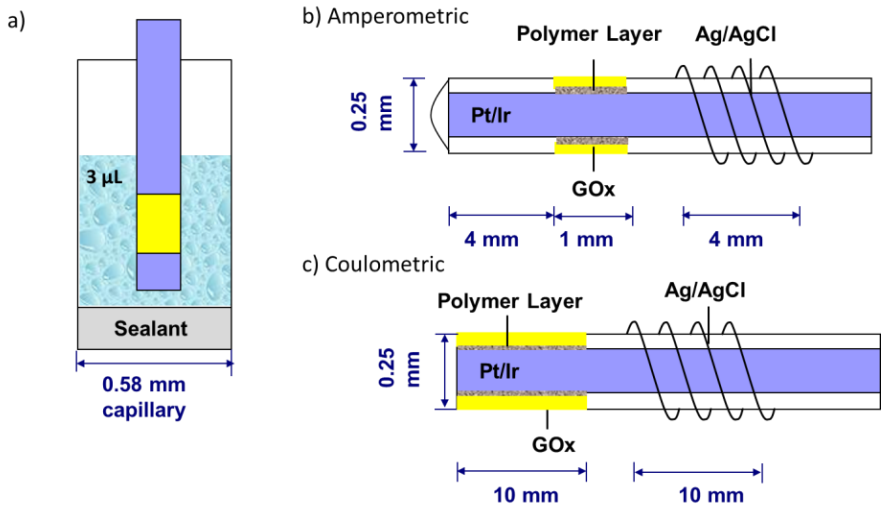

Figure 2.1. a) Schematic representation of the tear glucose detection in a glass capillary. b) Configuration of the amperometric sensor. c) Configuration of the coulometric sensor.

2.2.3 Calibration of Tear Glucose Sensors

The amperometric and coulometric sensors were calibrated using a four-channel BioStat potentiostat (ESA Biosciences Inc., Chelmsford, MA). After fabrication, the sensor was polarized at +0.6 V (*vs.* Ag/AgCl) in pH 7.4 phosphate buffered saline (PBS) for 3 h to reach a steady baseline. Three µL of glucose standard solution of varying concentrations (5-800 µM) were collected with a 0.58 mm i.d. microliter glass capillary tube (World Precision Instruments, Sarasota, FL) by capillary action. The bottom tip of the capillary was then sealed with a Critoseal wax (McCormick Scientific, Richmond, FL). It should be noted that the volume of test solution does not need to be precisely controlled in the amperometric measurement, but it has to be an exact 3 µL volume of solution for the coulometric test. The sensors were then carefully inserted into the capillary from the top opening without destroying the enzyme layer, especially for the amperometric sensor. For amperometric sensor, after the oxidation current was acquired for 5 min, a steady state current was recorded, and the sensor was removed from the glass

capillary and rinsed with deionized water for the next measurement of a higher concentration of glucose solution. A calibration curve was generated by plotting the recorded currents *vs.* the glucose concentrations. Generally, a linear regression fit is observed for the amperometric design. For the coulometric sensor, the oxidation current was also recorded and timed for 5 min after the sensor was exposed to the glucose solution (or tear fluid) within the capillary. Then the total electric charge passed through the working (Pt) and reference (Ag/AgCl) electrode in contact with the glucose solution was calculated by integrating the area under the *i*-t (current-time) response curve. In addition, the selectivity of sensor was examined in solutions of interfering species at their highest possible concentrations (i.e., 100 μM ascorbic acid, 100 μM uric acid, and 10 μM acetaminophen in PBS) in tear fluid. The % error that would occur in samples containing these levels of interferences was calculated by dividing the reported current from each interfering species by that observed from a 100 μM of glucose standard solution.

2.2.4 Rabbit Study Protocol

A total of 17 white rabbits (Myrtle's Rabbitry, Thompson's Station, TN) were used in this study to test the correlation of glucose levels between tear and blood samples over a wide range of blood glucose concentrations. A modified animal anesthesia protocol was applied based on previously reported studies[11] with the additional use of insulin. Further, in order to collect fresh tear fluids for each measurement, the rabbit was rested at a prone position so that any freshly produced tear fluid was guided from the lacrimal canal into the tear sac and nasal passage. Human insulin (Sigma, St. Louis, MO) was prepared by dissolving 1.45 mg into 10 mL 0.001 N HCl, then further diluted to 100

mL with saline, to make a 0.4 U/mL solution. One bolus of insulin (0.4 U/mL in saline, 0.4 mL) was given 1 h after anesthesia commenced, and additional boluses were employed as needed in order to reduce blood glucose levels to less than 5 mM in each rabbit. Every 30 min, 0.5 mL blood was drawn from the rabbit's carotid artery and the glucose concentration was measured by a Radiometer whole blood analyzer (Radiometer America Inc., Westlake, OH). At the same time, 3 μL of rabbit tear fluid was collected into the glass capillary and the current from the given type of glucose sensor placed into the tear fluid was recorded using the Biostat potentiostat. In each rabbit experiment, 12 pairs of blood glucose and tear glucose concentration data points were recorded for 7 h. Similarly as in the prior calibration step, for the amperometric sensors, the steady-state current value was recorded 5 min after the sensor was inserted into the capillary tube containing the tear fluid. For the coulometric sensor, the current over 5 min was integrated to provide the total charge, and this value was used to calibrate and also determine the concentration of glucose in the tear samples. The sensors were calibrated one day prior to the rabbit study and then re-calibrated in capillary tubes with standard glucose solution (200 μM in PBS) at the end of the 7 h experiment, and this calibration point was used to back calculate the rabbit tear glucose levels. Statistical data analysis was carried out to examine the correlation between the blood and tear glucose values within a given animal.

2.3. Results and Discussion

2.3.1 Analytical Performance of Amperometric Sensor

The amperometric sensor is based on a previous subcutaneous implantable glucose sensor design,[14] except that the outer polymer coating which restricts the glucose diffusion in high glucose concentrations for blood sample measurement was removed. Here, in order to achieve the low detection limit required for tear measurements, the enzymatic layer is in direct contact with glucose molecules in tear fluid. Typical response and calibration curves of the amperometric device are presented in Figure 2.2. The sensor exhibits a fast response to reach the steady-state current over a wide range of glucose concentrations (5-800 μM, Figure 2.2a), with an average sensitivity of 0.10 ± 0.01 nA/μM of glucose (n=3). It is capable of achieving a detection limit of 0.62 ± 0.03 μM (S/N=3, n=3), which provides the ability to detect very low levels of lacrimal glucose in tear samples. In addition, to reliably detect glucose concentrations in the tear fluid sample at a potential of +0.6 V (*vs.* Ag/AgCl), the sensor must exhibit good selectivity over electroactive species that can be present in tear fluid, such as ascorbic and uric acids, which will be oxidized and induce error in the detected glucose levels. Indeed, the concentration of ascorbic acid and uric acid in tear fluid are reported to be ~20 μM and 70 μM, respectively.[13] Therefore, we tested the amperometric response of the sensor towards 100 μM of uric acid and 100 μM of ascorbic acid, and 10 μM of acetaminophen as a small neutral interfering species (20 times lower than in blood, assuming a similar tear-blood dilution ratio as glucose). Due to the presence of underlying Nafion® layer and the electropolymerized layer of 1,3-diaminobenzene/resorcinol, the amperometric sensor exhibited excellent selectivity over these potentially interfering species, with the

error percentages of 2.1%, 5.8%, and 2.5% for ascorbic acid, uric acid, and acetaminophen, respectively. This provides a good indication that the amperometric devices can selectively respond to glucose without significant interference from these antioxidant species present in tear fluid.

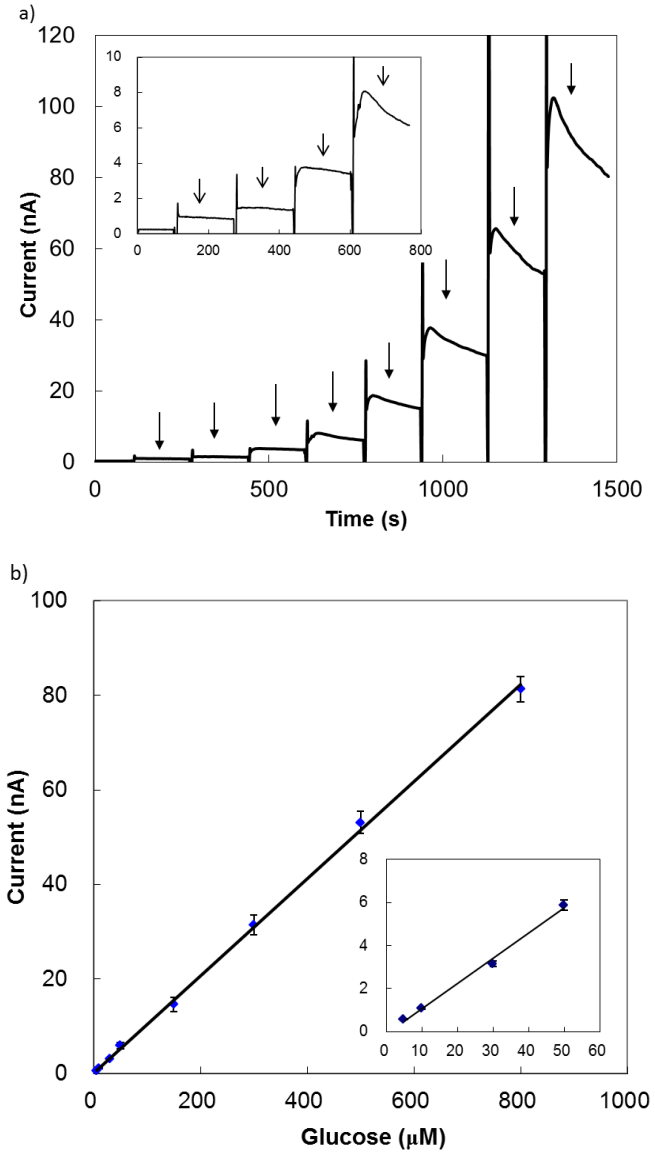

Figure 2.2. Calibration of tear glucose sensor using 3 μL solution in capillary. (a) Solutions in the order of 5 μM, 10 μM, 30 μM, 50 μM, 150 μM, 300 μM, 500μM, 800μM glucose. Inset: Interferents and low-end (5-50 μM) glucose response (note: the sensor is rinsed with water and soaked briefly in PBS buffer between each placement in capillary tube containing the test interferent or standard.) (b) Resulting calibration curve of tear glucose sensor. Inset: Low-end glucose calibration (5-50 μM). Error bars represent s.d. of n=3 replicate measurements of each standard within capillary tubes.

2.3.2 Analytical Performance of Coulometric Sensor

The coulometric glucose sensor design was developed in order to detect very low levels of glucose in tear fluid that may arise from the new insulin protocol that was implemented in this study. The coulometry approach provides a more convenient analytical method for future applications, potentially without the need for calibration, as well as enhanced sensitivity. Compared to the amperometric glucose sensor, there are two major differences in the new coulometric sensor design. The larger exposed enzymatic area on the Pt/Ir working electrode (4.0 mm^2) and the dip-coated enzyme layer of the coulometric sensors improve the efficiency for collection of peroxide produced from glucose. Indeed, this design employs a thinner enzyme layer and, therefore, it enhances the diffusion of glucose and peroxide to the electrode surface. Overall, the larger surface area of the sensor increases the surface to volume ratio, which greatly increases the rate of consumption of the glucose in the entire 3 μL sample within the capillary.

For small volume tear glucose testing, it is important to complete a glucose measurement in a reasonably short time period (1-5 min). A useful way of reducing response time is to accelerate the overall kinetics of the enzymatic reaction and diffusion by increasing temperature. Figure 2.3 shows representative response curves of the coulometric sensor at normal room temperature of 25^0C and at an elevated temperature of 50^0C. Indeed, a much faster coulometric current decay at the higher temperature suggests glucose in the sample solutions are consumed and depleted in a shorter time than at room temperature.

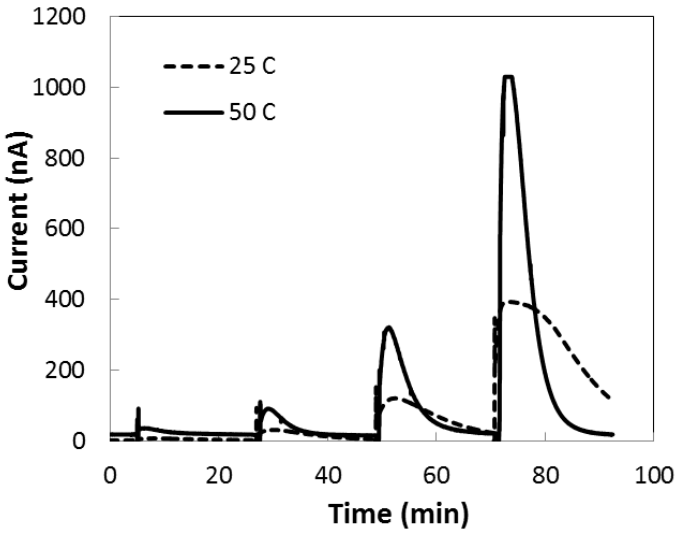

Figure 2.3. Response of coulometric tear glucose sensor using 3 μL solutions in capillary at RT (dotted line, 25^0C) and elevated temperature (solid line, 50 ^{0} C), solutions in the order of 10 μM, 50 μM, 200 μM, 800 μM glucose.

Further, by using the same electrode but acquiring and integrating data over different time periods, it is possible to compare the percentage of sample consumption over time (Figure 2.4). As shown, at 50^0C, 100% of glucose was depleted at the end of each 20 min measurement at various concentrations, and 71.5% of glucose was consumed within 5 min data acquisition time, while 52.7% of sample was depleted within a 3 min interval. Therefore, during the sensor calibration and real sample measurements, the temperature was raised to 50^0C and the total charge was acquired over a 5 min measurement period. Faster depletion rates of glucose should be possible with further increase in the surface area to volume ratio of the coulometric sensor/capillary configuration.

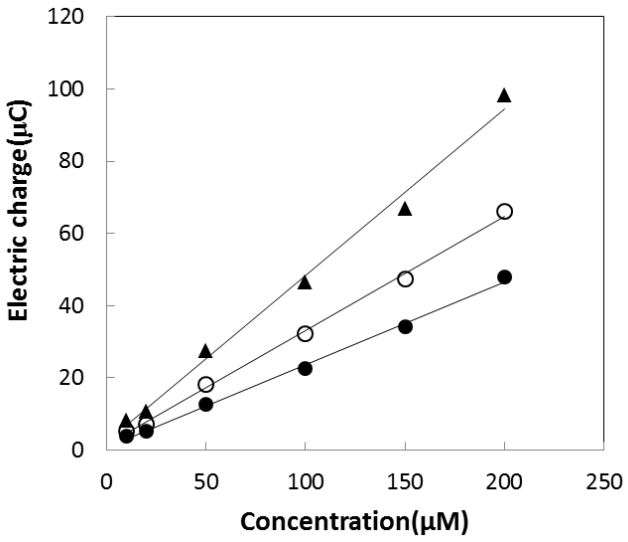

Figure 2.4. Calibration of coulometric tear glucose sensor using 3 μL solutions in capillary at elevated temperature (50 ^{0} C), with different data acquisition time periods: 3 min (solid circle), 5 min (hollow circle), 20 min (triangle).

The typical calibration curve for the coulometric tear glucose sensor in capillary tubes under this optimal higher temperature and shorter measurement time conditions (5 min) is shown in Figure 2.5. The sensor is capable of achieving a wide dynamic range (10-800 μM) and a very low detection limit of 0.38±0.13 μM (S/N=3, n=3) for the coulometric design. The coulometric sensor was then employed in rabbit studies along with the amperometric sensor to monitor tear fluid glucose levels. The measured tear glucose concentrations were compared with the results obtained with the amperometric sensors in order to examine whether the two methods provide similar correlations between tear and blood glucose values.

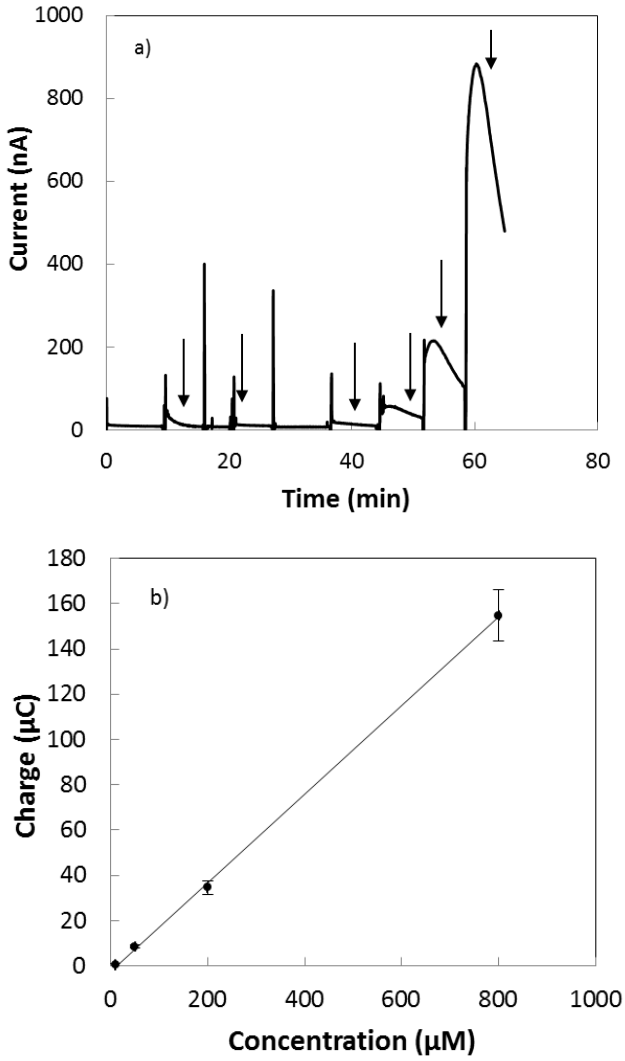

Figure 2.5. Calibration of coulometric tear glucose sensor using 3 µL solutions in capillary. (a) Solutions in the order of 100 µM ascorbic acid, 10 µM acetaminophen, 10 µM, 50 µM, 200 µM, 800 µM glucose. (note: the sensor was rinsed with water and soaked briefly in PBS buffer between each placement in capillary tube containing the test interferent or standard.) (b) Resulting calibration curve of tear glucose sensor. Error bars represent s.d. of n=3 replicate measurements of each standard within capillary tubes.

2.3.3 In Vitro Performance of Tear Glucose Sensor

Our group has previously reported data regarding a tear glucose detection system based on a needle-type amperometric electrode coupled with a glass micro-capillary configuration.[11] Such a miniature sensor is able to be inserted into a micro-capillary that holds microliter volumes of tear samples. In this earlier work, within 5 min, 5 µL of

rabbit tear fluid was carefully pulled into the capillary tube from the meniscus of the lower eyelids without inflicting any damage to the eye. The results showed a significant correlation between tear and blood glucose levels at the higher end range (7 mM -18 mM) in an anesthetized rabbit model, with variable correlation ratios for each individual animal.

It is known that anesthesia will cause an increase of blood glucose concentrations[12] by initially elevating blood glucose levels that continuously taper over an 8 h test period to levels that are slightly higher than normal (7-8 mM). For the present study, with a newly modified animal protocol, insulin was administrated into the rabbit's jugular vein to lower the elevated blood glucose levels 1 h after anesthesia was initiated. The use of insulin in the new animal model enabled us to examine whether a similar correlation exists between tear glucose and blood glucose cocentrations in this animal model at more normal and even hypoglycemic blood glucose levels. Figure 2.6 shows results from a pilot experiment with continuous infusion of insulin (4 U/mL in saline) into the rabbit ear vein for 75 min. The blood glucose dropped from an initial value of 10.4 mM (187.2 mg/dL) to 7.6 mM (136.8 mg/dL) in 30 min, and then gradually decreased to 0.6 mM (10.8 mg/dL) at the end of the 7 h experiment. Two separate coulometric sensors (Figure 2.6 a and b) were employed to measure glucose levels in rabbit's tear fluid. Both sensors were able to detect the very low corresponding glucose levels in tear fluid, which shared the same decreasing trend as the blood glucose, indicating that blood and tear glucose levels do indeed change in tandem over this wide concentration range. A linear least-square regression was obtained for the measured glucose levels in tears and blood samples for this pilot experiment. A strong Pearson's

correlation was observed with a determined r^2=0.9309 and 0.8302 (p<<0.05) for two separate coulometric sensors, as shown in Figure 2.6.

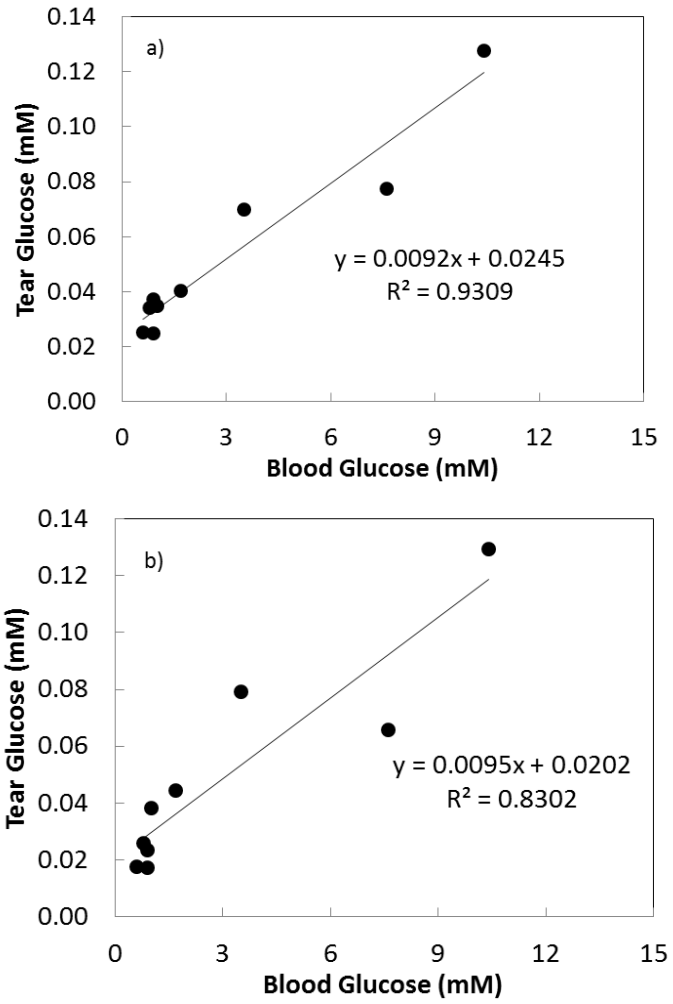

Figure 2.6. Tear and blood glucose level correlation results from one rabbit measured by two separate coulometric sensors a) and b) under a modified wide blood glucose range protocol.

However, since it is difficult for the animal to survive the surgery at the extreme hypoglycemic levels (< 3 mM) for a long time period, the initial insulin protocol was modified to provide an insulin bolus into the rabbit vein instead of the continuous infusion. The concentration of insulin was also decreased to one-tenth of the original

value, to 0.4 U/mL. In this way, the blood glucose drops from initial values in the range of 12-18 mM (216-324 mg/dL) to the range of 5-9 mM (90-162 mg/dL) in 30 min, and then gradually decrease to 2-3 mM (36-54 mg/dL) at the end of a 7 h experiment. A representative result from one rabbit using this optimal protocol is shown in Figure 2.7.

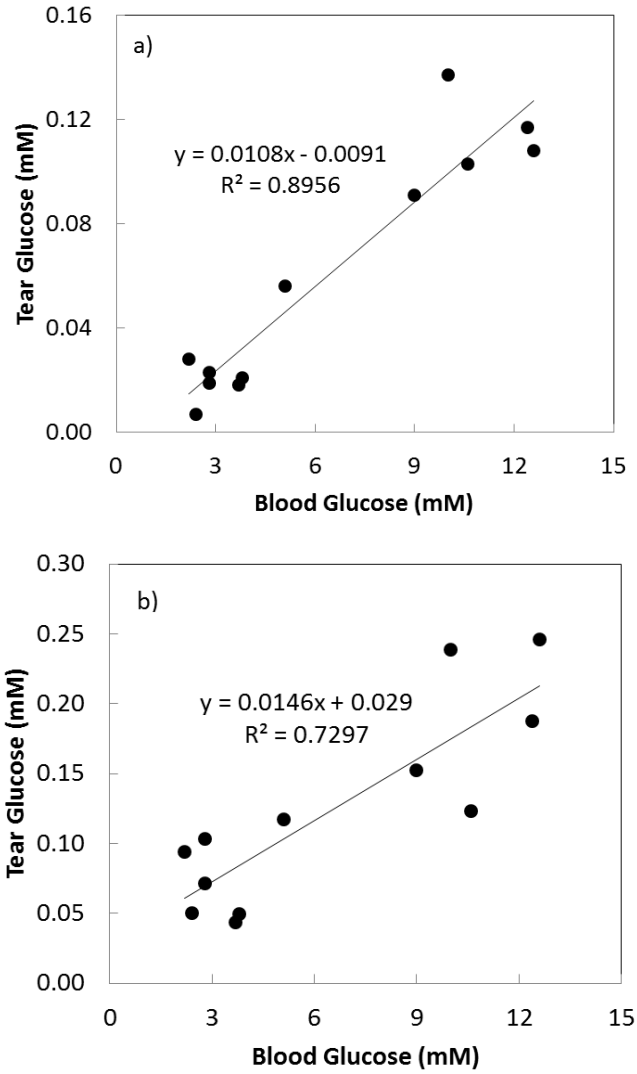

Figure 2.7. Tear and blood glucose level correlation results from one rabbit measured by (a) amperometric and (b) coulometric sensors under the optimized wide blood glucose range protocol. (Note: amperometric sensor used to detect glucose in left eye and the coulometric sensor used for right eye measurements.)

The rabbit was first left under anesthesia without insulin so as to collect samples at high glucose levels for 1 h. Then, one injection (0.4 mL) of the insulin solution was administrated, and the blood glucose dropped from 9.0 mM to 5.1 mM within 30 min, followed by the lowest point at 2.2 mM after 90 min. The Pearson's correlation analysis reveals a significant relationship between tear and blood glucose concentrations (r^2=0.8956, p<<0.05) and a linear regression shows a good fit of the data. In addition to the strong correlation across a wide glucose concentration range, the tear glucose levels (50-150 μM) measured by both amperometric and coulometric sensors at the normal blood glucose range (5-8 mM) are consistent with the most recent reports in the literature.[15] Separate correlation ratios are still observed in the modified animal protocol for different rabbit subjects, indicating the likely necessity of pre-calibrating the tear-blood ratio for each individual in potential real-world applications.

It is also important to note that tear glucose concentration from the left and right eye of the same rabbit subject (even with the same amperometric or coulometric sensors used) was quite different mainly due to different rates of tear production in each eye during the 7 h of anesthesia. This difference in tear glucose levels in each eye of the animals was frequently observed in these studies, despite the fact that rabbit was rested in a prone position to facilitate the tear drainage as much as possible. Indeed, visually it was easy to observe that several rabbits still preserved more tear fluid in one eye than the other. In Figure 2.8, tear fluid collected from left and right eyes of the same rabbit individual and measured with two coulometric sensors (of similar selectivity and sensitivity) showed different glucose levels during a 7 h anesthetized experiment.

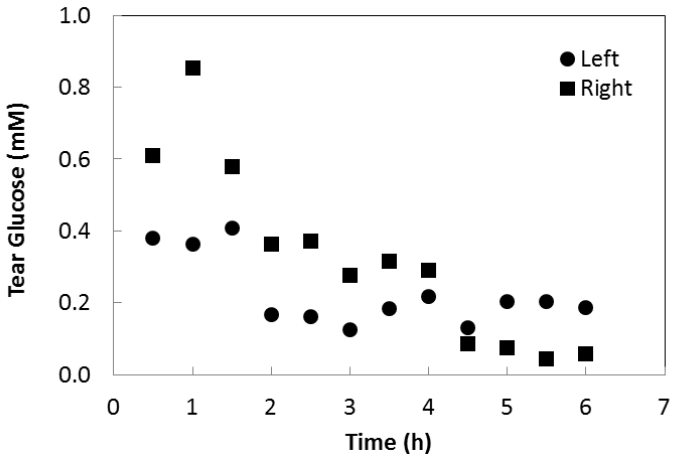

Figure 2.8. Tear and blood glucose level correlation results from one rabbit sampled from left eye (dot) and right eye (square) using coulometric sensors under the optimized wide blood glucose range protocol.

2.3.4 Correlation of Tear and Blood Glucose from Rabbit Model

The correlation between tear and glucose concentration has been investigated in a previous study using the amperometric sensor design.[11] Figures 2.9 and 2.10 show tear and blood glucose data from 6 rabbits under the optimal protocol used in this study for both the amperometric and coulometric sensor measurements. Though the measured tear glucose levels and blood glucose concentrations for individual rabbits clearly correlated (Figure 2.6 and 2.7), the total data set is widely dispersed (Figure 2.9a and 2.10a). This is mainly due to the individual difference (rabbit weight, initial glucose concentration, tear production rates in different eyes, etc.) from rabbit to rabbit, and thus the overall trend between tear and blood glucose level is undermined and could hardly be observed. Moreover, with the administration of insulin, each rabbit responded differently in time to the insulin to lower the blood glucose concentrations. Indeed, the exact number of boluses of insulin required to reach a normal or hypoglycemic levels of blood glucose

varied from animal to animal. Therefore, simply taking the average of all glucose concentrations for 6 rabbits at each measuring time point (30 min) to obtain a general trend is not applicable here.

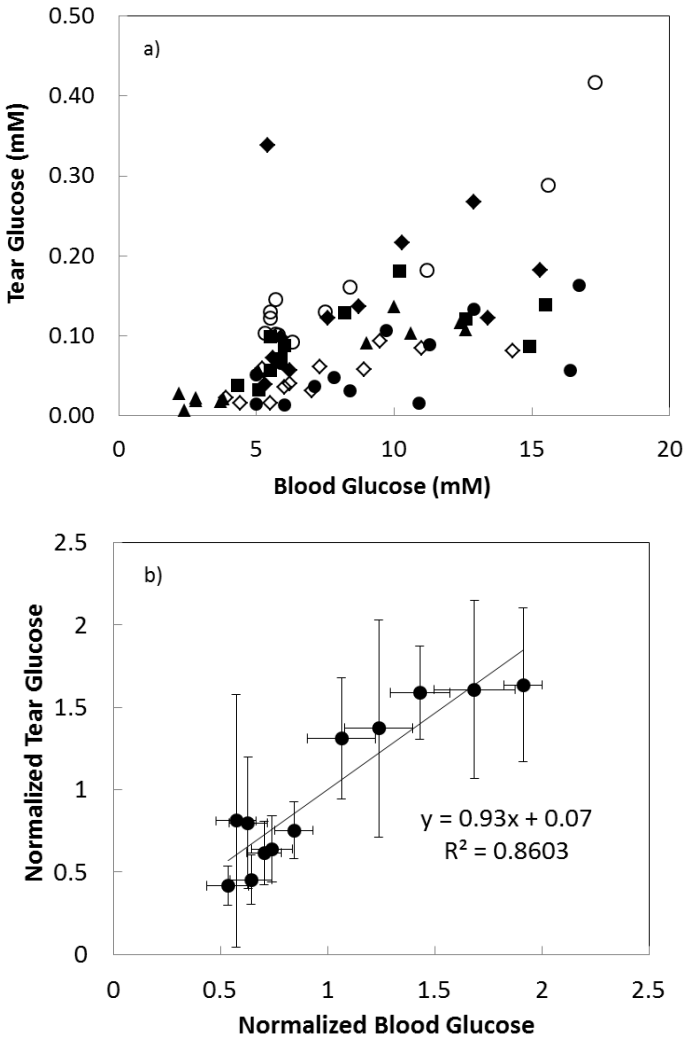

Figure 2.9. Amperometric results of correlation between tear and blood glucose levels using a rabbit model: a) All the data points of tear and blood glucose values of the total 6 rabbits. (b) The average values of both tear and blood glucose levels for all animals in study at every half hour time point fitted to least-squares linear regression.

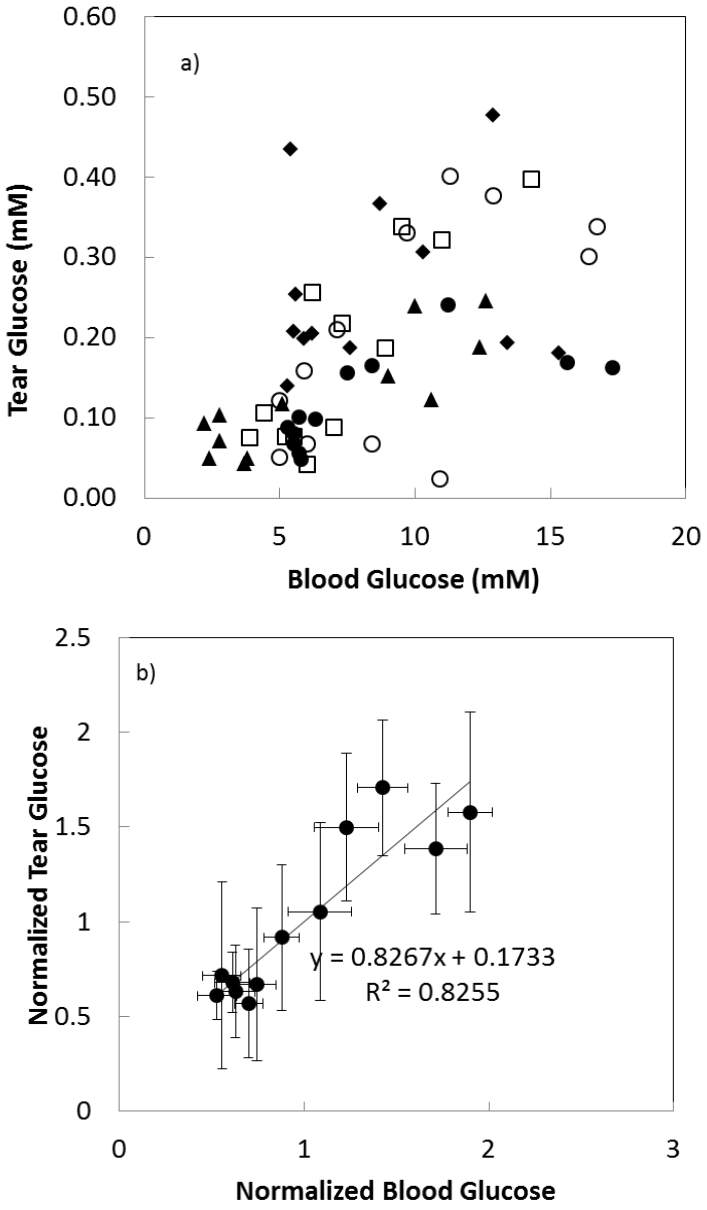

Figure 2.10. Coulometric results of correlation between tear and blood glucose levels using a rabbit model: a) All the data points of tear and blood glucose values of the total 6 rabbits. (b) The average values of both tear and blood glucose levels for all animals in study at every half hour time point fitted to a least-squares linear regression.

In order to draw a clearer conclusion of the global tear-blood glucose correlation, a simple normalization model can be used. For each data point (tear or blood glucose concentration) of sample i (i=1, 2, 3, …12) in experiment j (j=1, 2, 3,…6), we normalized

the concentration by dividing by the mean glucose levels (over the entire 7 h experiment) for each animal ($x'_{ij} = \frac{x_{ij}}{\frac{1}{n}\sum_i x_{ij}}$), a standard score method with minimum effect on data.[16] For a $x'_{ij} < 1$, it simply means that the measured glucose level is lower than the mean values of the rabbits, and a $x'_{ij} > 1$ indicates a higher than the mean glucose concentration.

Further, for each rabbit, the tear glucose concentrations were first paired with the corresponding blood glucose values that were measured at the same time point. Then the blood glucose concentrations were sorted and listed horizontally in Figures 2.9b and 2.10b. The *x* value of each data point is the average concentrations of blood glucose of 6 rabbits ($\overline{x_i} = \frac{1}{n}\sum_j x'_{ij}, j = 1,2,3 \ldots 6$). Similarly, the average tear glucose concentration of 6 rabbits crossing different experiments is presented as the *y* value data point. Error bars represent one standard deviation for 6 rabbits at the given glucose concentrations. Therefore, these error bars depict the individual glucose concentration variations for different animals, rather than representing the precision of the measurement itself.

For the normalized data shown in Figures 2.9b and 2.10b, the final linear regression models reveal a significant correlation between tear and blood glucose concentrations with the determined R square values ($r^2 = 0.8603$, $p \ll 0.05$ for amperometric sensor, and r^2=0.8255, $p \ll 0.05$ for coulometric sensor), indicating a reasonable linear relationship between measured tear and blood glucose levels. Clearly, it can be concluded that the tear glucose concentration does change in tandem with the blood glucose concentration, and the shared trend shows a good fitting to a simple linear regression model. However, separate correlation ratios are still observed in the modified

animal protocol for different rabbit subjects, indicating the necessity to ultimately pre-calibrate the tear-blood correlation for each individual in potential real-world applications.

2.3.5 Clarke Error Grid Analysis

Further, the gold standard Clarke error grid analysis[17, 18] can also be applied to evaluate the clinical accuracy of predicting blood glucose levels from electrochemical tear glucose measurements. First, the blood glucose values are calculated from the tear glucose concentrations that were sampled at the same time point based on the individual tear-blood correlation ratio (i.e., the slope from the tear-blood glucose concentration plot). The values were converted to mg/dl from mM in order to be plotted using the typical Clarke error grid analysis. These blood glucose values are plotted as the predicted blood concentrations on the y-axis, and the actual plasma glucose values that are measured directly by a Radiometer whole blood analyzer are plotted as the reference concentrations on the x-axis. In Figure 3.11a, the blood glucose concentrations predicted from the amperometric tear glucose measurements are plotted along with the reference values, and 91.7% of the results fall into the clinically acceptable zones A and B, strongly suggesting that the amperometric tear glucose measurement can provide a supplementary tool to monitor blood glucose levels with good clinical accuracy. For the coulometric sensor, results plotted via the Clarke error grid analysis method indicate that 84.3% of the predicted blood glucose values fall within zones A and B (Figure 3.11b.). Since the coulometric sensors utilized here were not fully optimized to consume all glucose in the tear test samples during the 5 min measurement period, it is likely that the lower % of

values in zones A and B *vs.* the amperometric sensor system, may reflect some variations in the kinetics of glucose consumption between different µL volumes of tear samples, relative to the consumption kinetics observed in the µL volumes of glucose calibration solutions.

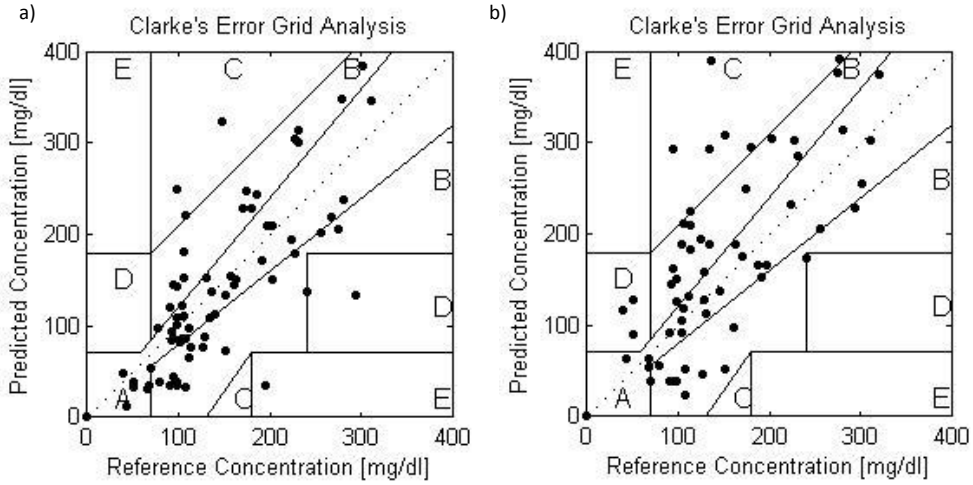

Figure 2.11. Clarke error grid analysis for evaluation of blood glucose values determined from the tear glucose concentrations measured by a) amperometric (Zone A= 48.61%, Zone B= 43.06%, Zone C= 4.17%, Zone D= 2.78%, Zone E= 1.39%) sensor and b) coulometric (Zone A=44.29%, Zone B= 40%, Zone C=10%, Zone D=5.71%) sensors in 6 rabbits.

2.4 Conclusions

We have developed simple electrochemical tear glucose biosensors based on amperometric or coulometric measurement methods coupled with a fluid collection glass micro-capillary configuration. These electrochemical sensors were employed in anesthetized rabbit experiments to detect tear glucose levels over a wide concentration range of blood glucose values. With the optimized administration of insulin, a clear correlation between tear and blood glucose levels was obtained over a wide range of glucose levels (from hypoglycemic to hyperglycemic); however, the degree of correlation

varies from animal to animal and the correlation ratio differs. This suggests that the ratio between blood and tear glucose varies significantly from animal to animal. Therefore, to use tear fluid as an alternate sample to evaluate blood glucose for human subjects, the approach will likely require a pre-calibration step to obtain the exact ratio between blood and tears glucose for each individual. Once this correlation is established for a given eye, the proper algorithm can be employed for the reported tear glucose results in order to reflect a corresponding value of blood glucose. With further improvements in its design, the new coulometric sensor, which measures the total charge resulting from total depletion of glucose from the sample tear volume, will likely enable more precise detection of glucose at much lower concentrations. This may not require any sensor pre-calibration, provided a reproducible and constant volume of tear fluid can be collected and that all the glucose present is consumed in the time course of the measurement. Efforts to utilize this new design with an even much smaller sample volume (< 1 μL) to measure the concentrations of glucose in human tear fluid is a future direction for this research (see Chapter 5).

2.5 References

1. Y. Ohashi, M. Dogru, and K. Tsubota, *Clinica Chimica Acta*, **2006**, *369*, 17-28.

2. D.K. Sen and G.S. Sarin, *Br. J. Ophthalomol.*, **1980**, *64*, 693.

3. J. LeBlanc, C. Haas, G. Vicente, and L. Colon, *Intens. Care Med.*, **2005**, *31*, 1442-1445.

4. J.T. Baca, D.N. Finegold, and S.A. Asher, *Ocul. Surf.*, **2007**, *5*, 280-293.

5. A. Tomlinson and S. Khanal, *The Ocular Surface*, **2005**, *3*, 81-95.

6. A. Romano and F. Rolant, *Metab. Pediatr. Syst. Ophthalmol.*, **1988**, *11*, 78-80.

7. J.D. Lane, D.M. Krumholz, R.A. Sack, and C. Morris, *Curr. Eye Res.*, **2006**, *31*, 895-901.

8. R. Chen, Z. Jin, and L.A. Colon, *J. Cap. Elec.*, **1996**, *3*, 243.

9. W.F. March, A. Mueller, and P. Herbrechtsmeier, *Diabetes Technol. Ther.*, **2004**, *6*, 782-789.

10. H. Yao, A.J. Shum, M. Cowan, I. Lähdesmäki, and B.A. Parviz, *Biosens. Bioelectron.*, **2011**, *26*, 3290-3296.

11. Q. Yan, B. Peng, G. Su, B.E. Cohan, T.C. Major, and M.E. Meyerhoff, *Anal. Chem.*, **2011**, *83*, 8341.

12. J.K. Saha, J. Xia, J.M. Gorndin, S.K. Engle, and J.A. Jakubowsku, *Exp. Biol. Med.*, **2005**, *230*, 777.

13. C.K.M. Choy, I.F.F. Benzie, and P. Cho, *Investigative Ophthalmology & Visual Science*, **2000**, *41*, 3293-3298.

14. Q. Yan, T.C. Major, R.H. Bartlett, and M.E. Meyerhoff, *Biosens. Bioelectron.*, **2011**, *26*, 4276.

15. M.X. Chu, T. Shirai, D. Takahashi, T. Arakawa, H. Kudo, K. Sano, S. Sawada, K. Yano, Y. Iwasaki, K. Akiyoshi, M. Mochizuki, and K. Mitsubayashi, *Biomed. Microdevices*, **2011**, *13*, 603-611.

16. Y. Dodge, ed. *The Oxford Dictionary of Statistical Terms*. 2006, Oxford University Press, USA; 6 edition (September 7, 2006).

17. W.L. Clarke, D. Cox, L.A. Gonderfrederick, W. Carter, and S.L. Pohl, *Diabetes Care*, **1987**, *10*, 622-628.

18. B.P. Kovatchev, L.A. Gonder-Frederick, D.J. Cox, and W.L. Clarke, *Diabetes Care*, **2004**, *27*, 1922-1928.

CHAPTER 3

RE-EXAMINATION OF THE DIRECT ELECTROCHEMICAL REDUCTION OF *S*-NITROSOTHIOLS

3. 1. Introduction

Nitrix oxide (NO), the elusive endothelial-derived relaxing factor (EDRF), is well recognized for playing critical roles in platelet inhibition, vasodilation, and wound healing.[1-3] However, NO does not exist to any significant degree in blood due to its rapid reaction with oxyhemoglobin to form methemoglobin and nitrate.[3] Therefore, the therapeutic delivery of localized NO on demand in biological system has been a very challenging task.

Previous research has demonstrated that physiological levels of NO ($0.5\text{-}4\times10^{-10}$ $mol\cdot cm^{-2}\cdot min^{-1}$) can be released from polymeric materials by incorporating NO donors (diazeniumdiolates or *S*-nitrosothiols) within the matrices.[4-7] The kinetics of NO release from such materials can be modulated by changing the polymer matrix or the structure of the NO donor. Other methods of preparing NO-releasing polymers consisting of small-molecule RSNOs donors, such as *S*-nitroso-N-acetyl-L-cysteine (SNAC) and *S*-nitrosoglutathione (GSNO), dispersed in hydrogels have been reported by the Oliveira[8] and Schoenfisch[9] groups. The NO delivery for these systems was accomplished by thermal, photochemical, or catalyst (copper ion, Cu^{+}) activation.

Our research interest focuses on employing a novel electrochemical method to modulate NO release from donors. This new design can provide a potential alternate method to realize quantitative NO release in a controlled manner. Indeed, it can be achieved by using either electrochemically active NO donor compounds (which can be electrochemically reduced or oxidized to give NO) or proton driven NO precursors (e.g., nitrite salts, diazeniumdiolates). In particular, *S*-nitrosothiols (RSNOs) are potent donors of NO and can release localized transient levels of NO under physiological conditions via various decomposition pathways (thermal, photolysis, catalytic metal ion reduction, etc.).[10] The S-NO group decomposes rapidly upon a one-electron reduction *in vivo*, and therefore provides a selective means to release NO from RSNOs in physiological systems. This reduction reaction can be catalyzed by Cu(I/II) or organoselenium species, such as proteins that contain Cu(I/II) centers or selenocysteine groups.[11]

Based on the known one-electron reduction chemical reactions that can liberate NO from RSNOs in solution, it was thought that electrochemical reduction of RSNOs could provide a potential alternate approach to realize quantitative NO release in a controlled manner. In fact, it has been reported previously that RSNOs can undergo a one-electron reduction and release NO on glassy carbon or hanging mercury drop electrodes at physiological pH.[12-14] Controlled potential electrolysis suggested that NO was released at cathodic potentials.[15] However, in these prior studies, the conclusion that NO was a product upon electrochemical reduction of RSNOs was based solely on cyclic voltammetry in which following reduction, sweeping to more positive working electrode potentials yielded an oxidation peak that corresponded to the potential where NO is typically oxidized. This previous research inspired us to consider a new method to create

NO releasing materials. By tuning the applied reduction potential via an electrode within a matrix with embedded RSNOs, a novel approach for creating voltage-triggered NO release materials could ultimately be developed. This type of control would allow fundamental studies to define necessary NO fluxes required to achieve specific therapeutic effects. Moreover, the use of a voltage trigger to initiate release provides a method of temporal control of the NO flux.

Toward this goal, preliminary studies were conducted to verify that both physiological (*S*-nitrosoglutathione (GSNO), *S*-nitrosocysteine (CysNO)) and synthetic RSNOs (*S*-nitroso-N-acetyl-DL-penicillamine (SNAP), *S*-nitroso-N-acetyl-L-cysteine (SNAC)) can be electrochemically reduced. However, during these studies, no evidence of NO gas production could be found at pH 7.4, indicating that NO is not necessarily the predominant reductive product, or a multiple-step electrochemical reaction, rather than a simple one-electron transfer, is involved in the electrolysis. All previous studies reported in the literature were carried out at pH 7.4, given that endogenous *S*-nitrosoglutathione would exist at this physiological pH. However, preliminary studies regarding the effect of pH on the electrochemical reductive pathway of RSNOs were also carried out in this thesis work at different pH 4.0 and 10, and it is reported here, for the first time, that pH is critically important to the electrochemical redution products formed from RSNO species. Indeed, to better understand the reaction and provide critical information to assess the potential application of using the electrochemistry of RSNOs in creating new electrochemical NO releasing devices, it is important to characterize the electrochemical decomposition path and sort out the actual reductive products. Hence, results from detailed solution and gas phase analysis via both electrochemical and spectroscopic

methods are presented in this chapter regarding the electrochemical reduction of *S*-nitrosothiols.

3.2. Materials and Methods

3.2.1 Materials

Glutathione (GSH), cysteine (Cys), N-acetyl-L-cysteine (NAC), *S*-nitroso-N-acetyl-DL- penicillamine (SNAP), ethylenediamine tetraacetic acid (EDTA), N-(1-naphthyl)ethylene diamine dihydrochloride (NED), sodium acetate, potassium phthalate obtained from Sigma-Aldrich (Milwaukee, WI) and sulfanilamide from Acros (Morris Plains, NJ) were used without further purification unless otherwise noted. A standard $NO_{(g)}$ stock solution was prepared from deoxygenated acidified nitrite solution. The generated gas was bubbled through 20% (wt%) NaOH solution to remove any interference nitrogen dioxide species and then collected in deoxygenated DI water for 30 min. Via use of a nitric oxide analyzer (NOA) (Seivers 280, Boulder, CO), the concentration of NO in a saturated solution was determined to be 1.9 mM at 25 °C and P_{NO}=1 atm. *S*-Nitrosoglutathione (GSNO), *S*-nitrosocysteine (CysNO), and *S*-nitroso-N-acetyl-L-cysteine (SNAC) were synthesized by nitrosating the sulfhydryl groups of the corresponding thiols (GSH, CySH, and NAC) in acidified nitrite solution, as reported in the literature.[16] The formation of the *S*-nitroso group was confirmed by a characteristic absorption at 335 nm via UV-Vis spectrophotometry. Phosphate buffered saline (PBS) and all other solutions were prepared with 18.2 $M\Omega \cdot cm^{-1}$ DI water from a Milli-Q system (Millipore Corp., Billerica, MA).

3.2.2 Electrochemical Reduction of RSNO

The RSNOs stock solutions (5 mM) were directly injected into a working buffer solution (PBS, 10 mM, pH 7.4) containing 0.1 mM EDTA (necessary to suppress metal ion impurities and prevent catalytic RSNO decomposition, especially from copper ions) to obtain the desired concentrations. All RSNO measurements were carried out in amber cells to avoid photolytic decay. A potentiostat (CHI 800B, Austin, TX) was used to examine the electrochemistry of RSNOs via cyclic voltammetry and chronoamperometry techniques. Preliminary cyclic voltammetry experiments of four different RSNOs (GSNO, CysNO, SNAC, SNAP) were tested on both polycrystalline gold and glassy carbon electrode surfaces (3 mm in diameter, CHI, Austin, TX) in 1 mM RSNO solutions prepared in deoxygenated PBS. GSNO was then selected as the model molecule for all other electrochemical reduction reactions studies due to its good stability (up to a few hours) and physiological abundance. Typically, a solution of 2 mM GSNO in stirred PBS was reduced at a potential of -0.8 V (vs. Ag/AgCl) on a Au mesh or glassy carbon electrode for 1 h, using a platinum coil behind a glass frit as the counter electrode. Before all electrochemical reactions, the cell was purged with either nitrogen or argon to prevent the oxidation of end products from any dissolved and headspace oxygen present.

3.2.3 Detection of NO

To assess whether NO is liberated during the electrochemical reduction of RSNOs, the reaction solution was constantly purged with $N_{2(g)}$ and the gas phase stream was monitored by a highly sensitive and selective chemiluminescence nitric oxide analyzer (NOA). An amber combination Echem-NOA cell (10 mL, Figure 3.1) was specially designed to conduct such combined electrochemical reduction and NO monitoring experiments.

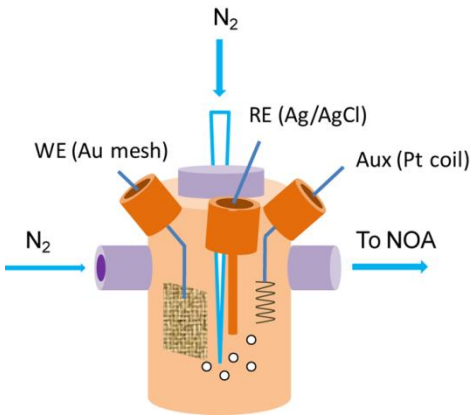

Figure 3.1. Schematic representation of the Echem-NOA cell set-up.

3.2.4 Detection of NO_2^-

The colorimetric Griess assay was conducted to measure nitrite (NO_2^-) produced from NO after RSNO reduction. A mixture of 15 mM sulfanilamide and 0.23 mM NED in 0.75 M HCl was prepared as the Griess reagent. Prior to sample measurement, the response of the Griess reagent towards a series of standard nitrite solutions was monitored by a UV-Vis spectrophotometer (Lambda 35, Perkin-Elmer, MA). The strong absorbance at a λ_{max} of 540 nm was plotted against NO_2^- concentrations to obtain the calibration curve. A 500 µL aliquot of the RSNO reduction solution was injected into a cuvette with 500 µL of Griess reagent and kept on the bench for 10 min to fully mix and react. The recorded absorbance at 540 nm was then fitted into the calibration curve to calculate the NO_2^- concentration.

3.2.5 Detection of Ammonia (NH_3)

Potentiometric measurement of ammonia was employed to evaluate whether NH_3 is one of the electrochemical reduction products of RSNOs. A high performance NH_3

gas sensor (Thermo Scientific, Beverly, MA) was used to measure the concentration of dissolved ammonia gas in GSNO solutions after electrochemical reduction. The sensor was mounted with Teflon gas-permeable membrane and preconditioned in 0.1 M NH_4Cl solutions overnight and then in 15 μM NH_4Cl for 30 min prior to use. Small aliquots of 1 mM NH_4Cl solution were first added into a 0.2 M NaOH solution to calibrate the response to NH_3 over a broad (10^{-6} to 10^{-2} M) range. A 2 mL sample solution of electrochemically reduced GSNO (reduction for 30 min at gold mesh electrode) was then introduced to a fresh 2 mL NaOH solution with a 1:1 dilution for measurement of ammonia in the electrolyzed GSNO solution.

3.2.6 Detection of NO^-/N_2O

Gas phase FT-IR spectroscopy (Spectrum BX, Perkin-Elmer, MA) was utilized to verify the existence of N_2O that would be produced from NO^- after GSNO decomposition. An amber electrochemical cell (50 mL) was aligned with a CaF_2 windowed (Pike Tech., Madison, WI) IR gas cell to collect the headspace gas from a GSNO solution after electrochemical reduction for 60 min at gold mesh electrode. Because of the high reactivity of N_2O with O_2, the GSNO solution was first purged with argon for 30 min prior to reaction and the IR gas cell was evacuated by vacuum before collecting the reductive headspace gas.

3.3. Results and Discussion

3.3.1 Preliminary Studies on the Electrochemical Reduction of RSNOs

For preliminary studies, cyclic voltammetric experiments were carried out for both physiological (GSNO, CysNO) and synthetic (SNAC, SNAP) RSNO species at polycrystalline gold and glassy carbon electrodes. As shown in Figure 3.2, the various RSNOs at 1 mM concentrations can be electrochemically reduced, exhibiting an irreversible cathodic wave at a potential of -0.8 V (vs. Ag/AgCl) on gold electrode surface at pH 7.4. The reduction of 1 mM $NO_{(g)}$ is overlaid as trace b in Figure 3.2, showing a different voltammogram pattern where the cathodic current starts increasing from -0.8 V and does not yet give a clear reductive peak even at -1.0 V. Therefore, it can be concluded that the observed cathodic peaks for the RSNO solutions are not due to the reduction of dissolved NO originating from RSNO self-decomposition (thermal, photo, etc.). Rather the reduction peak must be due to direct electrochemical reduction of the *S*-nitroso bond.

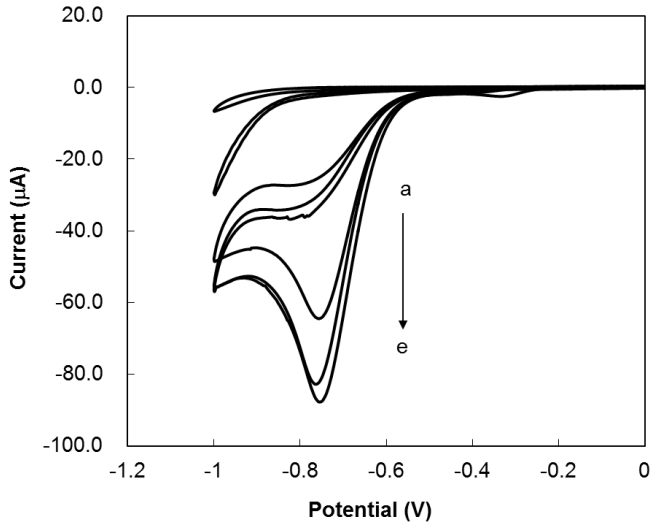

Figure 3.2. Cyclic voltammgrams of 1 mM NO and RSNOs in 10 mM PBS on a gold electrode at a scan rate of 0.05 V/s (vs Ag/AgCl), a: blank PBS, b: NO, c: SNAC, d: GSNO, e: CysNO.

The reduction peaks for RSNOs appear as totally irreversible waves in which the observed peak potential (E_p) is a function of scan rate, shifting in a negative direction with the increase in scan rate (υ) (Figure 3.3). This irreversible behavior suggests that the *S*-nitroso bond of GSNO has been electrochemically cleaved and can no longer be oxidized back on the electrode surface. Furthermore, plotting the peak current (i_p) versus the square root of scan rate ($\upsilon^{1/2}$) shows that i_p is proportional to $\upsilon^{1/2}$, indicating a diffusion controlled process (Figure 3.3 inset).[17]

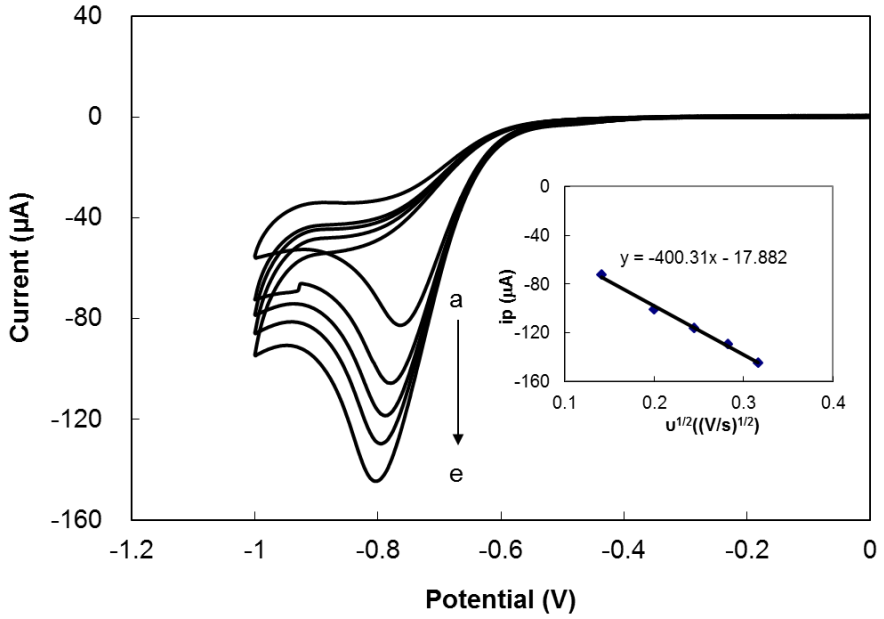

Figure 3.3. Cyclic voltammograms of 1 mM GSNO in 10 mM PBS on gold electrode at different scan rates (V/s) a to e: 0.02, 0.04, 0.06, 0.08, 0.10 V/s; inset: i_p versus $\upsilon^{1/2}$ fit into a linear regression.

Very similar data to that shown in Figures 3.2 and 3.3 above, are obtained when using a glassy carbon electrode as the working electrode for reduction of RSNOs (Figure 3.4). This suggests that the electrochemical reduction of RSNOs occurs by similar pathways on both types of electrodes.

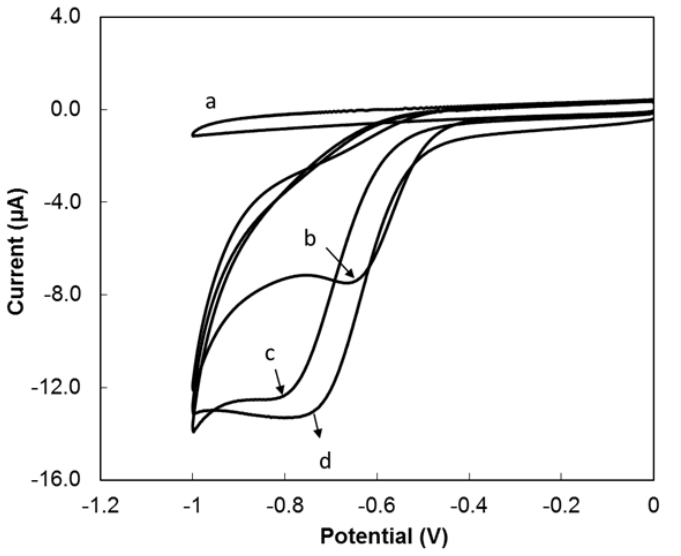

Figure 3.4. Cyclic voltammgrams of 1 mM RSNOs in 10 mM PBS on a glassy carbon electrode at a scan rate of 0.05 V/s (vs. Ag/AgCl), a: blank PBS; b: GSNO; c: SNAC; d: CysNO.

3.3.2 NO Produced from RSNOs

Chemiluminescence Detection

To further investigate the electrochemical reaction, a highly sensitive chemiluminescence nitric oxide analyzer (NOA) was used to assess whether NO is in fact liberated upon the electrochemical reduction of the *S*-nitroso bond of RSNOs. The generated NO can undergo a rapid reaction in the gas phase with ozone, yielding nitrogen dioxide (NO_2) in an excited state. As the excited electron returns to the ground state, a photon is emitted and detected as chemiluminescence. This highly specific, sensitive and reliable method is considered to be the gold standard for trace level NO detection.[18]

Surprisingly, when a cathodic potential of -0.8 V (vs. Ag/AgCl) was applied using a large area gold mesh working electrode (2.5 cm×3.5 cm, 100 mesh) and the solution (10

mM PBS, pH 7.4) was purged with nitrogen continuously (into NOA), no significant NO increase is observed via the NOA analyzer (Figure 3.5). Instead, the initial NO flux derived from the auto-decomposition of GSNO (about 4×10^{-12} mol/sec) actually decreases when the cathodic potential was applied (Figure 3.5). This is likely from the electrochemical reduction of NO at this potential, as observed from trace b in Figure 3.2. This result indicates that NO is not likely the predominant product of the electrochemical RSNO reduction reaction at pH 7.4, or a multiple-step electrochemical reaction rather than a discrete one-electron transfer is involved in the reduction of RSNOs.

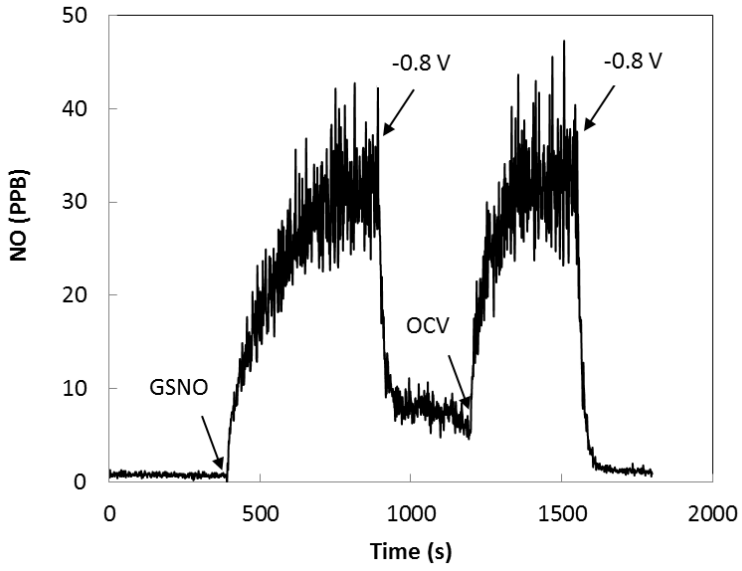

Figure 3.5. NO profile of 10 μM GSNO during electrochemical reduction at -0.8 V (vs. Ag/AgCl) and open-circuit voltage (OCV) on a gold mesh electrode surface.

Griess Assay for Nitrite Detection

Besides the chemiluminescence method to detect NO, a spectrophotometric Griess assay was employed to measure nitrite ion formed by the possible oxidation of NO with oxygen. In brief, under acidic conditions, sulfanilamide reacts with NO_2^- to form a

diazonium cation that further reacts with N-(1-naphthyl)ethylenediamine, producing a diazo molecule characterized by a strong absorbance at 540 nm.

This type of spectroscopic method is highly sensitive and can yield a detection limit as low as 1 μM. Thus, it is an ideal tool to monitor the level of any nitrite ions formed in the GSNO solutions as a function of the electrochemical reduction time of RSNOs. Unfortunately, when a sample of 1 mM GSNO solution was electrolyzed (at -0.8 V for 60 min at gold mesh electrode) and then analyzed by this method, there was very little absorbance at 540 nm (< 0.25 μM equivalent nitrite, Figure 3.6), further suggesting that no significant amount of NO was produced from the electrochemical reduction of GSNO at pH 7.4.

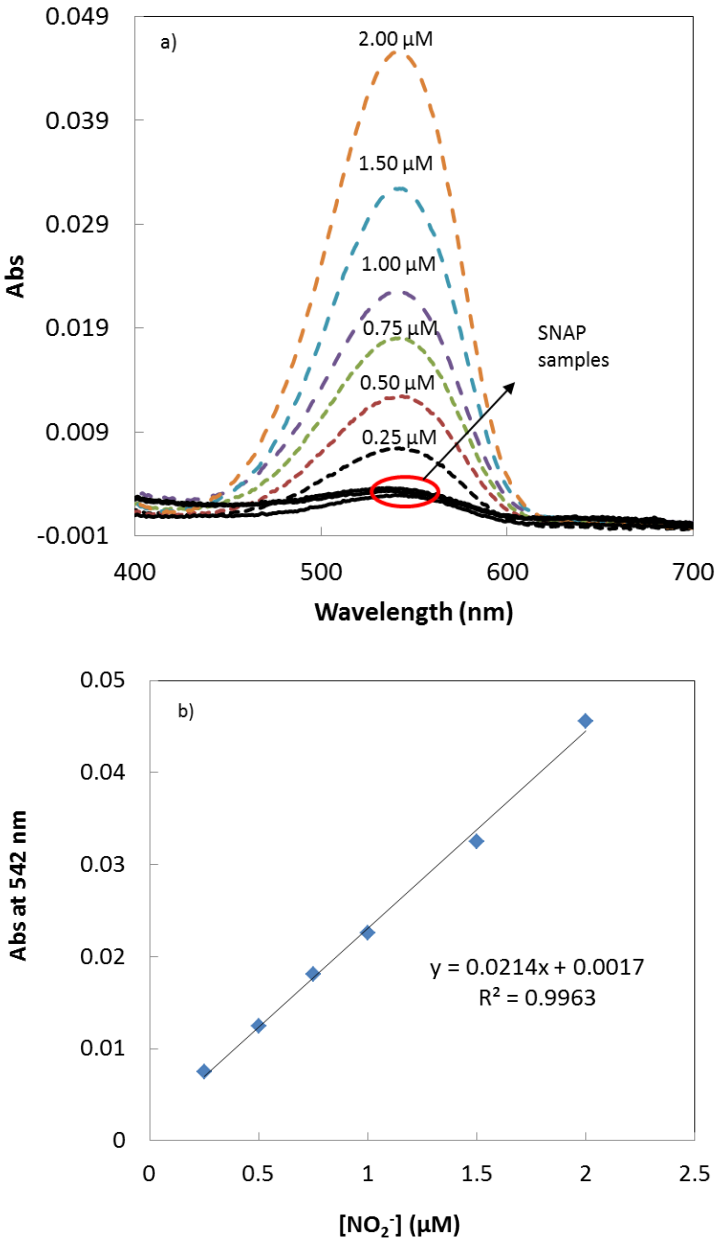

Figure 3.6. a) Response curves (dashed lines) towards concentrations (0.25, 0.50, 0.75, 1.00, 1.50, 2.00 µM) of $NaNO_2$, and the addition of SNAP samples under different periods of echem reduction on a gold mesh electrode (0 min, 30 min, and 60 min, bottom solid lines); b) Calibrations curves of standard $NaNO_2$ response.

3.3.3 Possible Reductive Products of RSNOs

Since all previous reports state that NO is the predominant reductive product from the electrochemical reduction of RSNOs at physiological pH,[12-14] the data shown in Figure 3.5 are rather surprising. Although most decomposition pathways of RSNOs mainly lead to the homolytic cleavage of the S-NO bond and formation of the NO free radical, these pathways may not be exclusive because the chemistry of these compounds is complex. Indeed, there are several possible candidates besides NO, such as ammonia gas, nitrosonium ions, and nitrosyl ions that may be produced.

Ammonia (NH_3)

Ammonia has been reported as one of the end products of the redox reaction between RSNO and high levels of a given thiol.[19] Therefore, we investigated whether direct electron transfer via an electrochemical method can also lead to the formation of ammonia in the RSNO solution that undergoes electrolysis at -0.8 V.

Severinghaus-type NH_3 electrodes are based on a gas-permeable membrane that separates the sample from an internal solution in which a glass electrode monitors the pH.[20] These devices are used to reliably measure dissolved ammonia and ammonium ions by adding base to convert ammonium to ammonia gas. Such electrodes have been approved by the United States Environmental Protection Agency (EPA) and are also described as a standard method for ammonia detection.[21]

Indeed, the ammonia electrode exhibits a fast response and wide dynamic range from 10^{-6} M to 10^{-2} M towards ammonia (Figure 3.7a), providing an excellent analytical tool to measure ammonia produced due to the electrochemical reduction of GSNO at a

large area gold mesh electrode. However, as shown in Figure 3.7b, after reduction of 2 mM GSNO for 30 min with stirring at pH 7.4, there is no immediate ammonia sensor response upon the addition of a sample of the GSNO solutions, except for a slow drift that is mostly due to accumulation of dissolved ambient ammonia. Moreover, there was no significant difference between samples that were blank PBS and ones that underwent 30 min of cathodic reduction, indicating no appreciable amount of ammonia is produced from the electrochemistry of GSNO.

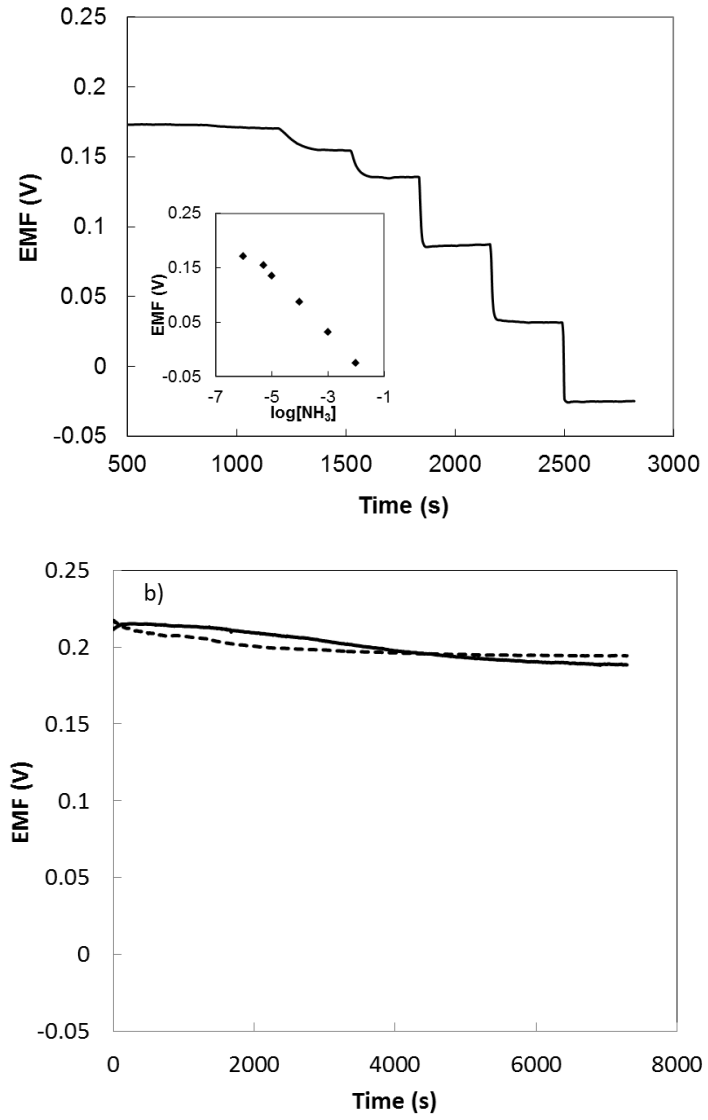

Figure 3.7. a) Response and calibration (inset) curves towards concentrations (10^{-6} to 10^{-2} M) of NH_3, exhibit a sub-Nerstian response with a slope of -53.7 mV/decade. b) EMF response with the addition of GSNO solutions (reduced at -0.8 V for 30 min, solid line) and the control blank PBS (dashed line).

Nitrosyl Ion (NO^-)

As previously reported, RSNOs can also react with thiols and produce NO^-, which under appropriate conditions can yield either nitrous oxide (N_2O) or peroxynitrite ($OONO^-$).[22] More specifically, NO^- can be an active intermediate that will undergo a fast

dimerization reaction to form N_2O at a rate of 8×10^6 M^{-1} s^{-1} under anaerobic conditions, or react with oxygen to form $OONO^-$ under aerobic condition.[23] The existence of NO^- is inferred by the detection of N_2O since it has an advantage of being infrared active with simple asymmetric stretch absorptions in IR spectroscopy at 2210-2230 cm^{-1} that is different from the linear stretching at 1780-1960 cm^{-1} for NO.[24]

Therefore, anaerobic headspace gas analysis was conducted to elucidate whether NO^-/N_2O is a reduction product from the electrochemical reaction of RSNOs at pH 7.4. Beforehand, a 2 mM solution of saturated NO in 100 mM PBS was reduced at a potential of -0.8 V (vs. Ag/AgCl) on the Au mesh electrode for 1 h. The gas phase FT-IR spectrum of the headspace gas shown in Figure 3.8 confirms the presence of N_2O at wavenumbers 2211 cm^{-1} and 2235 cm^{-1}, strongly indicating that N_2O is a reductive product of NO (stretching bands at 1790 and 1810 cm^{-1}) at -0.8 V on a Au surface. Another identifiable absorbance band at a lower wavenumber of 1630 cm^{-1} is probably due to trace amounts of NO_2 present. Most importantly, when a solution of 2 mM GSNO in 100 mM PBS (pH 7.4) undergoes the same electrochemical reduction on either Au or glassy carbon electrodes, bands at 2211 cm^{-1} and 2235 cm^{-1} appear to prove that N_2O is the major product of the electrochemical RSNO reduction (Figure 3.9).

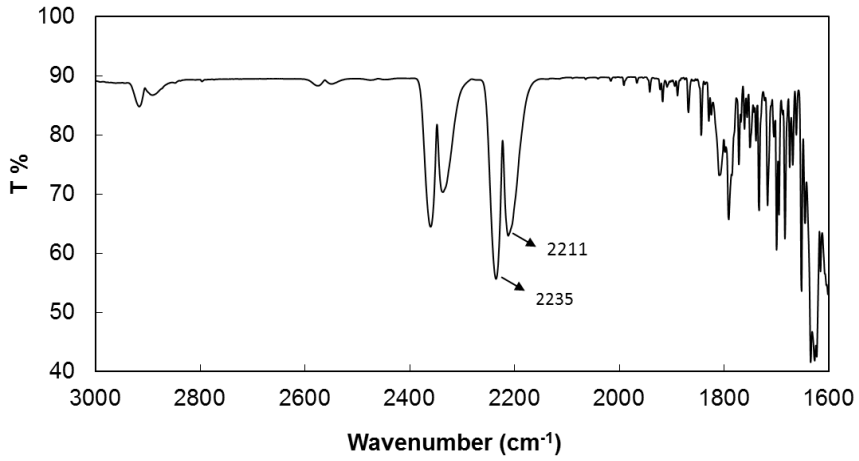

Figure 3.8. FT-IR spectrum of headspace gas from deoxygenated 2 mM NO in 100 mM PBS (pH 7.4), after reduction at -0.8 V (*vs.* Ag/AgCl) on Au mesh electrode for 1 h.

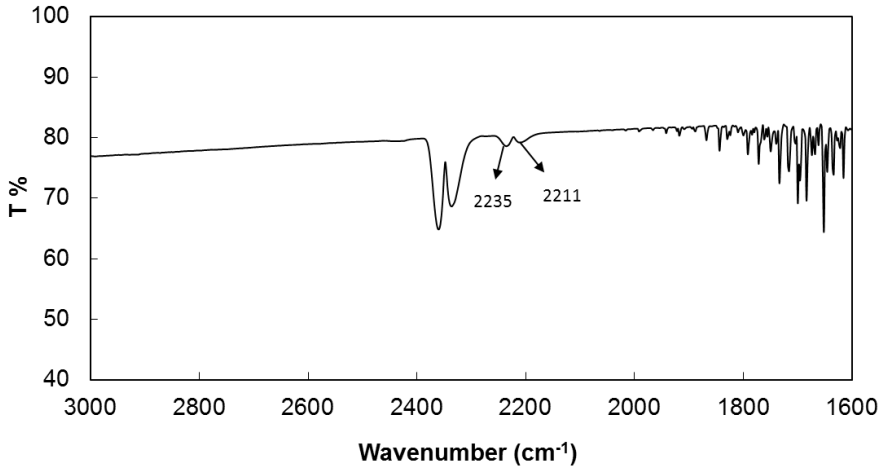

Figure 3.9. FT-IR spectrum of headspace gas from deoxygenated 2 mM GSNO in 100 mM PBS (pH 7.4), after reduction at -0.8 V (*vs.* Ag/AgCl) on Au mesh electrode for 1 h.

Moreover, a series of pulsed reduction potentials (between -0.6 V to -0.9 V) were applied to a gold mesh electrode in the presence of 100 μM GSNO in PBS solution at pH 7.4. The NOA results shown in Figure 3.10 exhibit an interesting "up-and-down" pattern when the applied voltage is switched between anodic (0 V) and cathodic potentials. The

reducing potentials result in an immediate NO decrease, and switching back to the oxidizing potential (0 V) leads to an increase of NO concentration. These results suggest that at pH 7.4 under reduction potentials between -0.6 V to -0.9 V, any NO that results from GSNO is further reduced into another reductive product, which can then be oxidized back to NO at a more anodic potential.

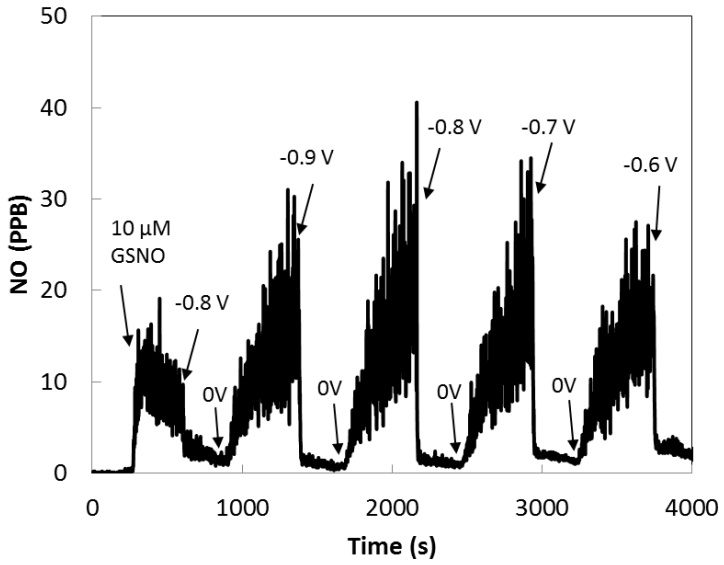

Figure 3.10. Nitric oxide profile of 10 μM GSNO in 100 mM PBS (pH 7.4), first in absence of any potential application, and then after different potentials are applied to gold mesh electrode.

Indeed, two possible reductive pathways may occur upon the electrochemical reduction of RSNOs (see Scheme 3.1 below) at pH 7.4. A one-electron transfer reaction (to form transient NO, Eq. 3.1) followed by an immediate second electron transfer (Eq. 3.2) to create N_2O (Eq. 3.4) is one possibility. Another option is a direct one-electron transfer process to two RSNOs molecules that will also produce N_2O via a nitrosyl intermediate (Eq. 3.3, 3.4).

$$RSNO + e^- \rightarrow NO^{\cdot} + RS^- \quad (3.1)$$

$$NO^{\cdot} + e^- \rightarrow NO^- \quad (3.2)$$

$$RSNO + e^- \rightarrow NO^- + RS^{\cdot} \quad (3.3)$$

$$2NO^- + H_2O \rightarrow N_2O + 2OH^- \quad (3.4)$$

Scheme 3.1. Proposed reactions for the electrochemical reduction of RSNOs.

To calculate the number of electrons transferred in the reactions, UV-Vis spectroscopy was utilized to quantitatively monitor the amount of RSNOs remaining in solution after bulk electrolysis of GSNO at -0.8 V. The characteristic absorbance of *S*-NO at 335 nm was detected before and after GSNO was reduced. With a molar extinction coefficient of 0.85 $mM^{-1}cm^{-1}$, the amounts of consumed GSNO after one hour of reduction was 5.94×10^{-6} mole. At the same time, the total charge passed through the electrochemical reaction was 1.83 coulombs, which was produced by 1.90×10^{-5} moles of electrons. Based on these results, an estimated number of electrons transferred is 3.2 per reaction. Clearly, this does not agree with either of the one-electron or two-electron transfer reactions suggested above. This could be explained by the many possible side reactions that can occur at the same time and would result in a more than the expected number of electrons. For example, one possibility is the reaction between HNO (produced by protonation of NO^-) and free thiols in solution, to further reduce HNO and produce hydroxylamine (NH_2OH) and a disulfide. A two electron reduction of the disulfide could occur at the reductive potentials applied in the above experiments, increasing the number of electrons observed under coulometric conditions. In theory, hydroxylamine can also be reduced, but the product of this electrochemical reduction

reaction is usually ammonia,[25] and hence there is no evidence that hydroxylamine, if formed, is also being reduced electrochemically at the potentials applied. In contrast, it is known that alkyl disulfides can be reduced in the range of -0.8 V to -1.0 V on gold electrode,[26] and hence the presence of significant levels of these species could explain the coulometry results.

3.3.4 pH Effect on Electrochemical Reduction of RSNO

All previous studies reported in the literature, as well as those described above were carried out at pH 7.4, given that endogenous *S*-nitrosoglutathione would exist at this physiological pH. However, preliminary studies regarding the effect of pH on the electrochemical reductive pathway of RSNOs were also carried out at pH 4.0 and 10. Figure 3.11 shows the cyclic voltammgrams of GSNO on gold disk electrode in pH 4.0 PBS at different scan rates. The negative shift at higher scan rate suggests an irreversible reduction of the *S*-nitroso bond. The cathodic peak potentials are similar to those shown in Figures 3.2 and 3.3, with only 50 mV more positive peak voltage occurring at pH 4.0 compared to pH 7.4.

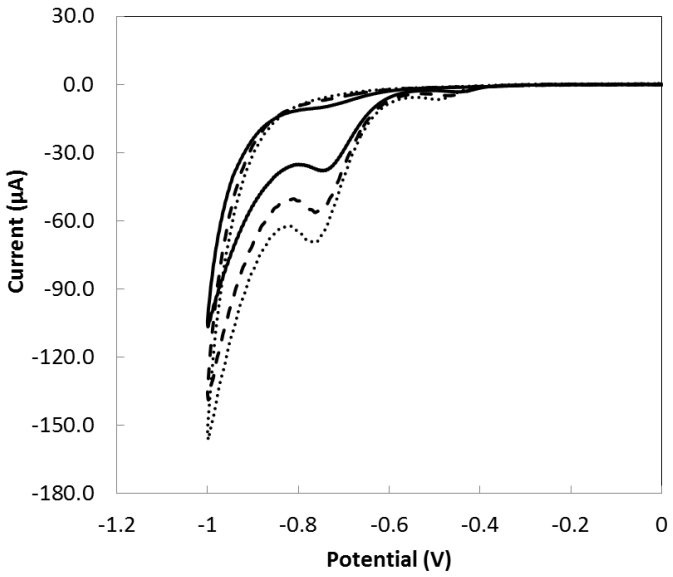

Figure 3.11. Cyclic voltammgrams of 1 mM GSNO in 100 mM PBS (pH 4.0) on gold electrode at different scan rates (V/s): 0.02 (solid line), 0.05 (dashed line), 0.08 (dotted line) V/s.

Most interesting, however, is that in a solution of 10 µM GSNO in 100 mM PBS at pH 4.0, when a cathodic potential of -0.8 V (vs. Ag/AgCl) is applied using a large area gold mesh working electrode (2.5 cm × 3.5 cm, 100 mesh) and the solution is purged with nitrogen continuously (into NOA), a significant NO burst is clearly observed via the NOA analyzer (Figure 3.12). Using a 5 min interval between application of -0.8 V and 0 V to the gold mesh electrode, an "on" and "off" pattern of NO release is observed. More importantly, by switching the potential on and off repeatedly, 97% of the total GSNO is converted into NO after 5 such cycles.

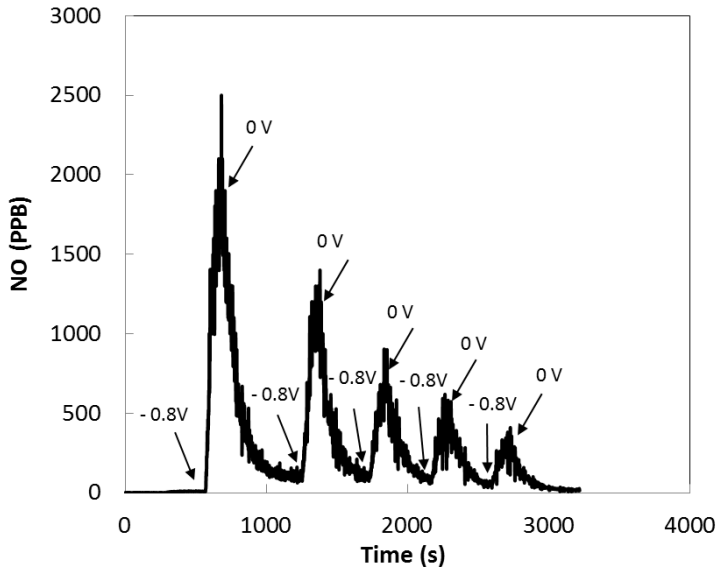

Figure 3.12. Nitric oxide profile of 10 μM GSNO in 100 mM PBS at pH 4.0, first in absence of any potential application, and then after cathodic potentials of -0.8 V and resting potentials of 0 V (*vs.* Ag/AgCl) are alternately applied to gold mesh electrode.

SNAP Species

The results for NO release experiments at pH 4.0 are clearly very different than observed at pH 7.4. To assess whether this difference carries over to other RSNO species, the electrochemical reduction of the synthetic SNAP (with longer half-live for up to a few hours at 37℃) at pH 4.0 in PBS was also examined. Similar quantitative NO release was observed at -0.8 V at pH 4.0 for this RSNO species (Figure 3.13).

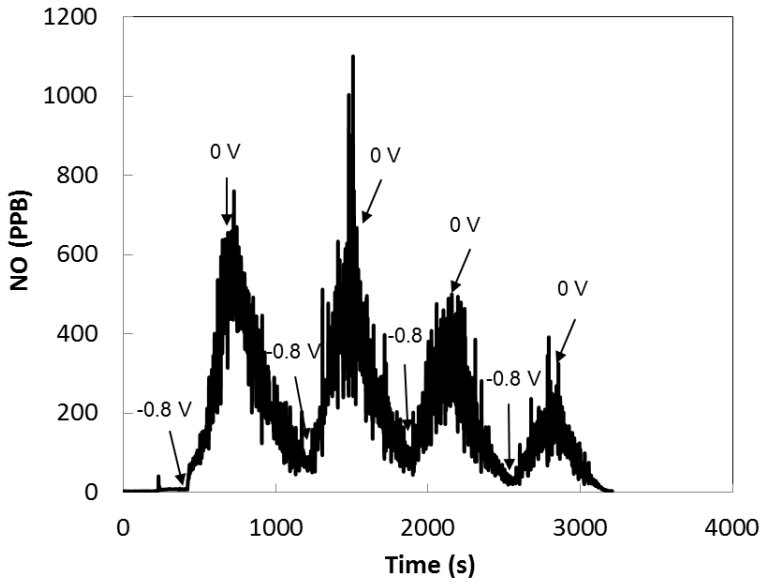

Figure 3.13. Nitric oxide profile of 10 μM SNAP in 100 mM PBS at pH 4.0, first in absence of any potential application, and then after cathodic potentials of -0.8 V and resting potentials of 0 V (*vs.* Ag/AgCl) are alternately applied to the gold mesh electrode.

Buffer Effect

In order to illuminate the decomposition mechanism of RSNOs under acidic conditions, a variety of buffers with different pHs were employed and compared for the electrochemical reduction reaction. Due to a better stability, SNAP was selected as the model molecule for electrochemical reduction on a gold mesh electrode. Phthalate (pH 3.0, pH 4.0), acetate (pH 5.0), and phosphate (pH 6.0) buffered solutions were employed to examine the buffer effect (Figure 3.14). It can be concluded that in acetate or phthalate buffers at pH 4 and 5, similar reductive NO release are observed when the cathodic potential at -0.8 V (*vs.* Ag/AgCl) is applied. However, at pH 6, unpredictable NO peaks are found. More specifically, as shown in Figure 3.14d, the first electrochemical pulse at -0.8 V did not induce any NO release. Instead, a slight decrease of NO (from the initial

auto-decomposition of SNAP) is observed, followed by an NO increase at 0 V. This is similar to the reduction pattern as found at higher neutral pH. Later, a second application of -0.8 V is able to successfully generate NO from the solution. Indeed, at pH 6, two different mechanisms of the electrochemical reduction of RSNO appear to exist at the same time. Therefore, pH 6 is not an ideal condition for controlled electrochemical reaction. Instead, both the phthalate and acetate buffers at pH 4.0 provide a suitable condition for the well-modulated NO release pattern from the SNAP molecule.

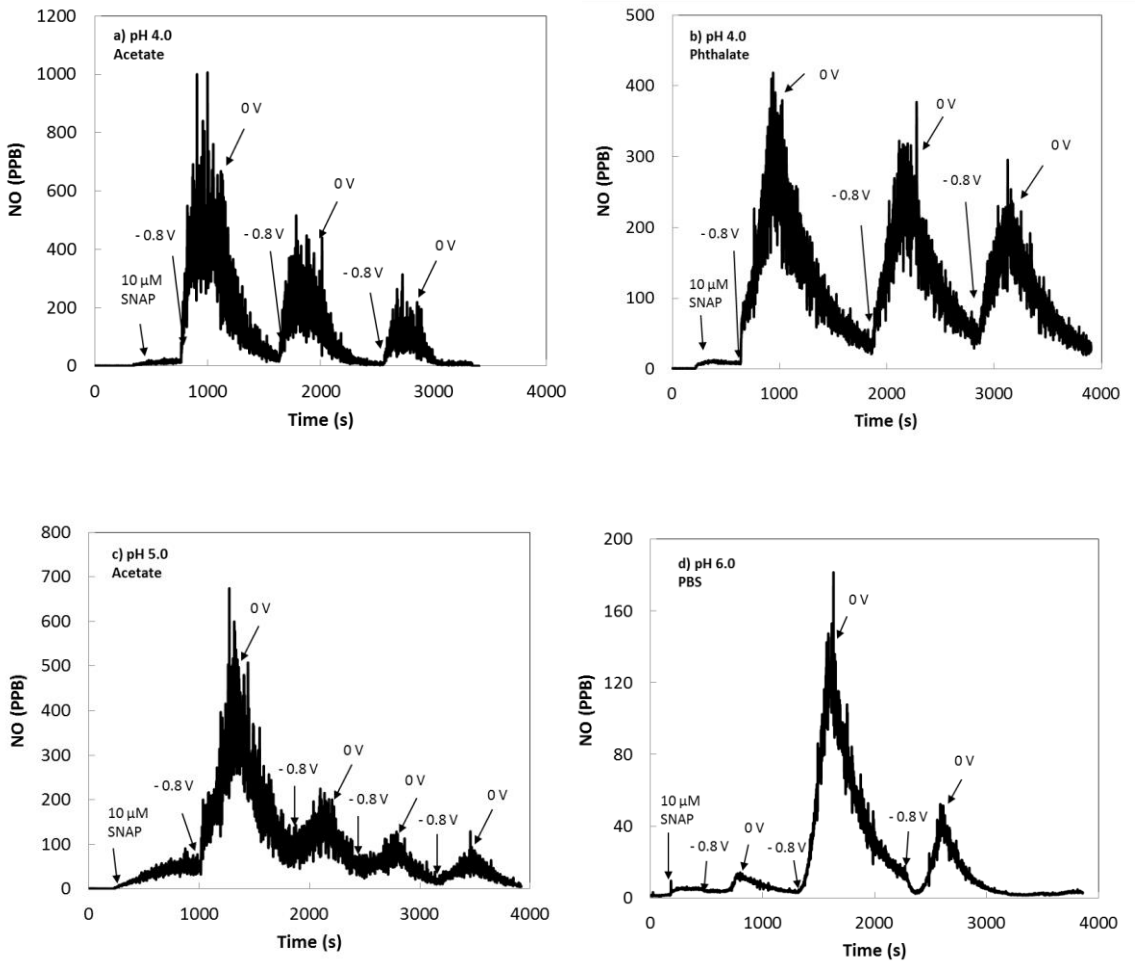

Figure 3.14. Nitric oxide profile of 10 µM SNAP in 100mM different buffers: a) phthalate buffer (pH 3.0), b) phthalate buffer (pH 4.0), c) acetate buffer (pH 5.0), d) phosphate buffer (pH 6.0), first in absence of any potential application, and then after cathodic potentials of -0.8 V and resting potentials of 0 V (*vs.* Ag/AgCl) are alternately applied to gold mesh electrode.

It should be noted that at more basic pH conditions, pH 10, the electrochemical reduction behavior is quite similar to that observed at pH 7.4 (except for a higher NO baseline due to poor GSNO stability at high pH), with no significant amounts of NO produced when cathodic potentials are applied onto gold mesh electrode (NO profile provided in Figure 3.15).

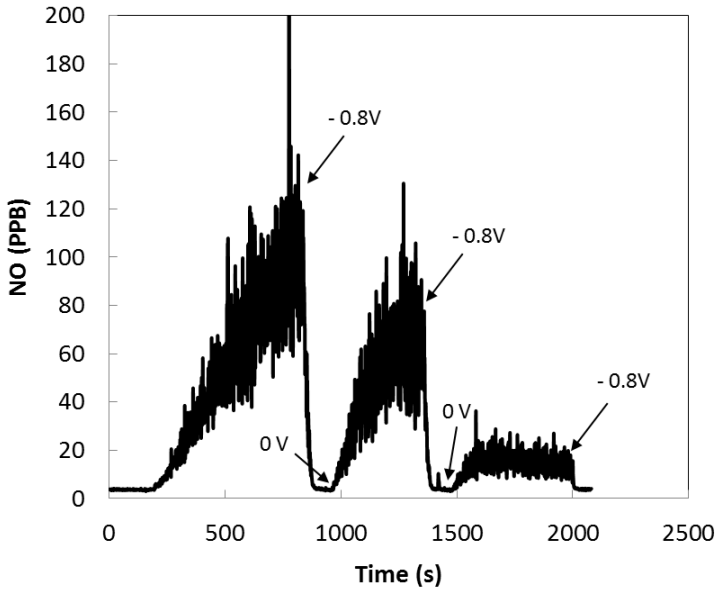

Figure 3.15. Nitric oxide profile of 10 μM GSNO in 100 mM PBS at pH 10.0, first in absence of any potential application, and then after cathodic potentials of -0.8 V and resting potentials of 0 V (*vs.* Ag/AgCl) are alternately applied to gold mesh electrode.

Overall, the reduction pathway of RSNOs at low pH most likely involve a proton that helps favor the direct one electron reaction, with protonation of the thiolate helping to drive the reaction to the right in accordance with Eq. 3.5:

$$RSNO + H^+ + e^- \rightarrow NO^{\cdot} + RSH \qquad (3.5)$$

Catheter Test

Further, as a proof-of-concept, a silicone rubber tubing based catheter was built for potential *in vivo* implantation and/or biofilm dispersion studies (Figure 3.16). Generally, 1 cm of gold was exposed from a Teflon coated gold wire (i.d., 76 μm) with a total length of 6 cm. The gold working electrode was coiled onto a 2 cm Ag/AgCl electrode (i.d. 250 μm, 5 mm apparent length after coiling) and then inserted into a 2 cm silicone rubber tubing (i.d. 510 μm). The polymeric tubing was sealed with silicone rubber glue (SR 3104, Dow Corning, MI) before and after inserting the electrodes. A volume of 3 μL of the buffered RSNO solution was introduced into the silicone rubber tubing by a micro-syringe without any bubbles (by visual check).

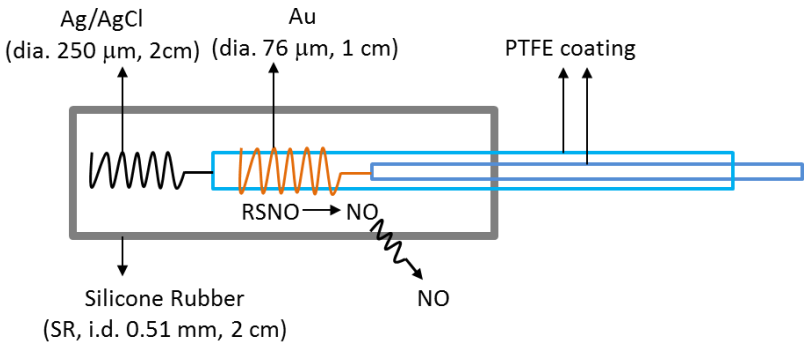

Figure 3.16. Schematic representation of the electrochemically modulated NO release catheter configuration, using gold working electrode and RSNO as the NO precursor.

Based on the results shown in Figure 3.14, phthalate buffer provides a stable condition for the electrochemical reduction of SNAP at pH 4. Therefore, 10 mM of SNAP was dissolved in 100 mM potassium phthalate buffer with 140 mM NaCl (to provide Cl^- source for the Ag/AgCl reference electrode) as the inner NO donor solution within the silicone rubber catheter. A preliminary result of the catheter with the

electrochemically modulated NO release pattern was observed in Figure 3.17. Similarly as observed in Figure 3.12, by using a 5 min interval between application of -0.8 V and 0 V to the gold wire electrode, an "on" and "off" pattern of NO release is clearly observed from the catheter. The catheter was removed at the end of the third electrochemical modulation cycles, and the amount of NO release decreased back to the baseline, indicating that no leakage of RSNO species occurred from the catheter.

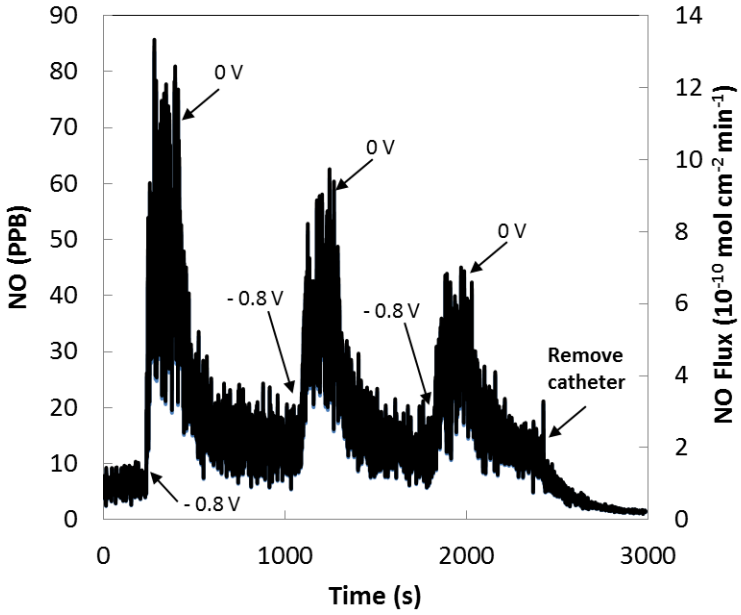

Figure 3.17. Nitric oxide profile of a catheter configuration filled with 10 mM SNAP in 100 mM phthalate buffer with 140 mM NaCl at pH 4.0, first in absence of any potential application, and then after cathodic potentials of -0.8 V and resting potentials of 0 V (*vs.* Ag/AgCl) are alternately applied to gold wire electrode.

However, the results in Figure 3.17 indicate that the amount of NO that had been released during the cathodic modulations decreases with the repeated cycles. It is further calculated that only 18% of total NO has been released from the 3 μL of SNAP that was initially filled into the 2 cm long catheter. Therefore, a possible explanation of the

reduced NO release is the passivation of the gold electrode surface by the produced free thiol species such as N-acetylpenicillamine (from SNAP), glutathione (from GSNO), and cysteine (from CysNO). A standard $K_3Fe(CN)_6$ solution was employed to examine the formation of self-assembled monolayer between the Au electrode surface and thiols. In Figure 3.18, a clear increase of redox peak separation of the ferri/ferro-cyanide species is found on the Au surface after using the same electrode for SNAP reduction for 30 min (dotted line) and soaked afterwards overnight (solid line), indicating the existence of an insulating Au-thiol layer.

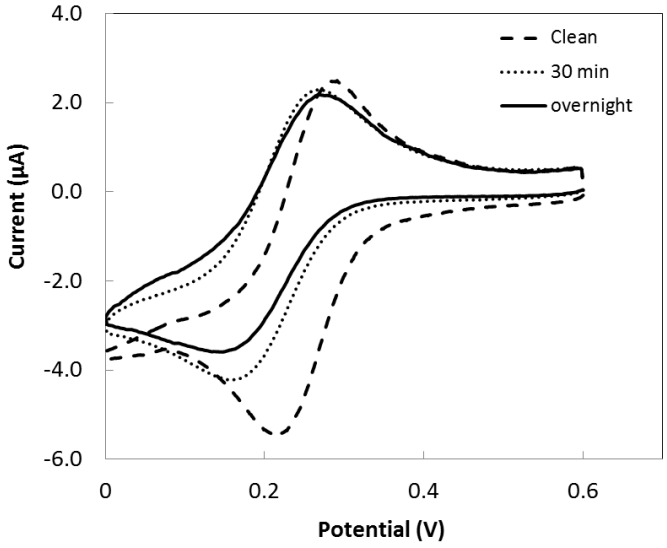

Figure 3.18. Cyclic voltammgrams of 1 mM $K_3Fe(CN)_6$/ 0.1 M KNO_3 solution on gold disk electrode that has been exposed to different reaction time periods in 10 μM SNAP in 100 mM phthalate buffer (pH 4.0): intact clean electrode before contacting SNAP solution (dashed line), after 30 min electrochemical reduction at -0.8 V (dotted line), soaked in 10 μM SNAP in phthalate buffer overnight (solid line).

3.4. Conclusions

Contrary to previous literature,[12-14] results reported in this chapter suggest that during the electrochemical reduction of RSNOs at voltages between -0.6 V to -0.9 V at pH 7.4, $NO_{(g)}$ is not the predominant product. Instead, the RSNO species are reduced to $N_2O_{(g)}$ and can only be converted back to NO by switching to a more oxidizing potential.

Two possible reductive pathways may occur upon the electrochemical reduction of RSNOs to explain the production of N_2O rather than NO. Further experiments aimed at accounting for all the possible electro-reduction reactions that lead to an unexpected high number of electrons from coulometric measurements at pH 7.4 are needed before final conclusions can be drawn. However, at pH 4.0, quantitative NO release from RSNOs at a gold working electrode does indeed take place at a cathodic potential of -0.8 V. Additional experiments aimed at examining and eliminating the surface Au-thiol interaction still need to be conducted in order to elongate the life-time of NO release from the electro-reduction of RSNOs in the catheter configuration. Nonetheless, based on preliminary results obtain here, it seems possible to use a reservoir of RSNOs at low pH to create biomedical devices (e.g., intravascular catheters) in which electrochemically modulated release of NO can be achieved to prevent clotting and infection.

3.5 References

1. N. Hogg, *Free Radi. Biol. Med.*, **2000**, *28*, 1478-1486.

2. A. Gow, A. Doctor, J. Mannick, and B. Gaston, *J. Chromatogr. B*, **2007**, *851*, 140-151.

3. D. Giustarini, A. Milzani, R. Colombo, I. Dalle-Donne, and R. Rossi, *Clin. Chim. Acta*, **2003**, *330*, 85-98.

4. M. Frost and M.E. Meyerhoff, *J. Am. Chem. Soc.*, **2004**, *126*, 1348-1349.

5. Z. Zhou and M.E. Meyerhoff, *Biomacromolecules*, **2005**, *6*, 780-789.

6. M.M. Batchelor, S.L. Reoma, P.S. Fleser, V.K. Nuthakki, R.E. Callahan, C.J. Shanley, J.K. Politis, J. Elmore, S.I. Merz, and M.E. Meyerhoff, *J. Med. Chem.*, **2003**, *46*, 5153-5161.

7. N.A. Stasko, T.H. Fischer, and M.H. Schoenfisch, *Biomacromolecules*, **2008**, *9*, 834-841.

8. S.M. Shishido, A.B. Seabra, W. Loh, and M.G.d. Oliveira, *Biomaterials*, **2003**, *24*, 3543-3553.

9. D.A. Riccio, K.P. Dobmeier, E.M. Hetrick, B.J. Privett, H.S. Paul, and M.H. Schoenfisch, *Biomaterials*, **2009**, *30*, 4494-4502.

10. D.L.H. Williams, *Acc. Chem. Res.*, **1999**, *32*, 869-876.

11. Y. Hou, Z. Guo, J. Li, and P.G. Wang, *Biochem. Biophys. Res. Comm.*, **1996**, *228*, 88-93.

12. N. Arulsamy, D.S. Bohle, J.A. Butt, G.J. Irvine, P.A. Jordan, and E. Sagan, *J. Am. Chem. Soc.*, **1999**, *121*, 7115-7123.

13. L. Soulere, J.-C. Sturm, L.J. Nunez-Vergara, P. Hoffmann, and J. Perie, *Tetrahedron*, **2001**, *57*, 7173-7180.

14. D.V. Vukomanovic, A. Hussain, D.E. Zoutman, G.S. Marks, J.F. Brien, and K. Nakatsu, *J. Pharm. Tox. Meth.*, **1998**, *39*, 235-240.

15. Y. Hou, J. Wang, F. Arias, L. Echegoyen, and P.G. Wang, *Bioorg. Med. Chem. Lett*, **1998**, *8*, 3065-3070.

16. J.S. Stamler and J. Loscalzo, *Anal. Chem.*, **1992**, *64*, 779-785.

17. A.J. Bard and L.R. Faulkner, *ELectrochemical Methods, fundamentals and applications*. Second Edition ed. 2001, Hoboken, NJ 07030: John Wiley & Sons.

18. P.H. MacArthur, S. Shiva, and M.T. Gladwin, *J. Chromatogr. B*, **2007**, *851*, 93-105.

19. A.P. Dicks, E. Li, A.P. Munro, H.R. Swift, and D.L.H. Williams, *Can. J. Chem.*, **1998**, *76*, 789-794.

20. M.D. Love, H.L. Pardue, and G. Pagan, *Anal. Chem.*, **1992**, *64*, 1269-1276.

21. L.H. Keith, *Compilation of EPA's Sampling and Analysis Methods, Second Edition*, ed. L.H. Keith. 1996, Boca Raton, FL 33431: Lewis Publisher.

22. R.J. Singh, N. Hogg, J. Joseph, and B. Kalyanaraman, *J. Biol. Chem.*, **1996**, *271*, 18596-18603.

23. N. Hogg, R.J. Singh, and B. Kalyanaraman, *FEBS letters*, **1996**, *382*, 223-228.

24. D.R. Willey, K.A. Ross, A.S. Mullin, S. Schowen, L.D. Zheng, and G. Flynn, *J. Mol. Spec.*, **1995**, *169*, 66-72.

25. V. Rosca, G.L. Beltramo, and M.T.M. Koper, *J. Electroanal. Chem.*, **2004**, *566*, 53-62.

26. H. Azehara, S. Yoshimoto, H. Hokari, U. Akiba, I. Taniguchi, and M. Fujihira, *J. Electroanal. Chem.*, **1999**, *473*, 68-74.

CHAPTER 4

ELECTROCHEMICAL MODULATION OF NITRIC OXIDE RELEASE FROM NITRITE SALTS AND DIAZENIUMDIOLATES

4.1 Introduction

As discussed in Chapter 1, it may be of therapeutic value to design a biomedical device that can deliver localized NO with the necessary dose on demand. Current strategies employed to modulate the controlled NO delivery include optical,[1, 2] thermal,[3, 4] and electrochemical methods.[5] Generally, photolytic and thermal modulations require the NO donor molecules to be light or heat sensitive, and this will cause stability issues during the storage and transport/shipping of the medical devices. With proper design, the electrochemical technique can provide a unique method for a generic galvanic and/or voltage control to a variety of readily available NO donors. More importantly, with the use of a simple potentiostat, very precise real time current and potential information that is associated with the NO release reaction can be obtained and further modulated. Therefore, electro-modulation of NO release can provide an alternative method to realize quantitative NO release in a better controlled manner.

This is achieved by using either electrochemically active compounds such as RSNOs (Chapter 3) or proton driven NO donors. It is possible to design controlled

NO release from pH sensitive NO donors via an electrochemically modulated proton production from aqueous solutions. Specifically, this approach can be achieved by using inorganic nitrite salts and diazeniumdiolates, where production of protons at an anode can locally activate NO release. By tuning the applied potential between working and reference electrodes in contact with an appropriate donor reservoir, a novel method of creating modulated NO delivery devices may be possible. This would allow fundamental studies to define necessary NO fluxes and NO release frequencies required to achieve specific therapeutic effects.

In theory, water can undergo a four-electron oxidation reaction to generate O_2 and four protons (oxygen evolution reaction, or OER, Eqn. 4.1), and this is well managed in green plants.[6, 7]

$$2H_2O \rightarrow 4H^+ + O_2 + 4e^- \qquad (4.1)$$

Therefore, by applying an oxidizing potential on the working electrode (e.g., Au, Pt, and glassy carbon), the local pH will be lowered by generating protons from water oxidation in a thin layer in proximity to the anode surface. However, in practice, the electrocatalytic water oxidation described in Eqn. 4.1 has been a challenge and a bottleneck in water splitting related research.[8] This is mainly due to its slow electrode kinetics. For example, while the thermodynamic potential for OER is at 0.62 V (*vs.* Ag/AgCl, unless otherwise stated) at pH 7 and 1 atm O_2, the actual electrode reaction occurs at a much more positive potential (overpotential, η) that reflects the slow electron transfer kinetics. Such high overpotential will not only cause a partial loss of energy, which consequently requires larger power input of medical devices, but more importantly,

it will sacrifice some of the locally released NO by electrochemically oxidizing it into nitrite (Eqn. 4.2) or nitrate (Eqn. 4.3) ions at the high anodic potential on the working electrode.[9]

$$NO + H_2O \rightarrow HNO_2 + H^+ + e \qquad (4.2)$$

$$NO + 2H_2O \rightarrow HNO_3 + 3H^+ + 3e \qquad (4.3)$$

Scheme 4.1. Possible NO oxidation reaction on the working electrode.

This will be a critical issue when the released NO has to diffuse through a polymeric catheter tubing wall to reach the target site. Thus, it is necessary to seek a proper electrocatalysis surface on which the water oxidation reaction occurs with a minimal value of η to yield sufficient proton production and, at the same time, prevent significant NO oxidation.

Fortunately, because of its essential role in splitting water and converting solar energy into chemical energy, there are intensive research efforts in OER related studies with a broad selection of catalytic electrode materials available.[10] Despite the active research explorations of new surface modifications for materials such as semiconductors[11] (e.g., crystalline silicon, gallium phosphide), our aim is to modify a conventional anode surface (Au, Pt, C) that can be easily engineered into a wire configuration with a catalyst on it to facilitate OER at lower potentials. Some metal complexes, (e.g., Ir and Ru[12, 13]) and metal oxides (e.g., IrO_2,[12, 13] Rh_2O_3,[14] Mn_2O_3,[15] and Co_3O_4[16]) can have high oxidation states that will catalyze water oxidation. Among them, iridium oxide was selected in this thesis work as the electrocatalyst for the water oxidation on an anode. Generally, the metal oxide materials can be prepared in different

forms, including thin film,[17, 18] nanoparticles,[19, 20] and colloids.[21, 22] Recently, the Murray group conducted mechanistic studies on achieving the lowest overpotential ($\eta \approx 0.15$ V) for the OER on glassy carbon electrodes deposited with a mesoporous film containing 2 nm diameter $Ir^{IV}O_x$ nanoparticles.[23, 24]

In the work reported in this chapter, the oxidation potential on an anode where the water oxidation occurs at the lowest overpotential was optimized (to provide sufficient proton generation and to prevent the oxidation of localized NO). Two different types of pH sensitive NO donors, nitrite salts and diazeniumdiolate species, were employed to fabricate an electrochemically modulated NO release catheter that can deliver physiologically levels ($0.5 \sim 4.0 \times 10^{-10}$ mol cm^{-2} min^{-1}) of localized NO on demand to potentially prevent clotting and infections.

4.2 Materials and Methods

4.2.1 Materials

Sodium nitrite, sodium chloride, sodium hydroxide, sodium acetate, sodium bicarbonate, potassium chloride, potassium phosphate monobasic, sodium phosphate dibasic, iron (III) chloride, hydrochloric acid (37%), and potassium hexachloroiridate(IV) were obtained from Sigma-Aldrich (Milwaukee, WI). A fluorescence pH probe, LysoSensor™ Yellow/Blue dextran (10,000 MW), was purchased from Life Technologies (Grand Island, NY). Diazeniumdiolates salts including methylamine hexamethylene methylamine NONOate (MAHMA/N_2O_2), spermine/N_2O_2, and proli/N_2O_2 are products of Cayman Chemical (Ann Arbor, MI). These chemicals were

used without further purification unless otherwise noted. Phosphate buffered saline (PBS) and all other solutions were prepared with 18.2 MΩ·cm^{-1} DI water from a Milli-Q system (Millipore Corp., Billerica, MA).

Gold and platinum wires (0.076 mm i.d., 0.13 mm o.d.) with Teflon® coatings were obtained from A-M Systems (Sequim, WA). The silicone rubber tubing (0.51 mm i.d., 0.94 mm o.d.) used to construct catheters was purchased from Helix Medial Inc. (Carpinteria, CA) and silicone rubber (RTV-3140) was a product of Dow Corning (Midland, MI). Carbon fibers (F22, 24k) were a gift from Toho Tenax America Inc., (Rockwood, TN).

4.2.2 Fluorescence Microscopy pH Measurement

Widefield single-molecule epifluorescence microscopy was performed as previously reported.[25] In brief, samples were imaged with a 1.40 NA oil-immersion objective in an Olympus IX71 inverted microscope and detected on a 512×512 pixel Photometrics Evolve EMCCD at a rate of 35 ms/frame. Samples were initially excited and then imaged under 488-nm illumination (Coherent Sapphire 488-50). Appropriate filters (Semrock 488-nm dichroic filter and Semrock 488-nm long-pass filter) were chosen to maximize signal and minimize scattered laser light.

4.2.3. Preparation of IrO_x Nanoparticles

The 2 nm iridium oxide nanoparticles were prepared as reported.[23, 26] In brief, 2.5 mM K_2IrCl_6 was dissolved in 0.1 M NaOH and heated at 90˚C for 20 min until the brown solution turned clear. The solution was then immediately cooled down in an ice bath, forming a light blue solution. The formation of IrO_x nanoparticles was validated by its

maximum absorbance at 580 nm using a UV-Vis spectrophotometer (Lambda 35, Perkin-Elmer, MA). Each batch of fresh solution was stored in a 4˚C refrigerator and used for up to one week.

4.2.4 Fabrication of Catheters

A silicone rubber tubing based catheter was prepared for potential *in vivo* implantation and/or biofilm dispersion studies. Generally, 1 cm of gold was exposed from a Teflon® coated gold wire (i.d., 76 μm) with a total length of 6 cm. Then, similarly, 2 cm of a Teflon® coated silver wire (i.d. 125 μm) were exposed and oxidized into Ag/AgCl as the reference/counter electrode with a total length of 8 cm. The working electrode (Au or Pt) was coiled onto the Ag/AgCl electrode (1 cm and 5 mm apparent length after coiling for the working electrode and reference electrode, respectively). The combination electrode was then inserted into a 2 cm silicone rubber tubing (i.d. 510 μm). A volume of 3 μL of the buffered sodium nitrite or diazeniumdiolates solution was introduced into the silicone rubber tubing without any bubbles (by visual check). The polymeric tubing was sealed with silicone rubber glue (SR 3104, Dow Corning, MI) before (distal end) and after inserting the electrodes. A potentiostat (CHI 800B, Austin, TX) was used to apply the electrochemical voltage or current required for water oxidation.

4.2.5 NO Measurement

Nitric oxide was measured with a real-time chemiluminescence nitric oxide analyzer (NOA). More specifically, in the catheter test, polymeric tubing containing the NO releasing agent and a two-electrode circuit was place into a glass cell. The cell was purged with nitrogen. Nitric oxide was continuously removed from the solution by using

a nitrogen bubbler and sweep gas into the reaction chamber. A combination Echem-NOA cell that is similar to the one designed in Chapter 3 (Figure 3.1) was used to conduct such combined electrochemical reaction and NO monitoring experiments.

4.3 Results and Discussion

4.3.1 Surface pH Measurements

An *in situ* fluorescent measurement was aligned with electrochemical settings to prove the production of protons and localized pH change from water oxidation at the anode surface. A LysoSensor™ Yellow/Blue pH dye was employed as the proton probe (Figure 4.1). The LysoSensor™ dye is an acidotropic probe that appears to accumulate in acidic conditions as a result of protonation. This protonation also relieves the fluorescence quenching of the dye by its weak base side chain, resulting in an increase in fluorescence intensity. Figure 4.2 shows the average fluorescence emission response of 1 μM dye in different pH buffer solutions ranging from 3 to 7. A significant increase of fluorescence intensity was observed when the pH dropped from 4 to 3. This probe is a sensitive indicator to monitor the local proton production at the surface of an electrode.

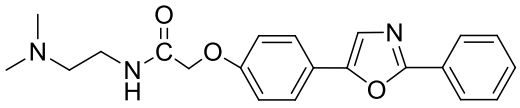

Figure 4.1. Chemical structure of pH probe LysoSensor™ Yellow/Blue.

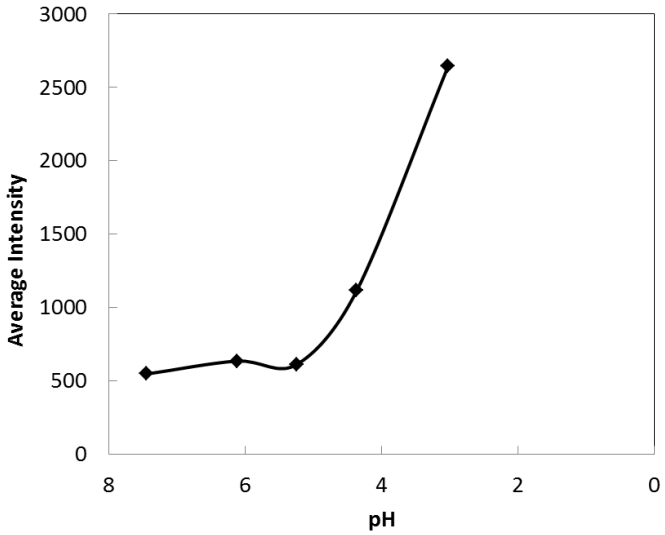

Figure 4.2. The pH-dependent fluorescence intensity response curve of 1 μM LysoSensor™ Yellow/Blue.

Further, two electrodes (Au working electrode and Ag or Ag/AgCl reference electrode) were placed onto a microscope slide within a thin layer of 1 μM LysoSensor™ dye in pH 7.4 PBS solution (Figure 4.3a). To eliminate evaporation of the small volume samples (~60 μL), the solution was sealed with a cover slip and glue. The electrodes were connected to a potentiostat (ESA Biosciences Inc., Chelmsford, MA) to apply positive potentials to oxidize water and release protons. The interface between the electrode surface and solution was imaged under the microscope (Figure 4.3b). When an anodic potential at +1.5 V (vs. Ag) was applied on the gold wire, an immediate increase of fluorescent intensity was observed (Figure 4.3c and d). Later, the fluorescent emission was quenched when the potential was switched to 0 V (Figure 4.3e). It should be noted that by switching to a less positive potential (i.e., +0.8 V), a smaller increase of fluorescent intensity was observed. These results prove that by tuning the anodic

potentials, the proton formation near the gold working electrode surface can be modulated.

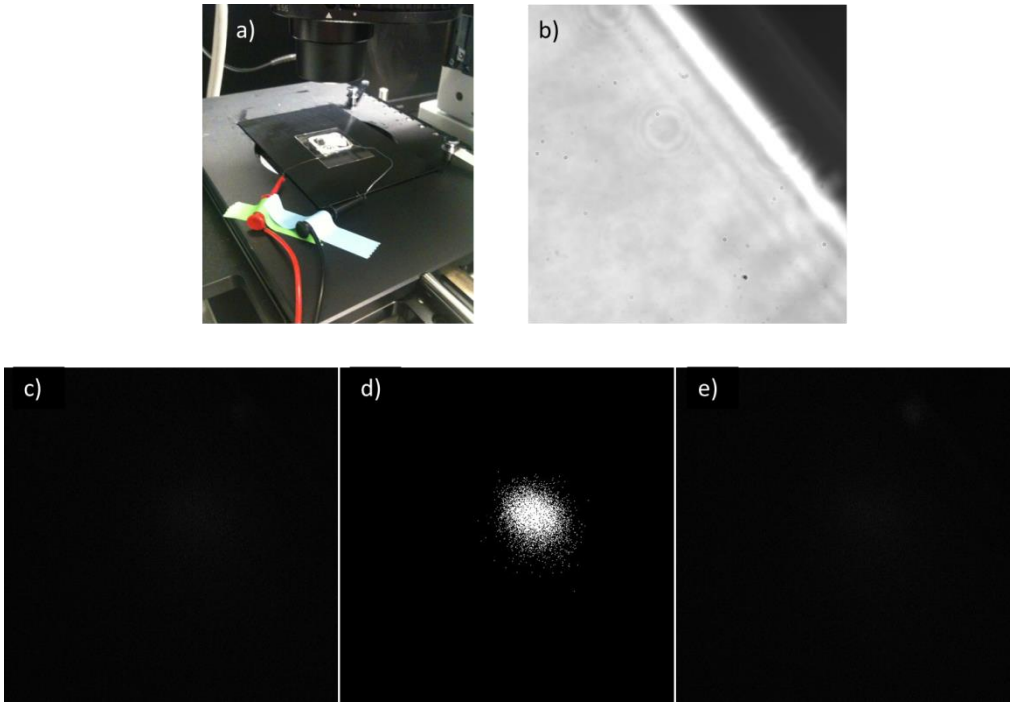

Figure 4.3. a) A picture of the combination echem-fluorescence measurement setup. b) Region of interest at the electrode and solution interface. c) Fluorescence image of the interface at 0 V. d) Intensified fluorescence image of the interface at +1.5 V. e) Fluorescence image of the interface going back to 0 V after d).

4.3.2 Electro-modulation of NO Release from Nitrite Salts

It is reported that acidified nitrite and NO play an important role in gastric host defense against swallowed pathogens.[27] Indeed, NO can function as an anti-microbial agent and is found in the stomach in a range of 10-100 ppm.[28] Chemically, when nitrite (p*K*a 3.4) is acidified, it produces nitrous acid (HNO_2, Eqn. 4.4) first, which spontaneously decomposes to nitric oxide (NO, Eqn. 4.5) and nitrogen dioxide (NO_2, Eqn. 4.6).

$$H^+ + NO_2^- \leftrightarrow HNO_2 \qquad (4.4)$$

$$2HNO_2 \rightarrow N_2O_3 + H_2O \qquad (4.5)$$

$$N_2O_3 \rightarrow NO + NO_2 \qquad (4.6)$$

This inspired us to consider employing the proton driven nitrite salts to electrochemically release NO by providing protons from water oxidation. Sodium nitrite is inexpensive and stable, and can be prepared at concentrated levels in miniature devices.

Bulk Solution Test

First, preliminary bulk solution tests were carried out in 1 M $NaNO_2$ solutions in a 10 mM phosphate buffered saline at pH 7.0 using a polycrystalline gold disk working electrode (dia. 3 mm), a commercial Ag/AgCl reference electrode (in 3 M KCl solution behind a frit), and a Pt coil counter electrode. As shown in Figure 4.4, when a series of anodic potentials were applied onto the Au electrode, different amounts of NO are released from the acidification of nitrite near the electrode surface. Starting from +0.75 V (*vs.* Ag/AgCl), apparent NO release is observed, and by turning the potential to 0 V, the amount of NO decreases back to baseline. When the potential is switched from 0 V to +0.8 V, a significant amount of NO is released immediately. At the same time, by holding the anodic potential at +0.8 V for 30 min, a relatively constant release of NO is achieved.

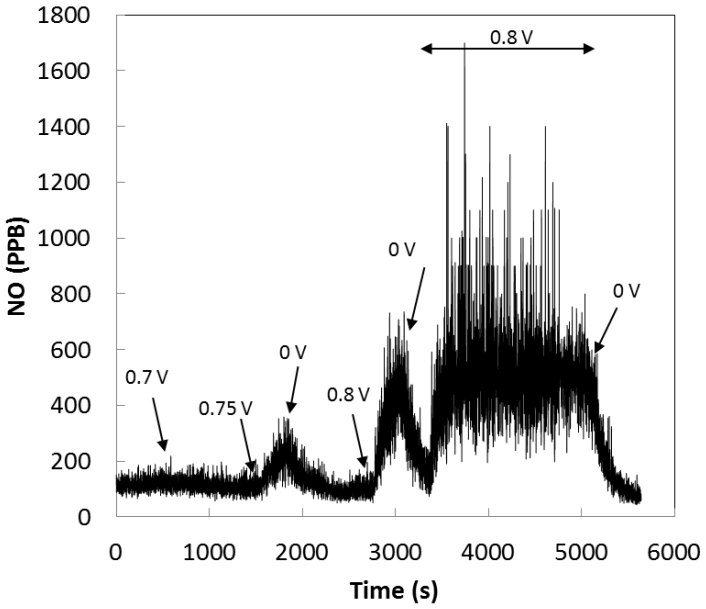

Figure 4.4. Nitric oxide release from the acidification of 1 M $NaNO_2$ in 10 mM PBS (pH 7.0) at a gold disk electrode surface with pulsed potentials applied.

Catheter Test

Further, a miniature catheter device was created based on the successful bulk solution test results. Figure 4.5 shows a schematic diagram of the catheter configuration, where Teflon® coated gold and Ag/AgCl wires were employed as the working and reference electrodes, respectively. The thin wires were coiled together and inserted into small silicone rubber tubing that was filled with buffered 100 mM $NaNO_2$ solution, and then sealed with silicone rubber glue. The catheter was left curing in PBS overnight.

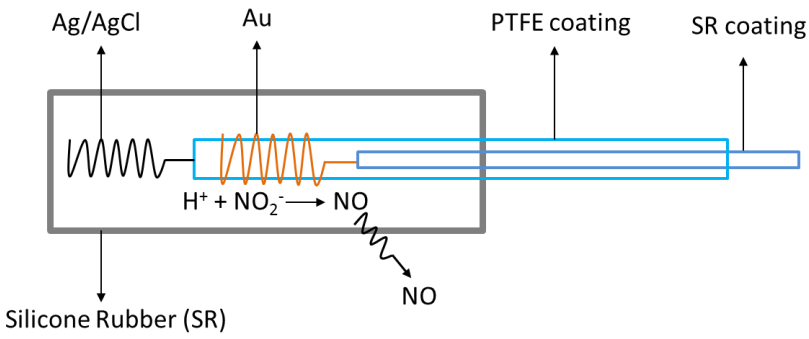

Figure 4.5. Schematic representation of the electrochemically modulated NO release catheter configuration, using a gold working electrode and $NaNO_2$ as the NO precursor.

In the catheter testing, a significant amount of NO is released when a positive potential at +0.75 V (vs. Ag/AgCl) is applied on the Au electrode (Figure 4.6a) for 2 h. Within the first 10 min, the maximum flux of NO is observed at 140 ppb, or 28×10^{-10} mol cm^{-2} min^{-1}. However, the flux of NO gradually decreases even though a constant anodic potential was applied on the Au electrode. At the same time, the anodic current observed on the working electrode decreases concurrently. This indicates that the potential applied between the Au and Ag/AgCl electrodes is not at a constant value.

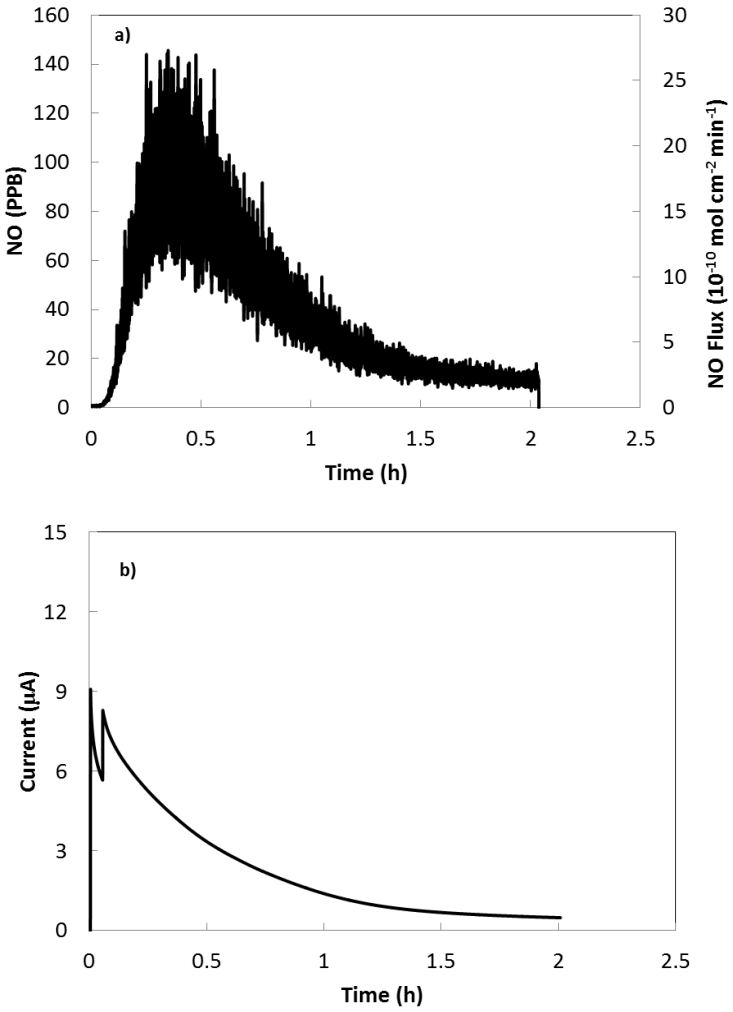

Figure 4.6. a) Nitric oxide released from a catheter containing 100 mM $NaNO_2$ in 10 mM PBS (pH 7.0). The potential was kept at +0.75 V on a small gold wire electrode surface for 2 h. b) The corresponding anodic current on the gold working electrode.

Indeed, it was observed that the color of the Ag/AgCl reference electrode turned from black to white at the end of the 2 h experiment, indicating that the AgCl layer is degraded due to the large current (μA) passed through this reference and counter electrode. Therefore, an additional cathodic potential was introduced after the oxidizing potential to regenerate the Ag/AgCl layer on the reference electrode. The potential was switched between +0.65 V and -0.20 V (*vs.* Ag/AgCl), each in a 5 min interval, for 16 h.

A relatively longer release of NO (flux>1, for 8 h) from a catheter configuration is observed using this modified potential sequence (Figure 4.7).

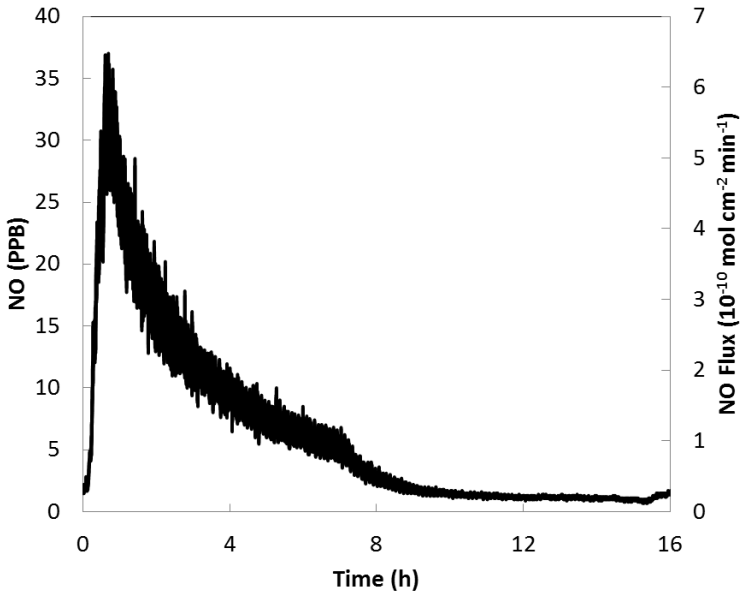

Figure 4.7. Nitric oxide release from a catheter containing 100 mM $NaNO_2$ in 10 mM PBS (pH 7.0) using a small gold wire electrode (dia. 76 μm, 1 cm) and Ag/AgCl (dia. 250 μm, 3 cm), pulsed between +0.65 V and -0.20 V (5 min each) for 16 h.

Further, a more stable electrochemical system with an additional large surface Pt auxiliary electrode was tested. In the 3-electrode system, when the potential is kept constant at +0.8 V on a gold wire (dia. 76 μm, 3 cm), a stable NO release is observed at 1.5 ppm (Figure 4.8a) in a bulk solution containing 1 M $NaNO_2$. The corresponding anodic current was kept relatively constant at ~ 5 mA.

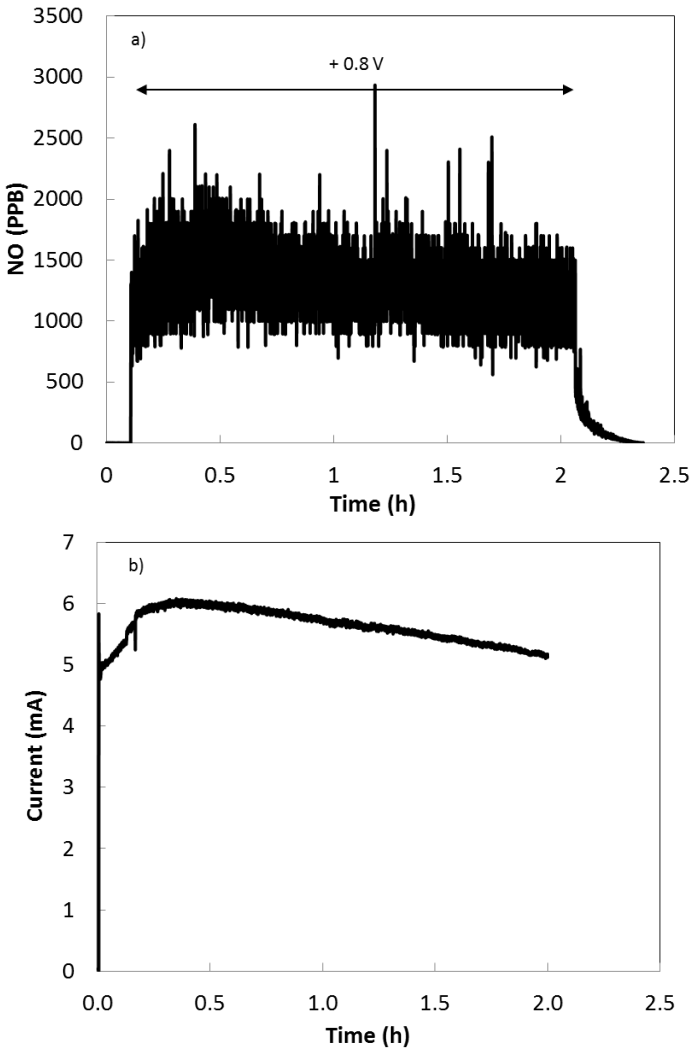

Figure 4.8. a) Nitric oxide release from the acidification of 1 M $NaNO_2$ in 10 mM PBS (pH 7.0) at small gold wire electrode surface with at +0.80 V for 2 h. b) The corresponding anodic current on the gold working electrode.

Another possible method to prevent the reference electrode from degrading is to employ a pseudo reference electrode, such as bare metal wires. Silver, Au and Pt wires were compared and it was found that both Ag and Pt can provide a relatively stable potential *vs.* the working electrode. Therefore, bare Ag was selected as the pseudo reference electrode in a bulk solution test with 1 M $NaNO_2$ (Figure 4.9). With this configuration, well-modulated NO release is achieved for 4 h without a significant drop

in the amount of NO. Later, in a catheter test using phosphate buffered 100 mM $NaNO_2$ solution, a modulated "on" and "off" NO release pattern is observed for the first 4 h. However, a significant decrease of NO flux still occurrs after the 8th hour (Figure 4.10). The pH of the filling solution was measured afterwards, and it increased from the initial 7.0 to 9.4. This is possibly due to the production of OH^- species on the bare Ag electrode.

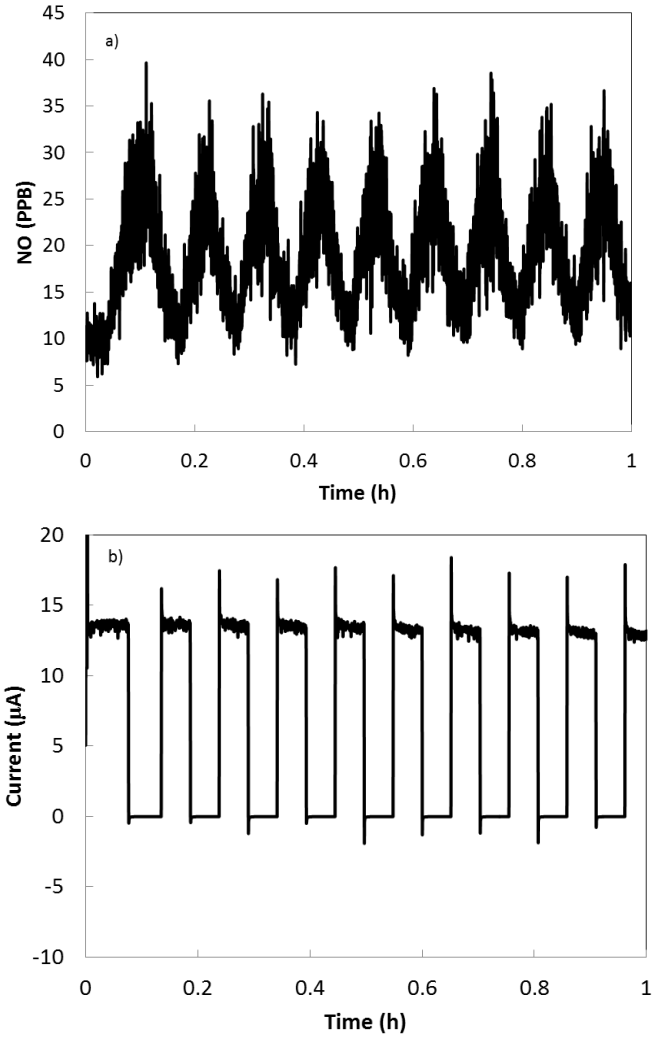

Figure 4.9. a) Nitric oxide release from the acidification of 1 M $NaNO_2$ in 10 mM PBS (pH 7.0) using a small gold wire electrode and bare Ag (dia. 250 µm, 3 cm), pulsed between +1.50 V and 0 V (5 min each) for 1 h. b) The corresponding anodic current on the gold working electrode.

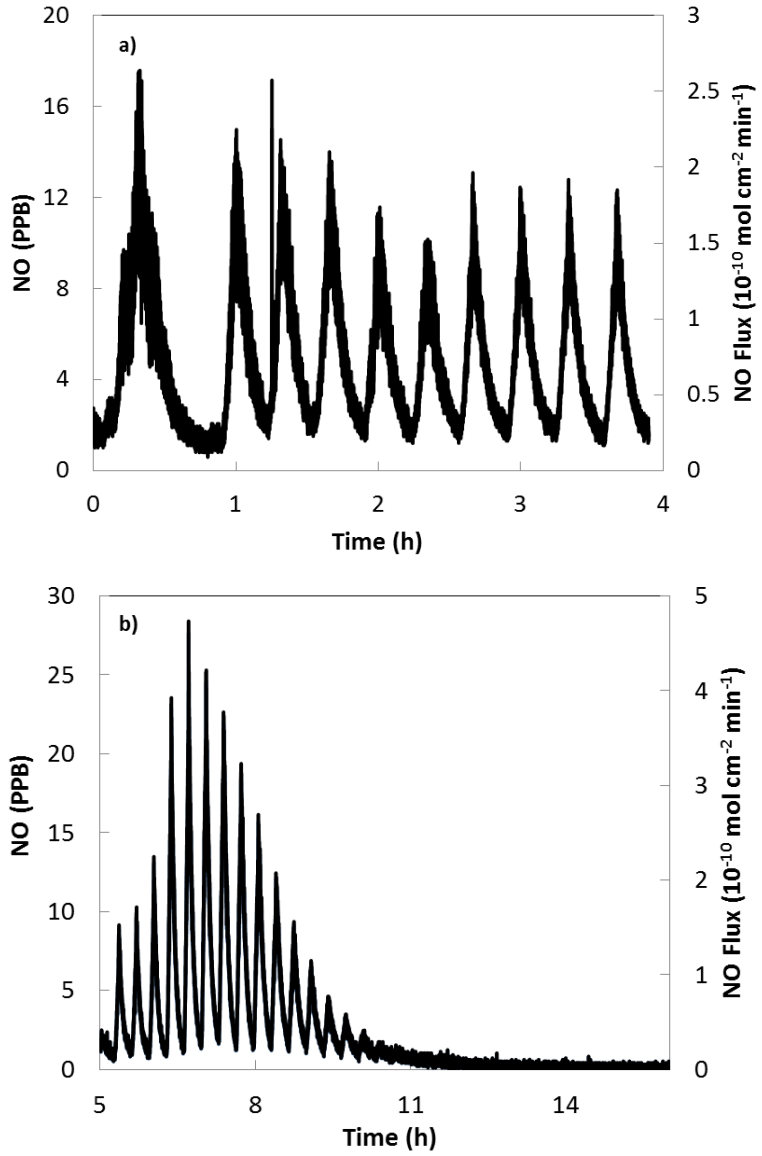

Figure 4.10. Nitric oxide release from a catheter containing 100 mM $NaNO_2$ in 10 mM PBS (pH 7.0) using a thin gold wire electrode (dia. 76 μm, 3 cm) and Ag/AgCl (dia. 250 μm, 3 cm), pulsed between +1.5 V and 0 V (5 min each) for a) 4 h and b) 15 h, periods.

One potential disadvantage of using the acidified nitrite salts as an NO donor is the production of nitrogen dioxide gas as a byproduct. Nitrogen dioxide can diffuse through the catheter wall, and is an oxidizing radical that can initiate a variety of destructive pathways in biology, including the formation of 3-nitrotyrosine, a

neurotoxin.[29] Therefore, it is necessary to explore other NO donors that will produce less or non-toxic side products from the NO release devices.

4.3.3 Electro-modulation of NO Release from Diazeniumdiolates

Diazeniumdiolates, a group of organic species containing two molecules of NO with an amine (*N*) or other nucleophilic site, can also release NO upon exposure to protons (see mechanism below).

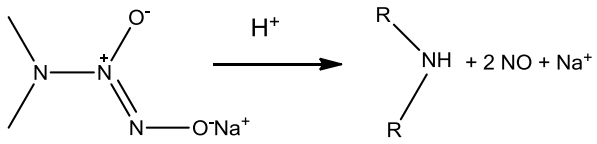

Scheme 4.2. The proton driven NO releasing mechanism from anionic diazeniumdiolates.

In the optimal catheter design, the NO gas will diffuse through the wall of the polymeric tubing, while the residual amine product will stay within the catheter. This pH sensitive NO donor is generally stabilized in the hydrophobic polymer matrix or stored in high alkaline solutions.[30] Therefore, it is possible to prepare water soluble diazeniumdiolates in high pH solutions (pH 11 or higher), and then by electrochemically generating protons (from water oxidation) in a thin layer proximal to the anode surface, localized NO will be released from the diazeniumdiolates molecules nearby. Another advantage of using diazeniumdiolates as the NO donor is that the water oxidation reaction will happen at a less positive potential under high pH conditions (to stabilize the donor), provided a good buffer is present to maintain the pH of bulk solution.

Bulk Solution Test

As a preliminary experiment, a gold wire working electrode (dia. 76 μm, 3 cm) and a bare Ag pseudo reference electrode (dia. 125 μm, 3 cm) were employed in 10 mL of 10 mM methylamine hexamethylene methylamine NONOate (MAHMA/N_2O_2) in a pH 12 NaOH/KCl solution. Indeed, at +0.65 V (*vs*. Ag), an increase of the amount of NO is clearly observed. By further increasing the potential to +1.50 V (*vs.* Ag), a larger NO release is seen (Figure 4.11a). This suggests that by switching the anodic potential on the working electrode, the NO release flux can be tuned.

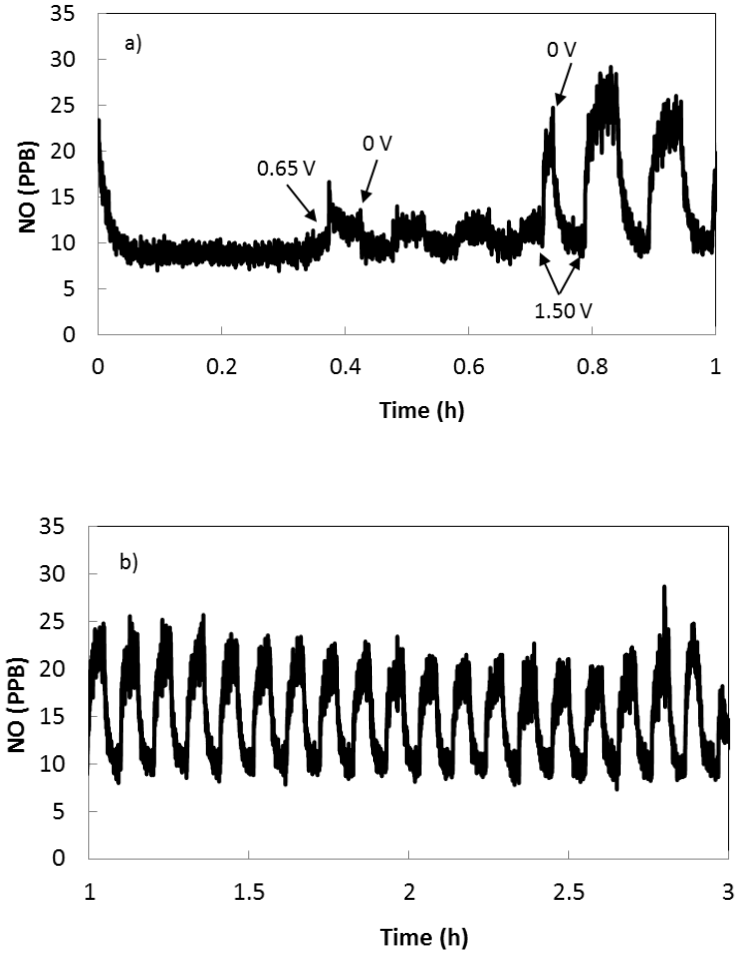

Figure 4.11. a) Nitric oxide release from the acidification of 10 mM MAHMA/N_2O_2 in NaOH/KCl solutions (pH 12.0) using a small gold wire electrode (dia. 76 μm, 3 cm) and a bare Ag (dia. 250 μm, 3 cm). The potential was pulsed between anodic potentials (+0.65 V and +1.50 V) and 0 V for 1 h and, b) the potential sequence was applied for 3 h.

Other diazeniumdiolates species such as spermine/N_2O_2 and proline/N_2O_2 were also examined as NO release candidates. However, due to their instability and sensitivity to pH, they failed to provide controlled release of NO from electrochemical modulation. For example, proline/N_2O_2 is very sensitive to proton concentrations and has a half-life of 1.8 s at 37˚C (pH 7.4). Therefore, low levels of proline-N_2O_2 solutions generally start with a high NO basal level (i.e., 20 ppb for 1 mM proline/N_2O_2) in pH 11, making it very challenging for precise dosage control. On the other hand, spermine/N_2O_2 has a relatively longer half-life of 39 min at 37˚C (pH 7.4), and requires more protons to sufficiently lower the local pH and initiate NO release. Hence, MAHMA/N_2O_2 (half-life=1 min, 37˚C, pH 7.4) was selected as the most suitable diazeniumdiolate species to design the echem-modulated NO release devices.

Catheter Test

To test the catheter concept, a reservoir of 50 mM MAHMA/N_2O_2 solution (in NaOH/KCl, pH 12) was placed into a silicone rubber tubing based catheter, along with thin wires of the working electrode and the reference electrode. As shown in Figure 4.12, by switching the potential between +0.65 V and 0 V on a Au electrode, NO release can be turned "on" and "off" electrochemically. By applying a constant positive potential (+0.65 V) on the working electrode, a constant NO release is achieved. It is noted that the first NO release peak in Figure 4.12 is significantly larger than the second and third ones when the same anodic potential was applied. This is mainly caused by the unbuffered solution (NaOH/KCl) used. When two molecules of NO are released from one diazeniumdiolate, one molecule of amine is produced as well. The NO further

diffuses through the wall of the silicone rubber tubing, while the amine stays in the filling solution as a scavenger for protons. To prevent such a titration effect, a good buffer solution is required to maintain the pH of the bulk solution within the catheter.

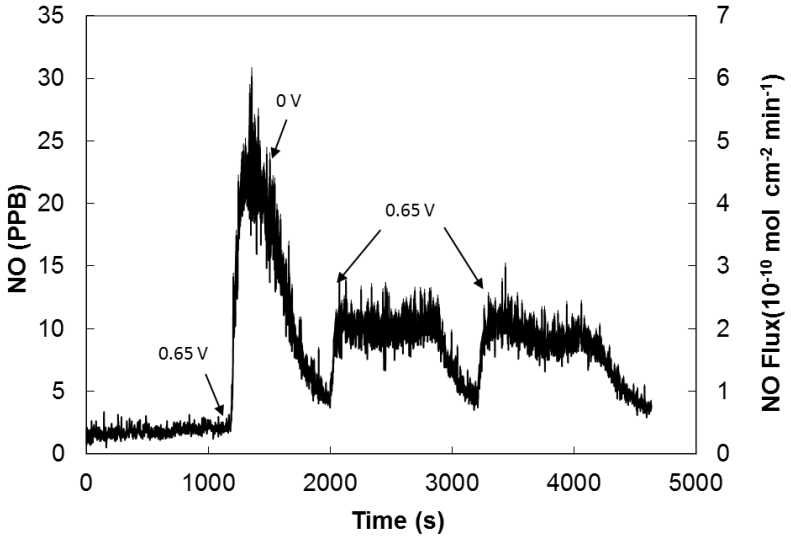

Figure 4.12. Nitric oxide release from a catheter containing 50 mM MAHMA/N_2O_2 in NaOH/KCl (pH 12), using a Au wire working electrode (dia. 76 μm, 1 cm) and Ag/AgCl reference electrode (dia. 125 μm, 3 cm). The potential was switched between +0.65 V and 0 V.

Carbonate buffer was employed to provide a stable pH in the bulk solution while protons were produced close to the surface of the working electrode. However, as shown in Figure 4.13, a decrease in NO release from a carbonate buffered catheter is still observed in a 12 h long term experiment. Only 3% of the total NO is actually released from 3 μL of a 50 mM MAHMA/N_2O_2 solution. The pH was tested afterwards, and it did not exhibit a significant change. However, the Ag/AgCl reference electrode was

again found to be white, indicating possible degradation. A pseudo bare Ag reference electrode was then employed into a long term catheter test; however, similar to the previous nitrite salt study, the pH of the solution increased significantly because of the formation of OH^- at the Ag electrode.

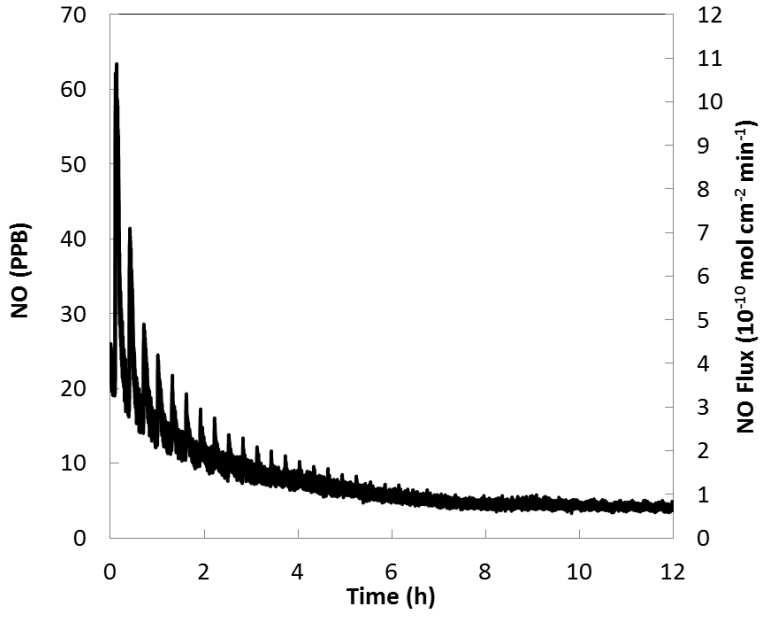

Figure 4.13. Nitric oxide release from a catheter containing 50 mM MAHMA/N_2O_2 in carbonate buffer (pH 11), using a Au wire working electrode (dia. 76 μm, 1 cm) and Ag/AgCl reference electrode (dia. 125 μm, 3 cm), with the potential switched between +0.60 V and 0 V for every 5 min.

4.3.4 IrO_x Modified Electrode for Electrochemically Modulated NO Release

In order to facilitate proton formation at a low anodic potential and prevent significant loss of NO from being oxidized on the working electrode, iridium oxide nanoparticles were employed as the electrocatalyst. They were prepared by thermal hydrolysis of K_2IrCl_6 at pH 13 and without addition of stabilizer ligands, as previously

reported by the Murray group.[23, 26] The formation of IrO_x particles was verified by the UV-Vis spectrum of the prepared solutions, with a λ_{max} at 580 nm (Figure 4.14).

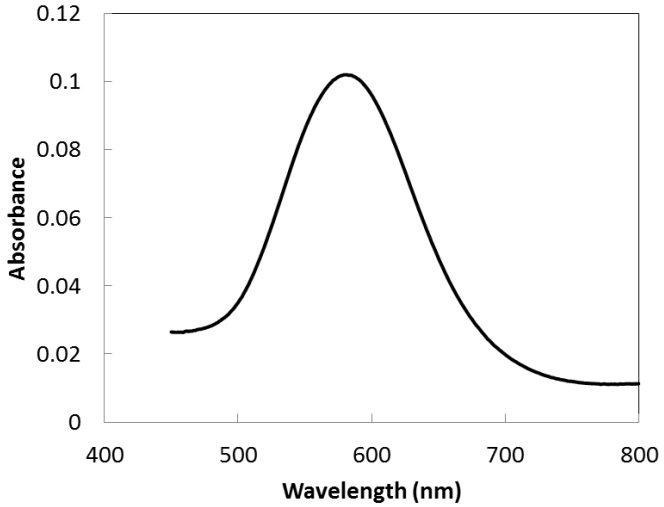

Figure 4.14. The UV-Vis spectrum of IrO_x nanoparticles dispersed in 0.01 M NaOH solution, with λ_{max} at 580 nm.

Further, the oxides particles were electrochemically deposited onto different anode surfaces (Au, Pt, and glassy carbon (GC) disk electrode) by an electro-floccuation process at +1.3 V (*vs.* Ag/AgCl) for 10 min. All Au, Pt, and GC electrodes with the conducting film exhibited an increased current as compared to the bare electrodes, and a noisy anodic current due to the copious O_2 gas evolution. Among the three electrodes examined, GC exhibits the most stable formation of an IrO_x layer, and the largest current increase over Au and Pt electrodes. As shown in Figure 4.15, on bare GC, due to high overpotential values, the oxygen evolution or proton generation reaction did not occur until the potential reaches 1 V (*vs.* Ag/AgCl). However, on the IrO_x nanoparticle modified surface, a more efficient oxygen evolution reaction occurrs at a lower potential

of +0.6 V, with a much larger current (~ 8 times). More importantly, the electrocatalytic layer did not exhibit significant NO oxidation when 0.2 mM of NO was added into the NaOH solution. This indicates that in the potential region of +0.6-0.8 V, water oxidation can be catalyzed by the iridium oxide nanoparticles without significant loss of NO.

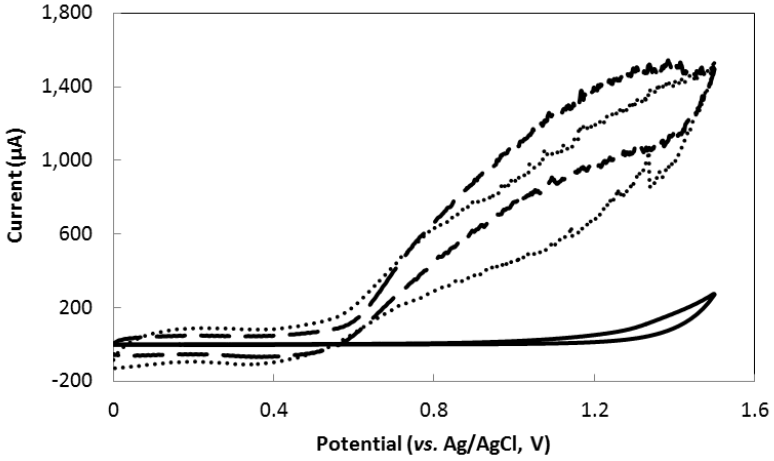

Figure 4.15. Cyclic voltammagrams of a GC electrode scanned between 0-1.5 V (*vs*. Ag/AgCl) in 100 mM NaOH (pH 13): a) on bare glass carbon disk electrode (dia. 4 mm), solid line; b) on GC electrode deposited with IrO_x nanoparticles, dotted line; c) GC-IrO_x electrode scanned in the same NaOH solution with the addition of 0.2 mM NO (dashed line).

To further evaluate the NO release enhancement derived from the IrO_x nanoparticles at lower potential, bare GC (Figure 4.16a) and GC-IrO_x (Figure 4.16b) electrodes were employed to release NO from a carbonate buffered bulk solution containing 1 mM MAHMA/N_2O_2 at pH 11. At +0.6 V (*vs.* Ag/AgCl), the GC-IrO_x clearly exhibits a higher amount of NO (~ 8 times) from a faster catalytic proton production reaction. It is worth mentioning that the optimal potential for NO release on the GC-IrO_x was found to be +0.6 V (*vs.* Ag/AgCl). This is also consistent with the cyclic voltammetry results presented in Figure 4.15, where a significant increase of current from the oxygen evolution reaction starts at +0.6 V. At higher potentials (i.e.,

+0.7 V and +0.8 V), a decrease of NO is observed, indicating partial oxidation of NO at this anodic potential.

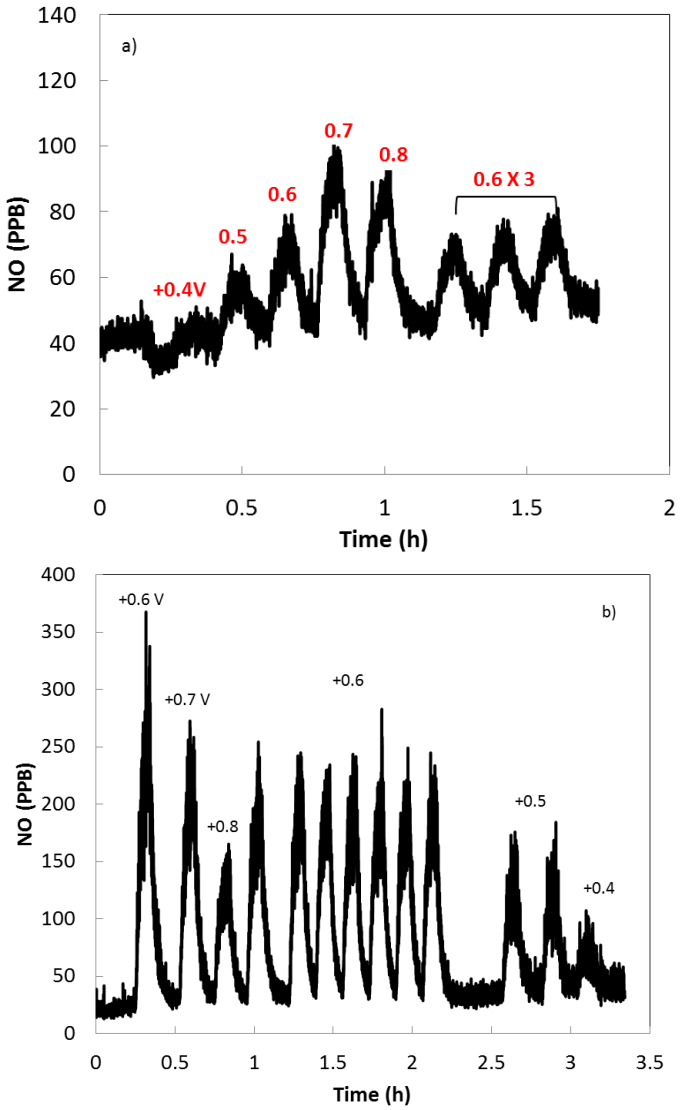

Figure 4.16. Nitric oxide release from a bulk solution containing 1 mM MAHMA/N_2O_2 in carbonate buffer (pH 11), using a GC disk working electrode (dia. 3 mm), Ag/AgCl reference electrode, and a coiled Pt counter electrode, with the potential switched between varying anodic potential (0.4-0.8V) and 0 V for every 5 min. a) bare GC electrode; b) GC electrode with the IrO_x particles deposited on.

However, the IrO_x film is known to be unstable on most electrode surfaces,[31] and carbon is by far the most suitable material that enables mechanically stable and reproducible layers of the oxide particles to reside these on.[32, 33] Therefore, carbon fibers were employed as the anode to provide a flexible electrode to eventually fabricate a medically relevant NO release catheter. Carbon fibers are also a less expensive material than the previously used rare metal wires (e.g., Au and Pt).

First, a 4 cm length of a carbon fiber bundle (dia. 7 μm, 200 threads) was examined with a Ag/AgCl (dia. 125 μm, 5 cm) as the reference in a bulk solution of 1 mM MAHMA/N_2O_2 in a carbonate buffer solution at pH 11 (Figure 4.17a). By switching the potential on the IrO_x modified carbon fiber (CF-IrO_x) working electrode between +0.6 V and 0 V, the NO release is well controlled by the potential. More importantly, due to the better proton generation property of the IrO_x catalyst and a larger surface area of the carbon fiber electrodes (than the gold wires), a larger amount of NO was released from the less concentrated diazeniumdiolate solutions (compare Figure 4.11 and 4.17). The CF-IrO_x electrode was also incorporated into a silicone rubber tubing catheter that is the same configuration as the previous one (Figure 4.5). As shown in Figure 4.17b, the NO release from the catheter containing 5 times lower concentration of diazeniumdiolate donor (10 mM) and the CF-IrO_x with a Ag/AgCl reference does indeed achieve a comparable NO flux pattern to the previous results using a bare Au wire working electrode. This provides a good indication that CF-IrO_x is a suitable electrode material for the design of electrochemically modulated NO release devices. However, more research is needed in order to achieve a long term NO release (> 8 h) in a catheter design, focusing on the preparation of a more stable and robust reference electrode.

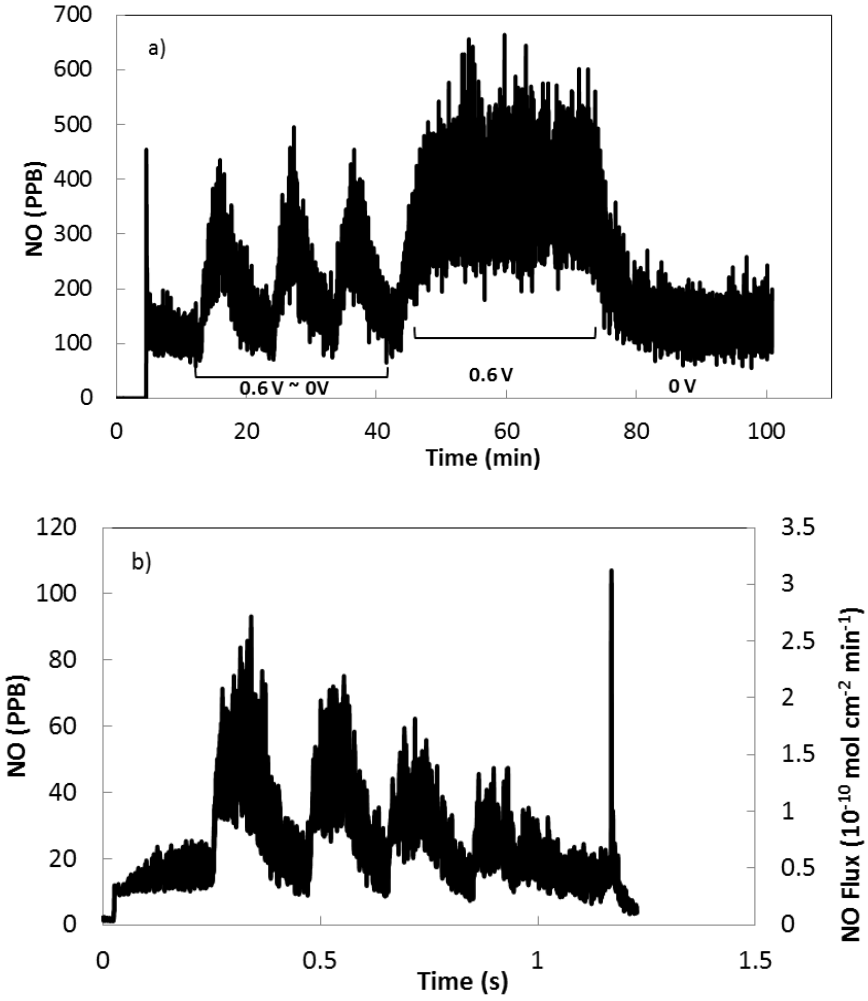

Figure 4.17. Nitric oxide release from a) 1 mM MAHMA/N_2O_2 bulk solution in carbonate buffer (pH 11), b) a catheter containing 50 mM MAHMA/N_2O_2 in carbonate buffer (pH 11), using a CF-IrOx wire working electrode (dia. 7 μm, 4 cm) and Ag/AgCl reference electrode (dia. 125 μm, 3 cm), with the potential switched between +0.60 V and 0 V for every 5 min.

4.4 Conclusion

In this chapter, it has been demonstrated that it is possible to achieve well controlled NO release from pH sensitive NO donors via electrochemical modulation. Two types of pH sensitive NO donors were investigated, and a buffered solution containing these donors was placed into a silicone rubber tubing catheter as well. In the catheter design, diazeniumdiolates are a more suitable donor candidate, while nitrite salts are not appropriate, since they produce a toxic side product, NO_2, that can diffuse through the catheter wall. With the optimal design, a physiologically relevant flux of NO ($>1\times10^{-10}$ mol cm^{-2} min^{-1}) can be released from the catheter for up to 8 h. Additionally, iridium oxide nanoparticles were deposited onto a carbon fiber electrode by electro-fluoccuation. The modified carbon fiber electrode exhibited a superior ability to release larger amounts of NO at a lower anodic applied potential. Current limitations for this research include the degradation of the reference/counter electrode, and consequently a relatively short NO release life time. Future studies will mainly involve searching for a more stable and robust reference/counter electrode to carry the large anodic current during water oxidation. A better engineered design to fit a 3 electrode setup into the catheter would also provide a stable electrochemical cell for a potentially longer life time of the NO release catheter.

4.5 Reference

1. M. Frost and M.E. Meyerhoff, *J. Am. Chem. Soc.*, **2004**, *126*, 1348-1349.

2. A.A. Eroy-Reveles and P.K. Mascharak, *Future Med. Chem.*, **2009**, *1*, 1497-1507.

3. J.A. Hrabie and L.K. Keefer, *Chem. Rev.*, **2002**, *102*, 1135-1154.

4. M. Marazzi, A. Lopez-Delgado, M.A. Fernandez-Gonzalez, O. Castano, L.M. Frutos, and M. Temprado, *J. Phys. Chem. A*, **2012**, *116*, 7039-7049.

5. L. Hofler, D. Koley, J. Wu, C. Xi, and M.E. Meyerhoff, *RSC Advances*, **2012**, *2*, 6765-6767.

6. N.S. Lewis and D.G. Nocera, *PNAS*, **2006**, *103*, 15729-15735.

7. M.G. Walter, E.L. Warren, J.R. McKone, S.W. Boettcher, Q. Mi, E.A. Santori, and N.S. Lewis, *Chem. Rev.*, **2010**, *110*, 6446-6473.

8. P.E.M. Siegbahn, *Dalton Trans.*, **2009**, *0*, 10063-10068.

9. Y. Lee, B.K. Oh, and M.E. Meyerhoff, *Anal. Chem.*, **2003**, *76*, 536-544.

10. J. Barber and P.D. Tran, *J. R. Soc. Interface*, **2013**, *10*, 1-16.

11. D.G. Nocera, *Acc. Chem. Res.*, **2012**, *45*, 767-776.

12. P.G. Hoertz, Y.-I. Kim, W.J. Youngblood, and T.E. Mallouk, *J. Phys. Chem. B*, **2007**, *111*, 6845-6856.

13. W.J. Youngblood, S.-H.A. Lee, Y. Kobayashi, E.A. Hernandez-Pagan, P.G. Hoertz, T.A. Moore, A.L. Moore, D. Gust, and T.E. Mallouk, *J. Am. Chem. Soc.*, **2009**, *131*, 926-927.

14. K. Kvastek and V. Horvat-Radosevic, *J. Electroanal. Chem.*, **2001**, *511*, 65-78.

15. M.M. Najafpour, F. Rahimi, E.M. Aro, C.H. Lee, and S.I. Allakhverdiev, *J. R. Soc. Interface*, **2012**, *9*, 2383-2395.

16. B.S. Yeo and A.T. Bell, *J. Am. Chem. Soc.*, **2011**, *133*, 5587-5593.

17. J.D. Blakemore, N.D. Schley, M.N. Kushner-Lenhoff, A.M. Winter, F. D'Souza, R.H. Crabtree, and G.W. Brudvig, *Inorg. Chem.*, **2012**, *51*, 7749-7763.

18. A. Minguzzi, F.R.F. Fan, A. Vertova, S. Rondinini, and A.J. Bard, *Chem. Sci.*, **2012**, *3*, 217-229.

19. M.M. Najafpour and S.I. Allakhverdiev, *Int. J. Hydrog. Energy*, **2012**, *37*, 8753-8764.

20. F.E. Osterloh, *Chem. Soc. Rev.*, **2013**, *42*, 2294-2320.

21. M. Carraro, A. Sartorel, F.M. Toma, F. Puntoriero, F. Scandola, S. Campagna, M. Prato, and M. Bonchio, *Artificial Photosynthesis Challenges: Water Oxidation at Nanostructured Interfaces*, in *Photocatalysis*, C.A. Bignozzi, Editor. **2011**, Springer-Verlag Berlin: Berlin. p. 121-150.

22. F. Jiao and H. Frei, *Energy Environ. Sci.*, **2010**, *3*, 1018-1027.

23. T. Nakagawa, C.A. Beasley, and R.W. Murray, *J. Phys. Chem. C*, **2009**, *113*, 12958-12961.

24. A.A. Gambardella, S.W. Feldberg, and R.W. Murray, *J. Am. Chem. Soc.*, **2012**, *134*, 5774-5777.

25. Y. Liao, S.K. Yang, K. Koh, A.J. Matzger, and J.S. Biteen, *Nano Letters*, **2012**, *12*, 3080-3085.

26. T. Nakagawa, N.S. Bjorge, and R.W. Murray, *J. Am. Chem. Soc.*, **2009**, *131*, 15578-15579.

27. R.S. Dykhuizen, R. Frazer, C. Duncan, C.C. Smith, M. Golden, N. Benjamin, and C. Leifert, *Antimicrobial Agents and Chemotherapy*, **1996**, *40*, 1422-1425.

28. H. Björne, E. Weitzberg, and J.O. Lundberg, *Free Radi. Biol. Med.*, **2006**, *41*, 1404-1412.

29. M. Kirsch, H.G. Korth, R. Sustmann, and H. de Groot, *Biological Chemistry*, **2002**, *383*, 389-399.

30. D.J. Waterhouse, J.E. Saavedra, K.M. Davies, M.L. Citro, X. Xu, D.A. Powell, G.J. Grimes, G.K. Potti, and L.K. Keefer, *J. Pharm. Sci.*, **2006**, *95*, 108-115.

31. S.A.M. Marzouk, *Anal. Chem.*, **2003**, *75*, 1258-1266.

32. J.E. Baur and T.W. Spaine, *J. Electroanal. Chem.*, **1998**, *443*, 208-216.

33. Y.X. Zhao, N.M. Vargas-Barbosa, E.A. Hernandez-Pagan, and T.E. Mallouk, *Small*, **2011**, *7*, 2087-2093.

CHAPTER 5

CONCLUSIONS

5.1 Summary of Results and Contributions

Electrochemistry-based diagnostic devices have been widely applied in modern medicine, especially in point-of-care clinical analysis in hospitals and doctor's offices. In this Ph.D. dissertation, we have employed miniaturized classical enzyme-based electrochemical sensor devices to measure very low concentrations of glucose levels in tear fluid using a micro glass capillary tube configuration. Furthermore, a novel method that utilizes electrochemical modulation to deliver nitric oxide (NO) on demand from catheter tubing was also described. This new catheter design can be incorporated in a multi-lumen catheter configuration to help prevent clotting and infection of such indwelling medical devices.

In Chapter 2, needle-type amperometric and coulometric sensor devices were fabricated based on a previously reported subcutaneous glucose sensor configuration.[1] Both amperometric and coulometric sensors were combined with a micro glass capillary tube in which only 3 μL of tear fluid was needed to detect the lacrimal glucose concentrations. These electrochemical sensors can reliably measure very low glucose levels with a limit of detection of less than 1 μM (0.62 ± 0.03 μM and 0.38 ± 0.13 μM for amperometric and coulometric sensors, respectively, S/N=3, n=3) and exhibit excellent

selectivity over possible interference species (i.e., ascorbic acid, uric acid, and acetaminophen) with less than 10% error at their highest possible concentrations in tear fluid. Further, these miniature electrochemical devices were employed in an anesthetized rabbit model to detect the tear glucose levels in live animals and, more importantly, to examine whether a correlation between tear glucose and blood glucose concentrations exists. It was found that there was a positive correlation between the lacrimal glucose levels and the blood glucose concentrations in a total of 17 (6 under the optimal protocol) rabbit studies over a wide range of blood glucose values (3-20 mM). These results provide a good indication that tear glucose measurements may be a supplementary tool to assist routine blood glucose monitoring with blood glucometer devices for diabetics. However, as found,[2] separate correlation ratios are still observed in the animal model from different rabbit subjects and even from eye to eye, indicating the necessity of pre-calibrating the tear-blood glucose ratio for each individual in potential real-world applications. Once a correlation is obtained for a given eye, the proper algorithm may be employed to use tear glucose values to reflect the corresponding concentration of blood glucose.

In Chapters 3 and 4, a different view on applying electrochemical techniques in the biomedical field was focused on improving the biocompatibility of implantable medical devices. This was pursued by designing a novel NO delivery catheter from which the amount and duration of NO can be modulated by electrochemical methods. By proper control, NO can be delivered on demand to prevent clotting and infection on the surface of polymeric catheters. In this dissertation, two different electrochemical strategies were employed toward this ultimate goal.

In Chapter 3, electrochemically active species, *S*-nitrosothiols (RSNOs), were examined as a potential NO donor that can release NO locally by electrochemical reduction. Based on prior literature, NO is the reported common product from electrochemical reduction of RSNOs at physiological pH. However, studies here indicate that at pH 7.4, the reduction of RSNOs (-0.6 V to -0.9 V, *vs.* Ag/AgCl), does not yield a significant amount of NO. Instead, gas analysis suggested that RSNOs are reduced to nitrous oxide (N_2O) at pH 7.4 and can only be converted back to NO at more oxidizing voltages. Interestingly, at pH 4.0, a direct one-electron reduction of RSNOs appeared to occur and generates significant amounts of NO from RSNO species. Therefore, it seems possible to use a reservoir of RSNOs at low pH to create biomedical devices (e.g., intravascular catheters) in which electrochemically modulated release of NO can be achieved to prevent clotting and infection.

In Chapter 4, it was shown that it is possible to design controlled NO release on demand from pH sensitive NO donors via electrochemical modulation. The anodic potential has been optimized to facilitate the water oxidation reaction to occur at the lowest overpotential (to provide sufficient protons and to prevent the oxidation of localized NO). Two different types of pH sensitive NO donors, nitrite salts and diazeniumdiolate species, were employed to fabricate an electrochemically modulated NO release catheter. In the catheter design, diazeniumdiolates are a more suitable donor candidate, while nitrite salts are not optimal, as they produce a toxic side product, NO_2, that can diffuse through the catheter wall. With careful design, a physiologically relevant flux of NO ($>1\times10^{-10}$ mol cm^{-2} min^{-1}) was released from the catheter for up to 6 h. Additionally, iridium oxide nanoparticles were deposited onto a carbon fiber electrode by

electro-fluoccuation. The modified carbon fiber electrode exhibited a superior ability to release larger amounts of NO at a lower anodic potential than the bare electrodes.

5.2 Future Work

5.2.1 Strip-type Electrochemical Tear Glucose Sensor

The use of miniature electrochemical sensors for tear glucose measurements is a novel method with very few reports to date. However, the current design discussed in this dissertation requires 3 μL of tear fluids to be collected into a glass capillary for each measurement. Efforts to utilize the electrochemical sensor design with an even smaller sample volume (< 1 μL) to measure the concentrations of glucose in human tear fluid is a future direction for this research. Further miniaturization of the capillary sensors described in Chapter 2 would require significant engineering efforts. However, there already are many blood glucometer type electrochemical strips in the commercial market that utilize <1 μL of blood samples for accurate measurements of blood glucose. Therefore, a logical question to ask is whether any of these already existing electrode strips can be used with a high current sensitivity potentiostat to measure the low levels of glucose found in tear fluid.

Indeed, ongoing research by Kyoung Ha Cha in this lab has focused on employing such disposable strip-type electrochemical sensors to detect tear glucose with only 0.5 μL of solutions collected. Generally, such strips are pre-coated with two reagents inside: one is the enzyme that reacts directly with the glucose molecule to remove its two available electrons, and another one is the mediator molecule which takes the electrons from the

enzyme to the working electrode surface, where the current signal is monitored via end oxidation reaction.[3, 4] The mediator is usually a small chemical capable of existing in both an oxidized and a reduced form, and generally with high electrode kinetics to transfer electrons.[5] In Figure 5.1, a schematic diagram of a commercially available generic glucose test strip is shown with the fundamental structural components.

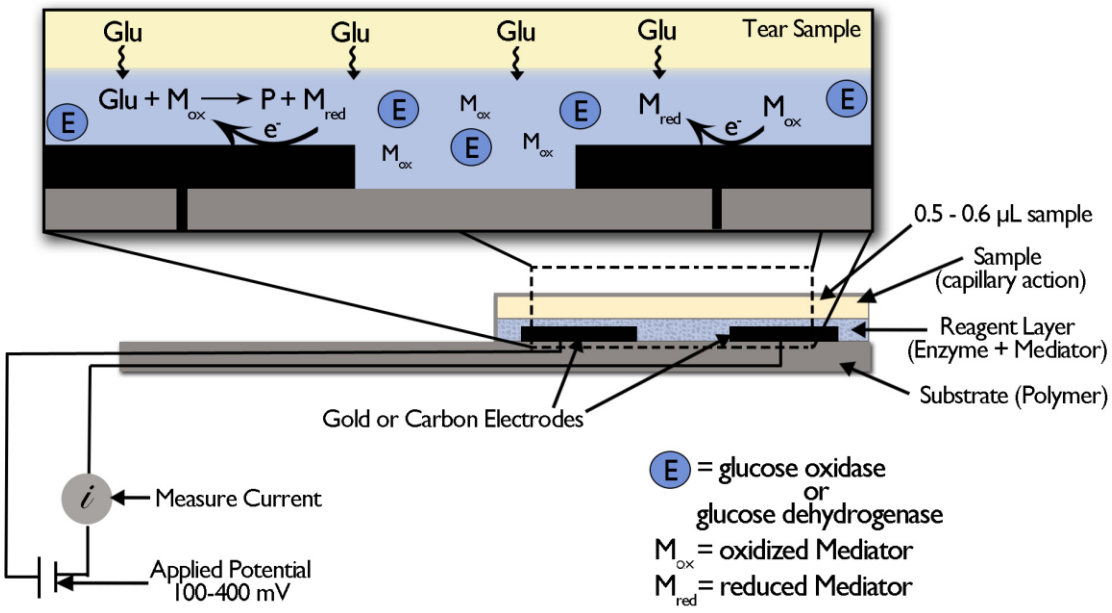

Figure 5.1. Diagram of testing tear glucose concentrations using commercially available blood glucometer test strips.

A large number of currently available glucose test strips were examined to obtain the ideal sensor that can sensitively measure low levels of tear glucose and block the electrochemically active interference species as well. The disposable strip was connected to a highly sensitive Biostat potentiostat (ESA Biosciences Inc., Chelmsford, MA) at

+0.15 V (*vs.* Au) for the electrochemical oxidation reaction with minimal errors (<10%) from ascorbic acid (100 μM), uric acid (100 μM), and 10 μM acetaminophen (10 μM) of their highest possible concentrations in tear fluid. Using the optimal strip, preliminary results from amperometric measurements over a range of low glucose concentrations (0-800 μM) in pH 7.4 PBS have been observed. After the sensor was exposed to 0.5 μL of glucose solution, an immediate increase of current was observed (Figure 5.2a), and the current was recorded at a 5 s mark for each measurement. The *i*-t results from low concentrations of glucose (0-100 μM) are fitted into a linear regression calibration curve in Figure 5.2b. It is noted that the strip-type sensor exhibits a polynomial regression fitting over a wide range of low glucose concentrations (0-800 μM), with a limit of detection of 7 μM (S/N=3).

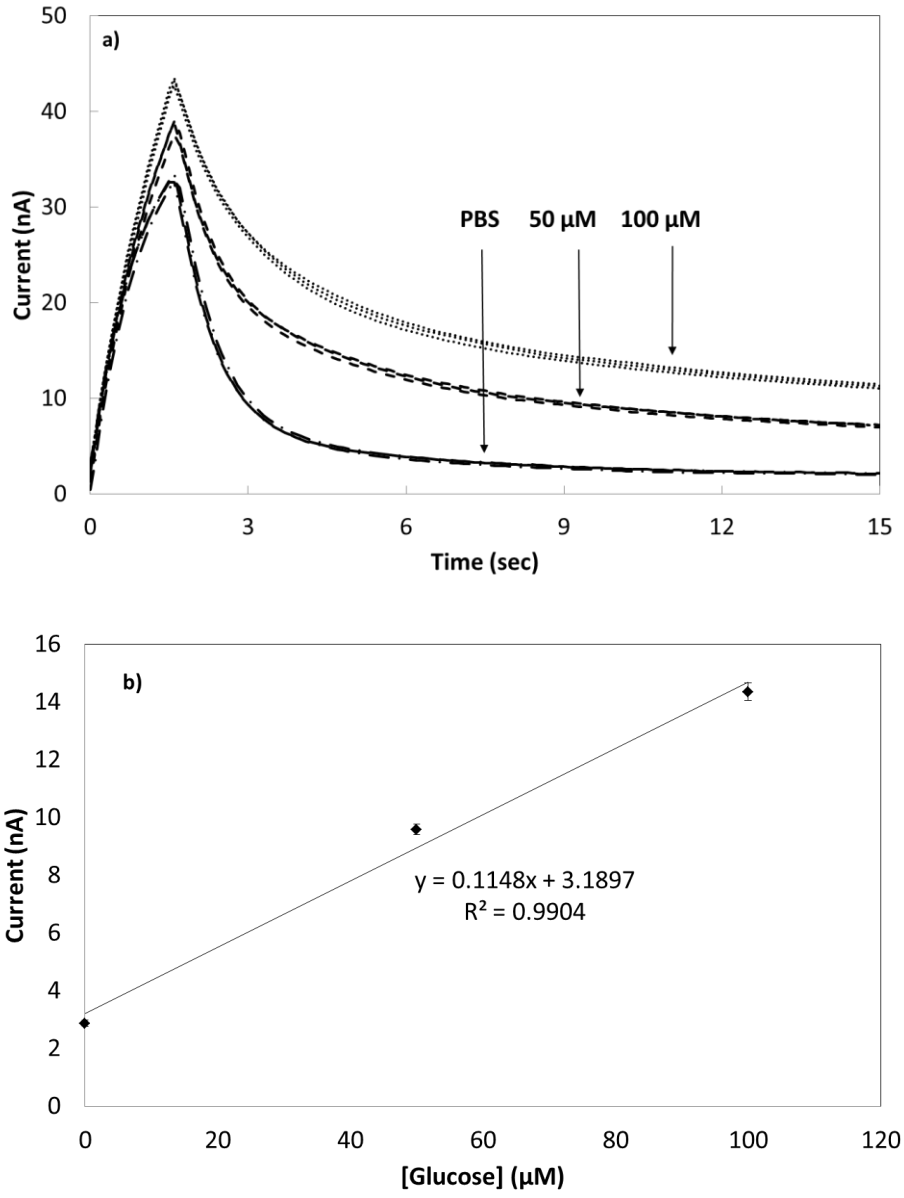

Figure 5.2. a) Response curve of single-use strip sensor to different concentrations of glucose (0-100 µM) in PBS (pH 7.4) at +0.15 V (*vs.* Au), each concentration was tested with 3 strips. b) the corresponding calibration curve. Error bars represent s.d. of n=3 replicate measurements of each standard solutions.

This strip-type sensor is now employed in an anesthetized animal study protocol (see Chapter 2) to evaluate its efficacy of monitoring glucose levels in rabbit tears. At the same time, the blood glucose values are monitored by the commercial whole blood

Radiometer instrument so that to examine whether the correlation between tear glucose as measured with the strips and blood glucose concentrations exists.

5.2.2 Long-term NO Delivery Catheter

As a proof-of-concept, it has been demonstrated in this dissertation work that two different types of NO donors (RSNO and diazeniumdiolates) can be placed into a silicone rubber catheter along with two electrodes to achieve electrochemically modulated NO delivery. However, the current limitation of these systems is the life-time of the NO delivery, apparently due to the inability to maintain a truly reliable and durable reference electrode. Therefore, future work should focus on the design of a better reference electrode in order to enhance the life time of these catheters (> 12 h).

First, Ag/AgCl is by far the most successful non-polarized electrode to reliably maintain a stable potential in miniature sensor designs.[6] The AgCl layer is generally formed on the surface of bare Ag electrode by chemical (soak in $FeCl_3$/HCl solution) or electrochemical oxidation (cycle between 0 to 1 V in HCl solution). Therefore, it is possible to electrochemically regenerate the AgCl layer by simply adding a cathodic potential on the working electrode (oxidizing potential on the reference electrode) after the water oxidation reaction. For example, in a catheter that contains diazeniumdiolates at pH 11, when an oxidizing potential of +0.6 V is applied on the working electrode, Eqn 5.1 and 5.3 (Table 5.1) are most likely to occur on the working electrode and reference (Ag/AgCl) electrode, producing proton and Ag, respectively. When a cathodic potential is applied on the working electrode at -0.4 V, an oxidizing potential on the reference

electrode will possibly facilitate the formation of $AgCl_{(s)}$ (Eqn. 5.7). Equations 5.3 and 5.7 are characterized by fast electrode kinetics, meaning that a sufficient high current can be passed through the electrode with high efficiency of the redox reaction. It is observed that in a catheter containing 10 mM diazeniumdiolates ($MAHMA/N_2O_2$) in pH 11 carbonate buffered solution, the anodic current at +0.6 V (*vs.* Ag/AgCl) is twice larger than the cathodic current at -0.4 V on a carbon fiber electrode surface. Therefore, in the optimal design, a cathodic potential at -0.4 V (*vs.* Ag/AgCl) will be turned on for 2 min after the potential is kept at +0.6 V for 1 min to regenerate equivalent amount of AgCl layer on the Ag/AgCl reference electrode.

App. E	Possible Half Rxns	Calculations	E' (V)
On WE: **+ 0.6 V**	**5.1)** $\boldsymbol{2H_2O \leftrightarrow 4H^+ + O_2 + 4e}$	$E' = 1.23 + \frac{0.059}{4}\lg[H^+]$	1.07
	5.2) $4OH^- \leftrightarrow 2H_2O + O_2 + 4e$	$E' = 0.401 - \frac{0.059}{2}\lg[OH^-]$	0.44
On Ref:	**5.3)** $\boldsymbol{AgCl_{(s)} + e \leftrightarrow Ag + Cl^-}$	$E' = 0.222 - 0.059\lg[Cl^-]$	0.28
On WE **-0.4 V**	**5.4)** $\boldsymbol{O_2 + 4H^+ + 4e \leftrightarrow 2H_2O}$	$E' = 1.23 + \frac{0.059}{4}\lg[H^+]$	1.07
	5.5) $O_2 + 2H^+ + 2e \leftrightarrow H_2O_2$	$E' = 0.695 + \frac{0.059}{2}\lg[H^+]$	0.37
	5.6) $O_2 + 2H_2O + 4e \leftrightarrow 4OH^-$	$E' = 0.401 - \frac{0.059}{4}\lg[OH^-]$	0.44
On Ref	**5.7)** $\boldsymbol{Ag + Cl^- \leftrightarrow AgCl_{(s)} + e}$	$E' = 0.222 - 0.059\lg[Cl^-]$	0.28

Table 5.1. Possible half reactions and the corresponding thermodynamic cell potentials on the working electrode and reference electrode surfaces.

Additionally, the Ag/AgCl electrode may be better sustained by adding some solid AgCl precipitate into the electrolyte solution. On one hand, the potential of Ag/AgCl is determined by the Ag^+ concentration in solution ($Ag^+ + e \leftrightarrow Ag_{(s)}$), which is inversely related to the chloride concentration through the solubility product constant of AgCl (K_{sp}= 1.77×10^{-10}). Therefore, in theory, the AgCl precipitate along with a Ag electrode can function as a reference electrode, provided a saturated AgCl solution is maintained. Moreover, the low concentration of soluble AgCl in solution can be reduced on the Ag/AgCl electrode surface when anodic potential is applied on the working electrode (Eqn. 5.3). In this way, the degradation of AgCl layer on the reference electrode surface may be alleviated. One possible side product yielded from the anodic potential sequence is HCl (proton from working electrode and Cl^- from reference electrode). However, in the basic solution where diazeniumdiolate is stabilized, the HCl can be readily neutralized by high concentrations of OH^- nearby.

Moreover, as described in Chapter 4, stable applied potential sequences can be maintained on the working electrode using a pseudo reference electrode (i.e., bare Ag). However, the production of OH^- species from the reference/counter electrode (from water reduction, Eqn 5.6) will titrate the pH of the bulk solution and therefore decrease the available amount of protons that react with diazeniumdiolates to release NO. A possible solution for this is to create two separate lumens for the working electrode and the reference electrode compartments in a multi-lumen catheter, where the reference electrode is in one lumen behind an ion conducting electric pathway (i.e., similar to the commercial Ag/AgCl electrode) and the working electrode is in another lumen with the NO donor solution (see Figure 5.3). The reference and working compartments can be

filled with the same buffered solutions to eliminate possible osmolality problems. In this way, the increase of pH from the production of OH^- on the pseudo reference electrode can be restrained in the reference lumen without changing the pH of the NO donor solutions. Therefore, a longer NO release can be achieved from the working electrode lumen that is under a constant pH conditions.

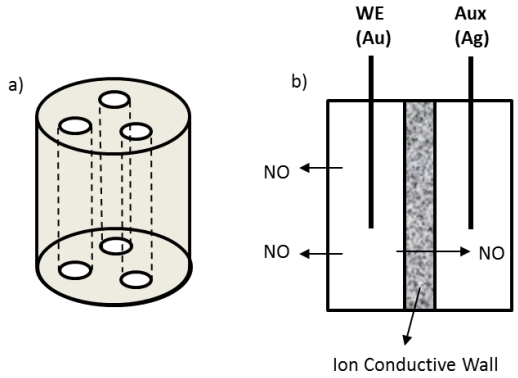

Figure 5.3. a) A schematic configuration of a triple-lumen catheter. b) The cross-section view of two separate lumens with the working electrode and reference electrode compartments.

5.3 References

1. D.S. Bindra, Y. Zhang, G.S. Wilson, R. Sternberg, D.R. Thevenot, D. Moatti, and G. Reach, *Anal. Chem.*, **1991**, *63*, 1692-1696.

2. Q. Yan, B. Peng, G. Su, B.E. Cohan, T.C. Major, and M.E. Meyerhoff, *Anal. Chem.*, **2011**, *83*, 8341.

3. M. Montagnana, M. Caputo, D. Giavarina, and G. Lippi, *Clinica Chimica Acta*, **2009**, *402*, 7-13.

4. S.E. Clarke and J.R. Foster, *Br. J. Biomed. Sci.*, **2012**, *69*, 83-93.

5. J. Hones, P. Muller, and N. Surridge, *Diabetes Technol. Ther.*, **2008**, *10*, S10-S26.

6. M.W. Shinwari, D. Zhitomirsky, I.A. Deen, P.R. Selvaganapathy, M.J. Deen, and D. Landheer, *Sensors*, **2010**, *10*, 1679-1715.